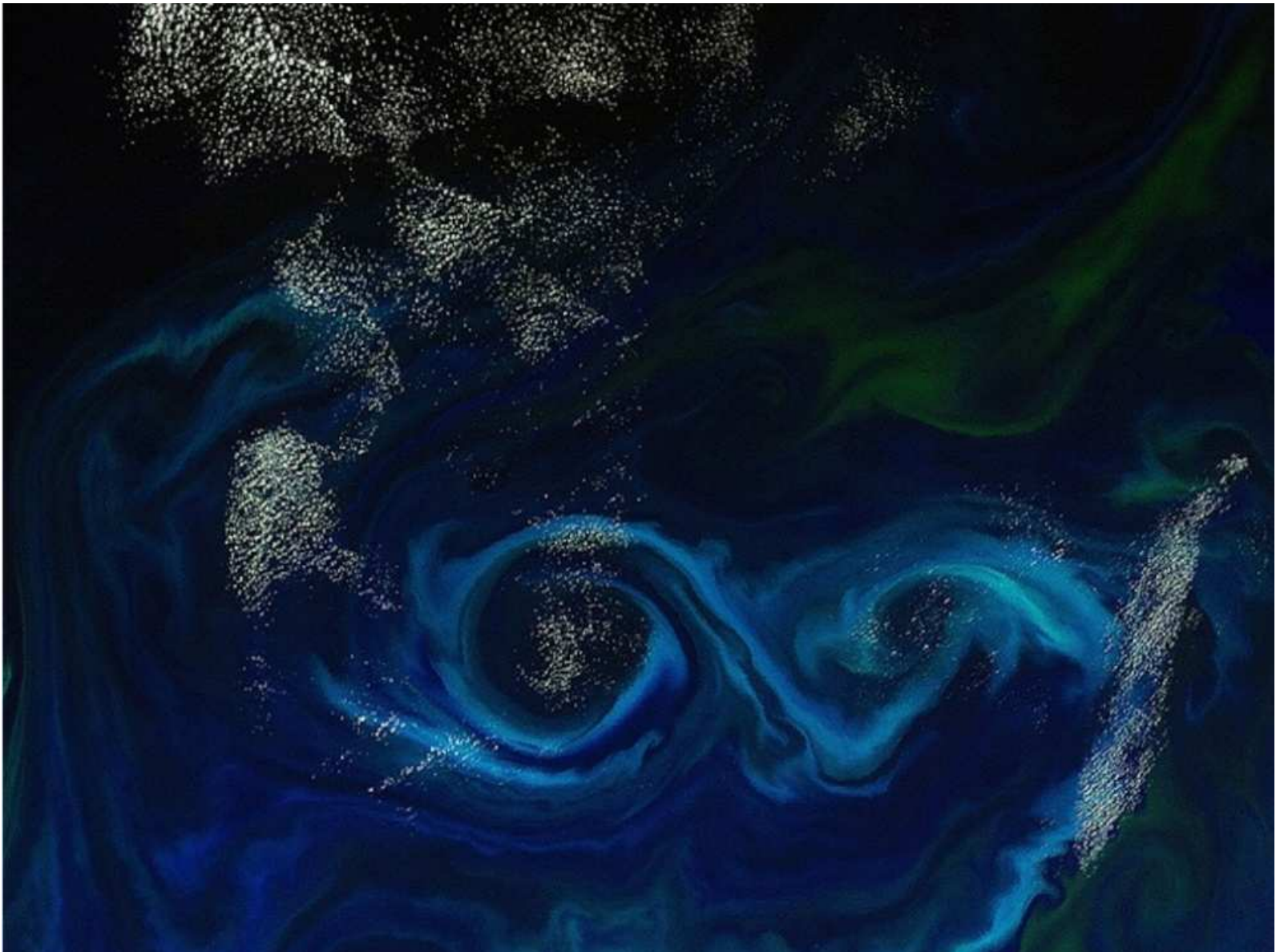


IUTAM Symposium on

Motile Cells in Complex Environments



Udine, May 15–18, 2018

SYMPOSIUM SCHEDULE-AT-A-GLANCE

Tuesday, 15 May	
17:00-19:00	Registration and Welcome Reception at CISM

Wednesday, 16 May	
8:30-9:00	On-site registration
9:00-9:15	Welcome Address
9:15-10:00	Invited Lecture: G. Boffetta , M. Cencini, F. De Lillo
10:00-10:30	Keynote Lecture: W. Clifton, R.N. Bearon , M.A. Bees
10:30-11:00	Coffee Break
11:00-12:48	Session #1 (regular talks)
12:48-14:15	Lunch Break
14:15-15:00	Invited Lecture: K. Gustavsson, F. Berglund, P.R. Jonsson, B. Mehlig
15:00-15:30	Keynote Lecture: R.G. Winkler
15:30-16:00	Keynote Lecture: A. Ardekani , N. Desai, V. Shaik
16:00-16:30	Coffee Break
16:30-18:00	Session #2 (regular talks)

Thursday, 17 May	
9:00-9:45	Invited Lecture: W.C.K. Poon
9:45-10:15	Keynote Lecture: L. Rao, P.Garg, G. Subramanian
10:15-10:40	Coffee Break
10:40-12:28	Session #3 (regular talks)
12:28-14:00	Lunch Break
14:00-14:30	Keynote Lecture: A.Mathijssen, N. Figueroa-Morales, G. Junot, E. Clement, A. Lindner , A. Zöttl
14:30-15:00	Keynote Lecture: N.M. Oliveira, K.R. Foster, W.M. Durham
15:00-15:54	Session #4 (regular talks)
15:54-16:20	Coffee Break
16:20-17:50	Session #5 (regular talks)
20:00-22:00	Social Dinner

Friday, 18 May	
9:00-9:45	Invited Lecture: S. Fielding
9:45-10:15	Keynote Lecture: I. Pagonabarraga
10:15-10:50	Session #6 (regular talks)
10:50-11:10	Coffee Break
11:10-12:58	Session #7 (regular talks)
12:58-13:10	Closing
13:10-14:30	Lunch Break

TABLE OF CONTENTS

<u>SYMPOSIUM SCHEDULE-AT-A-GLANCE.....</u>	<u>0</u>
<u>WELCOME.....</u>	<u>2</u>
ORGANIZING COMMITTEE	3
SCIENTIFIC COMMITTEE	3
<u>USEFUL INFORMATION.....</u>	<u>4</u>
<u>SOCIAL DINNER.....</u>	<u>4</u>
<u>MEETING VENUE.....</u>	<u>4</u>
PALAZZO GARZOLINI DI TOPPO WASSERMANN	5
CENTRO INTERNAZIONALE DI SCIENZE MECCANICHE - CISM	5
CASA DELLA CONTADINANZA, CASTELLO DI UDINE	5
<u>INVITED LECTURES</u>	<u>6</u>
<u>INSTRUCTIONS TO SPEAKEARS AND SESSION CHAIRS.....</u>	<u>8</u>
<u>SPONSOR.....</u>	<u>9</u>
<u>PROGRAM SUMMARY.....</u>	<u>11</u>
<u>ABSTRACTS</u>	<u>15</u>

WELCOME

Welcome to the IUTAM Symposium on Motile Cells in Complex Environments (MCCE 2018) in Udine (Italy), May 15-18, 2018.

The Symposium brings together experts in the complementary fields of physics, applied mathematics, chemistry, biology, life sciences, and engineering to discuss multidisciplinary theoretical, numerical and experimental approaches to predict the behaviour of active complex fluid systems characterized by the presence of motile living cells. Cell motility is a multifaceted interdisciplinary challenge for a wide community of scientists, with applications ranging from medical to bio-technological and environmental issues. Cells often grow and move within complex fluid environments: Examples include motile phytoplankton cells giving rise to bio-convective patterns in turbulent flows, but also suspensions of swimming bacteria that can form biofilms under adverse conditions and swarm to colonize solid surfaces. Depending on the targeted biological system, such environments may be characterized both by high and low Reynolds numbers, thus involving a broad spectrum of spatial and temporal dynamics that are not easy to model.

The Symposium provides the opportunity to compare and contrast the different available approaches, giving a global overview of the most significant advancements in the field. It also serves the purpose of identifying the main open issues and research pathways that the community should focus on in the future. To these aims the Symposium brings together internationally renowned scientists from all horizons (analytical, numerical, and experimental) to foster scientific exchange and strengthen interdisciplinary work among engineers, applied mathematicians, physicists, and biologists through invited lectures, and contributed talks.

The Symposium spans a wide selection of topics in biological fluid mechanics from single swimmer propulsion and navigation mechanisms to synchronized and collective motion, focusing on how active cells may use hydrodynamic interaction as well as biochemistry to coordinate their locomotion. Topics of interest are also the dynamics and rheology of active fluids, fluid-structure interactions in bio-inspired systems, growth of tissues, and surface colonization. The interest on these topics has exploded in recent years, as demonstrated by the wealth of experimental or numerical results that have been produced and by the many resulting (and sometimes competing) theories that have been developed.

The conference is hosted by the Università degli Studi di Udine, which we gratefully acknowledge for

providing funding and resources. The conference convenes at the Palazzo Garzolini di Toppo-Wasserman, located next to the city center of Udine.

As we are all aware, the efforts required in organizing and holding this kind of scientific events are extensive. Sincere appreciation is expressed to the organizing committee members for their exemplary efforts. The productive co-operation with the International Center of Mechanical Sciences is also gratefully acknowledged. The financial support provided by CINECA, the largest Italian supercomputing center, is also thankfully acknowledged. Finally, gratitude is expressed to all the invited speakers, authors, session chairpersons and attendees, whose contributions and efforts have made this Symposium a great success.

On behalf of the Organizing Committee,

Cristian Marchioli
MCCE 2018 Chairman

Eric Climent
MCCE 2018 Co-Chairman

ORGANIZING COMMITTEE

- Cristian Marchioli, University of Udine, IT, **CHAIR**
- Eric Climent, IMFT Toulouse, FR, **co-CHAIR**
- Marina Campolo, University of Udine, IT
- Giorgio Honsell, University of Udine, IT
- Alfredo Soldati, TU Wien, AT

SCIENTIFIC COMMITTEE

- Arezoo Ardekani, Purdue University, US
- Rachel Bearon, University of Liverpool, UK
- Eric Climent, IMFT Toulouse, FR
- Cristian Marchioli, University of Udine, IT
- Ignacio Pagonabarraga, University of Barcelona, ES
- Roman Stoker, ETH Zurich, SU
- Ganesh Subramanian, Jawaharlal Nehru Center for Advanced Scientific Research, IN
- Roland G. Winkler, Institute for Advanced Simulation, Forschungszentrum Julich, DE

USEFUL INFORMATION

Registration Desk Hours

Tuesday, 15 May: 17:00-19:00, Palazzo del Torso (CISM).

Wednesday, 16 May: 8:30-9:00, Palazzo Garzolini di Toppo-Wassermann.

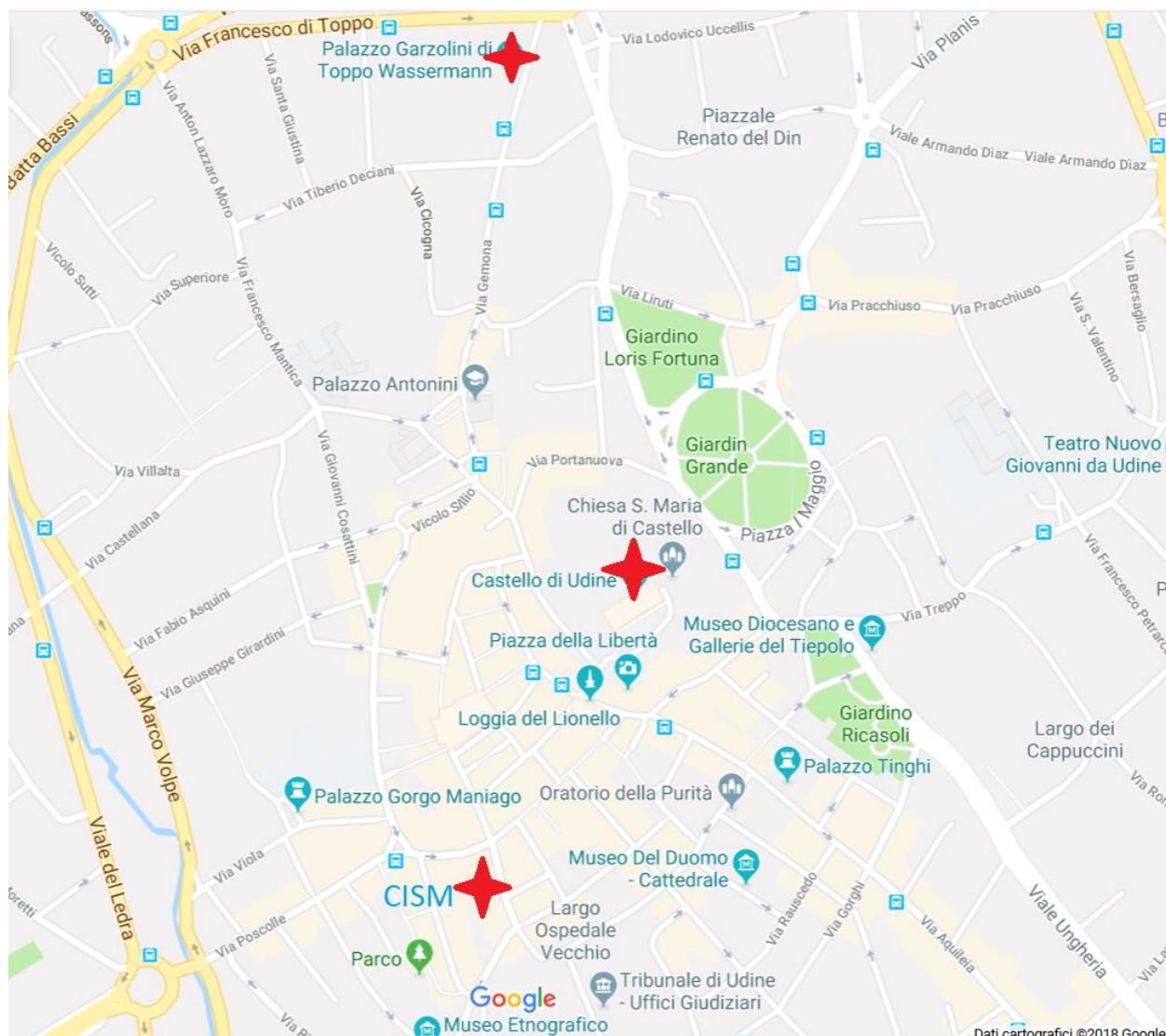
Wireless Internet

Participants who would like to access the Internet at Palazzo Garzolini di Toppo-Wassermann can use the wireless network Eduroam.

SOCIAL DINNER

The Social Dinner will be held on Thursday, May 17, 2018 at Casa della Contadinanza, Castello di Udine (20:00 -22:00).

MEETING VENUE



PALAZZO GARZOLINI DI TOPPO WASSERMANN



Located in Via Gemona 90, Udine, Italy, the Toppo Wassermann College (named for Count Francesco Toppo Wassermann) was a boarding school from 1900 until closing in the 1981-82 school year. The name Toppo Wassermann is now linked to, among other local institutions, a library, a primary school and the School of Excellence of the University of Udine.

CENTRO INTERNAZIONALE DI SCIENZE MECCANICHE - CISM



CISM, International Centre for Mechanical Sciences, is a non-profit organization, founded in 1968 to favour the exchange and application of the most advanced

knowledge in mechanical sciences, in interdisciplinary fields like robotics, biomechanics, environmental engineering and in other fields (mathematics, information and system theory, operations research, computer science, artificial intelligence).

Located in the Palazzo del Torso in the center of Udine, CISM is international in both scope and structure: the Scientific Council, rectors, lecturers are selected from among the acknowledged authorities in their respective fields the world over.

CISM is funded by the Friuli Venezia Giulia Region, the Province of Udine and the city of Udine, and local public and private institutions, together with other member institutions in Europe and abroad. Further financial support comes from the National Research Council of Italy (CNR), and from UNESCO.

CISM also has consolidated working relations with AIMETA, ECCOMAS, ERCOFTAC, EUROMECH, GAMM, IFToMM and IUTAM.

CASA DELLA CONTADINANZA, CASTELLO DI UDINE



Casa della Contadinanza is located on the top of Udine Hill. The view from there toward the Friuli mountains is impressive but the Casa (House) is a non extraordinary reconstruction of the XX century of an old building originally in town. Inside there is a restaurant serving regional foods at reasonably price.

There is no public transport to the hill and you have to walk for about 500-700 meters to reach the top of the hill. Near the Casa della Contadinanza there is the "castle" of Udine, ancient residence of the lieutenant of Venice and a present museum of arts and hystory of the city.

INVITED LECTURES

Wednesday, 16 May

9:15, Palazzo Garzolini, Room 4
Chair: E. Climent

GYROTACTIC PHYTOPLANKTON SWIMMING IN
LAMINAR AND TURBULENT FLOWS

Guido BOFFETTA, M. Cencini.F. De Lillo

University of Torino, IT



Wednesday, 16 May

10:00, Palazzo Garzolini, Room 4
Chair: E. Climent

ENHANCED SEDIMENTATION OF ELONGATED
PLANKTON IN SIMPLE FLOWS

W. Clifton, Rachel BEARON, M.A. Bees

University of Liverpool, UK



Wednesday, 16 May

14:15, Palazzo Garzolini, Room 4
Chair: W.M. Durham

PREFERENTIAL SAMPLING AND SMALL SCALE
CLUSTERING OF GYROTACTIC MICROSWIMMERS
IN TURBULENCE

K. Gustavsson, F.Berglund, P.R. Jonsson, Bernhard. MEHLIG

University of Gothenburg, SE



Wednesday, 16 May

15:00, Palazzo Garzolini, Room 4
Chair: W.M. Durham

ROLE OF HYDRODYNAMICS IN CELL MOTILITY:
MESOSCALE HYDRODYNAMIC SIMULATIONS

Roland G. WINKLER

Institute for Advanced Simulation,
Forschungszentrum Jülich, DE



Thursday, 17 May

9:00, Palazzo Garzolini, Room 4
Chair: A. Lindner

PAINTING WITH BACTERIA, THREE WAYS

Wilson C.K. POON

University of Edinburgh, UK



Wednesday, 16 May

15:30, Palazzo Garzolini, Room 4
Chair: W.M. Durham

OIL --MICROBE INTERACTIONS: ROLE OF
CHEMOTAXIS AND HYDRODYNAMICS

Arezoo ARDEKANI, N. Desai, V. Shaik

Purdue University, US



Friday, 18 May

9:00, Palazzo Garzolini, Room 4
Chair: C.Marchioli

HYDRODYNAMICS AND PHASE BEHAVIOUR OF
ACTIVE SUSPENSIONS

Suzanne FIELDING

Durham University, UK



Thursday, 17 May

9:45, Palazzo Garzolini, Room 4
Chair: A. Lindner

SHEAR-INDUCED MIGRATION AND BANDING
INSTABILITIES IN BACTERIAL SUSPENSIONS

L. Rao, P. Garg, Ganesh SUBRAMANIAN

Jawaharlal Nehru Centre for Advanced
Scientific Research, IN



Thursday, 17 May

14:00, Palazzo Garzolini, Room 4

Chair: R.G. Winkler

OSCILLATORY SURFACE RHEOTAXIS OF
SWIMMING E. COLI BACTERIA



**A.Mathijssen, N. Figueroa-Morales, G.
Junot, E. Clement, Anke LINDNER, A.
Zöttl**

ESPCI ParisTech, FR

Thursday, 17 May

14:30, Palazzo Garzolini, Room 4

Chair: R.G. Winkler

BACTERIAL CHEMOTAXIS DURING BIOFILM
FORMATION



**N.M. Oliveira, K.R. Foster, William M.
DURHAM**

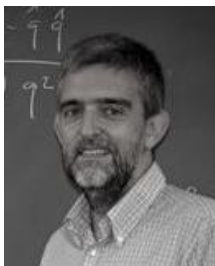
University of Sheffield, UK

Friday, 18 May

9:45, Palazzo Garzolini, Room 4

Chair: C.Marchioli

TBA



Ignacio PAGONABARRAGA

University of Barcelona, ES

INSTRUCTIONS TO SPEAKERS AND SESSION CHAIRS

1. The presentation room will be equipped with a PC and an LCD projector. Laser presentation pointers can be provided upon request of the Chair person and depending on availability;
2. Speakers are kindly asked to upload their presentations in the PC assigned to the room; speakers may also use their own laptop;
3. The default software for presentation is PowerPoint running on Microsoft OS;
4. To avoid time losses due to technical issues, speakers are kindly requested to test their presentation well beforehand;
5. In case of technical difficulties, it is the speaker's responsibility to contact the staff person ahead of the scheduled time of the presentation;
6. Please prepare a good quality portable PDF version of the presentation in the case other formats are not supported by the PC;
7. Invited plenary talks will be assigned 40 minutes for presentation, plus additional 5 minutes for questions and change of speaker;
8. Invited keynote talks will be assigned 26 minutes for presentation, plus additional 4 minutes for questions and change of speaker;
9. Regular contributed talks will be assigned 15 minutes for presentation, plus additional 3 minutes for questions and change of speaker;
10. A monitor display will be used to time the sessions; this timing will be enforced by the Session Chair;
11. Chair persons are kindly asked to strictly maintain the schedule.

SPONSOR

IUTAM

International Union of Theoretical and Applied Mechanics

iutam.org

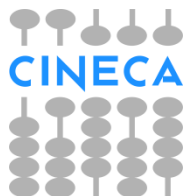


The International Union of Theoretical and Applied Mechanics, was probably founded when Theodore von Kármán, professor in Aachen (Germany), held a conference in Innsbruck in September 1922 to discuss questions of hydrodynamics and aerodynamics. Today, IUTAM counts more than 500 active members, representing 50 countries and 20 affiliated organisations. The original IUTAM website was established in connection with the ICTAM 2000 internet activities by the Secretary-General of ICTAM 2000, Prof. James W. Phillips at UIUC, on request by the IUTAM Bureau. During the Closing Ceremony of ICTAM 2000 in Chicago, a citation was presented to Prof. Phillips by the President of IUTAM. The website is maintained under the responsibility of the Secretary-General of IUTAM.

CINECA

Consorzio Interuniversitario per il
Calcolo Automatico

www.cineca.it



Cineca is a no-profit Consortium, made up of 70 Italian universities, 5 Italian Research Institutions and the Italian Ministry of Education. Today it is the largest Italian computing center, one of the most important worldwide. With more seven hundred employees, it operates in the technological transfer sector through high performance scientific computing, the management and development of networks and web based services, and the development of complex information systems for treating large amounts of data. It develops advanced Information Technology applications and services, acting like a trait-d'union between the academic world, the sphere of pure research and the world of industry and Public Administration.

CISM

International Centre of Mechanical
Sciences

www.cism.it



CISM, International Centre for Mechanical Sciences, is a no-profit organization, founded in 1968 to favour the exchange and application of the most advanced knowledge in the mechanical sciences, in interdisciplinary fields like robotics, biomechanics, environmental engineering and in other fields (mathematics, information and system theory, operations research, computer science, artificial intelligence). The principal activity of the Centre is the organization of courses, seminars, workshops, symposia, and conferences to present the state of the art of these sciences to researchers. It also provides advanced training for engineers operating in industry. CISM is funded by the Friuli Venezia Giulia Region, the Province of Udine and the city of Udine, and local public and private institutions, together with other member institutions in Europe and abroad. Further financial support comes from the National Research Council of Italy (CNR), and from UNESCO. CISM also has consolidated relations with AIMETA, ECCOMAS, ERCOFTAC, EUROMECH, GAMM, IFToMM and IUTAM.

UNIUD

University of Udine

www.uniud.it



The University of Udine was founded in 1978 as part of the reconstruction plan of Friuli after the earthquake in 1976. Its aim was to provide the Friulian community with an independent centre for advanced training in cultural and scientific studies. Udine and its University are a point of reference in a region that is historically a meeting place and crossroads of different worlds and cultures. Geographically situated in the centre of the European Union, the University of Udine plays an active role in a close network of relations, committed to sharing its knowledge and ideas. Since its establishment, Udine University has pursued the policy of internationalisation, aimed at preparing students and forging relations and partnerships with universities and institutions in Europe and the rest of the world. Udine University collaborates not only within Europe but across the globe and has long-standing connections with Africa, India and China.

PROGRAM SUMMARY

May 15, 2018	TUESDAY	WHERE	CHAIRPERSON
17:00-19:00	Registration and Welcome Reception	CISM	
May 16, 2018	WEDNESDAY		
8:30-9:00	Onsite registration	Palazzo Garzolini	
9:00-9.15	Opening: Welcome address		C.Marchioli
9:15-10:00	INVITED LECTURE: <u>G. Boffetta</u> , M. Cencini, F. De Lillo Gyrotactic phytoplankton swimming in laminar and turbulent flows		E. Climent
10:00-10:30	KEYNOTE LECTURE: W. Clifton, <u>R.N.Bearon</u> , M.A. Bees Enhanced sedimentation of elongated plankton in simple flows		E. Climent
10:30-11:00	Coffee Break		
	REGULAR SESSION 1		
11:00-11:18	F. Toschi, E. Calzavarini, F. Schmid Lagrangian modelling of copepod dynamics		G. Boffetta T.J. Pedley
11:18-11:36	K. Guseva, U. Feudel Colonization of moving marine aggregates by bacteria		
11:36-11:54	S. Colabrese, K. Gustavsson, A. Celani, L. Biferale Flow navigation by smart microswimmers via reinforcement learning		
11:54-12:12	E. Climent, S. Lovecchio, W.M. Durham, R. Stocke Vertical migration of motile phytoplankton chains through turbulence		
12:12-12:30	A. Soldati, S. Lovecchio, F. Zonta, C. Marchioli Thermal stratification hinders gyrotactic micro-organism rising in free-surface turbulence		
12:30-12:48	M. Borgnino, I. Tuval, F. De Lillo, G. Boffetta Buoyancy regulation of non-motile phytoplankton in a turbulent flow		
12:48-14:15	Lunch break		
14:15-15:00	INVITED LECTURE: K. Gustavsson, F. Berglund, P.R. Jonsson, <u>B. Mehlig</u> Preferential sampling and small-scale clustering of gyrotactic microswimmers in turbulence		W.M. Durham
15:00-15:30	KEYNOTE LECTURE: <u>R.G. Winkler</u> Role of hydrodynamics in cell motility: Mesoscale hydrodynamic simulations		W.M. Durham
15:30-16:00	KEYNOTE LECTURE: <u>A. Ardekani</u> , N. Desai, V. Shaik Oil-microbe interactions: role of chemotaxis and hydrodynamics		W.M. Durham
16:00-16:30	Coffee Break		

REGULAR SESSION 2

16:30-16:48	L. Zeng, T.J. Pedley Distribution of gyrotactic micro-organisms in complex three-dimensional flows: Horizontal shear flow past a vertical circular cylinder	R.N. Bearon B. Mehlig
16:48-17:06	T.J. Pedley and L. Zeng Gravitational motion induced by gyrotactic micro-organisms near a vertical wall in a horizontal stagnation point flow	
17:06-17:24	S. Maretvadakethope, E. Keaveny, Y. Hwang Gyrotactic trapping can be hydrodynamically unstable	
17:24-17:42	C. Marchioli, S. Lovecchio, A. Soldati Micro-swimmer dynamics in free-surface turbulence subject to wind stress	
17:42-18:00	I. Aronson, B. Winkler, F. Ziebert Confinement and substrate topography control 3D cell migration	

May 17, 2018**THURSDAY**

9:00-9:45	INVITED LECTURE: <u>W.C.K. Poon</u> Painting with bacteria, three ways	Palazzo Garzolini	A. Lindner
-----------	--	-------------------	------------

9:45-10:15	KEYNOTE LECTURE: L. Rao, P. Garg, <u>G. Subramanian</u> Shear-induced migration and banding instabilities in bacterial suspensions		A. Lindner
------------	--	--	------------

10:15-10:40	Coffee Break		
-------------	--------------	--	--

REGULAR SESSION 3

10:40-10:58	S. Nambiar, G. Subramanian Divergence of the velocity variance in interacting swimmer suspensions	A. Ardekani B. Delmotte
-------------	--	----------------------------

10:58-11:16	N. Giuliani, A. De Simone Optimizing performance of micro-swimmers: The role of hydrodynamic interactions	
-------------	--	--

11:16-11:34	V. Meschini, G. Noselli, M. Chinappi, R. Verzicco, A. De Simone Study of biological and bio-inspired swimming at low Reynolds numbers using an immersed boundary method	
-------------	--	--

11:34-11:52	S. F. Schoeller, E. Keaveny Linking individual and collective dynamics of sperm in suspension	
-------------	--	--

11:52-12:10	M. Mousavi, T. Eisenstecken, G. Gompper, R. G. Winkler E-coli swimming and scattering at surfaces. A mesoscale simulation study	
-------------	--	--

12:10-12:28	G. Sinibaldi, V. Iebba, M. Chinappi Swimming and rafting of E-coli microcolonies at air-liquid interfaces	
-------------	--	--

12:28-14:00	Lunch Break	
-------------	-------------	--

14:00-14:30	KEYNOTE LECTURE: A. Mathijssen, N. Figueroa-Morales, G. Junot, E. Clement, <u>A. Lindner</u> , A. Zöttl Oscillatory surface rheotaxis of swimming E. coli bacteria	R.G. Winkler
-------------	--	--------------

14:30-15:00	KEYNOTE LECTURE: N.M. Oliveira, K.R. Foster, <u>W.M. Durham</u> Bacterial chemotaxis during biofilm formation	R.G. Winkler
REGULAR SESSION 4		
15:00-15:18	C.T.Kreis, A. Fragkopoulos, T. Ostapenko, T. Bøddeker, O. Bäumchen Photoactive microbes – Light-switchable adhesion and motility in confinement	I. Pagonabarraga
15:18-15:36	J. Arlt, V. A. Martinez, A. Dawson, T. Pilizota, W. C.K. Poon Painting with light-powered bacteria: Smart-templated self assembly using microswimmers	
15:36-15:54	B. Delmotte, M. Driscoll, A. Donev, P. Chaikin Hydrodynamic genesis of colloidal creatures	
15:54-16:20	Coffee Break	
REGULAR SESSIONS 5		
16:20-16:38	R. Pioli, E. Secchi, L. Isa, R. Stocker Capillary deposition of microorganisms in a microfluidic channel for the study of cells in spatially controlled environments	I. Aronson G. Subramanian
16:38-16:56	M.M. Villone, M. Trofa, M.A. Hulsen, P.L. Maffettone Numerical design of a T-shaped microfluidic device for the detection of diseased cells through deformability-based separation	
16:56-17:14	R. Martinez, F. Alarcon, D. Rogel-Rodriguez, J. Ramirez, J. L. Aragonés, C. Valeriani Flocking particles with asymmetric obstacles: A model for isolation and sorting motile cells and unicellular organisms	
17:14-17:32	A. Basoni, G. Gonnella, D. Marenduzzo, E. Orlandini, A. Tiribocchi A minimal physical model for cell migration in presence of obstacles	
17:32-17:50	F. Giavazzi, C. Malinverno, A. Ferrari, G. Scita, R. Cerbino Endocytic reawakening of motility and flocking in jammed epithelia	
20:00-22:00	Social Dinner	
May 18, 2018	FRIDAY	
9:00-9:45	INVITED LECTURE: <u>S. Fielding</u> Hydrodynamics and phase behaviour of active suspensions	C.Marchioli
9:45-10:15	KEYNOTE LECTURE: <u>I. Pagonabarraga</u> TBA	C.Marchioli
REGULAR SESSIONS 6		
10:15-10:33	A. Zöttl, J. M. Yeomans Large speed enhancement of swimming bacteria in dense polymeric fluids	L. Ploux
10:33-10:51	C. Devailly, A. Dawson, J. Arlt, J. Schwarz-Linek, A. Morozov, W.C.K. Poon, V. Martinez Scaling of bacteria swimming in polymer solutions	

10:51-11:10	Coffee Break	
11:10-11:28	D. Brumley, F. Carrara, A. Hein, Y. Yawata, S. Levin, R. Stocker Bacteria push the limits of sensory precision to navigate dynamic seascapes	S. Fielding W.C.K. Poon
11:28-11:46	J. Lagrone, L. Fauci, R. Cortez Simulating Bacterial Motility in Confined Environments	
11:46-12:04	A. Dehkharghani, N. Waisbord, J. Dunkel, J. Guasto Transport of swimming bacteria in porous media flows	
12:04-12:22	M. Veuillet, C. Soraru, A. Airoudj, Y. Goubeyre, E. Gaudichet-Maurin, V. Roucoules, L. Ploux Relationship between bacterial motility and biofilm preventive properties on coatings with from soft to stiff mechanical properties	
12:22-12:40	B. Delmotte, E. Keaveny, F. Plouraboué, E. Climent Transport and diffusion of micro-particles in active suspensions	
12:40-12:58	K. Qi, E. Westphal, G. Gompper, R.G. Winkler A Spheroidal Squirmer in Shear Flow	
12:58-13:10	Closing	
13:10-14:30	Lunch Break	

ABSTRACTS

Day	Page
Wednesday, 16 May	16-41
Thursday, 17 May	42-75
Friday, 18 May	76-90

Gyrotactic phytoplankton swimming in laminar and turbulent flows

Guido Boffetta¹, Massimo Cencini² and Filippo De Lillo¹

¹Dipartimento di Fisica and INFN, Università di Torino
via P. Giuria 1, 10125 Torino, Italy

²Institute of Complex System of CNR
Address

Abstract

This contribution discusses the dynamics of gyrotactic swimmers in laminar and turbulent flows. A generalized gyrotactic model, which takes into account the presence of fluid acceleration, is verified by means of laboratory experiments of gyrotactic cells in a rotating cylinder. The model is then implemented in numerical simulations of fully turbulent flows, where clustering of gyrotactic swimmers is observed and characterized as a function of swimming parameters. Finally, clustering of a heterogeneous population of cells, characterized by a distribution of swimming parameters, is discussed.

Keywords: turbulence, phytoplankton, gyrotaxis

1. Introduction

The mathematical model for gyrotactic algae was introduced by Pedley and Kessler [1, 2] on the basis of the observation that bottom-heavy swimming micro-organisms focus in the center of a pipe when the fluid flows downwards. The swimming direction \mathbf{p} results from the competition between gravity-buoyant torque, due to bottom-heaviness, and the shear-induced viscous torque and evolves according to

$$\dot{\mathbf{p}} = \frac{1}{2B} [\hat{\mathbf{z}} - (\hat{\mathbf{z}} \cdot \mathbf{p})\mathbf{p}] + \frac{1}{2}\omega \times \mathbf{p} + \Gamma_r \quad (1)$$

where $\omega = \nabla \times \mathbf{u}$ is the vorticity at the position of the cell, $B = 3\nu/(hg)$ is a characteristic orientation time which depends on viscosity ν , gravity $\mathbf{g} = -g\hat{\mathbf{z}}$ and on the displacement h of the cell center of mass relative to the geometrical center. The stochastic term Γ_r represent rotational diffusion of the swimming direction as a results of irregularities in the swimming behavior.

Due to the small size and the small density mismatch with the fluid, gyrotactic cells are represented as point-like, spherical and neutrally buoyant particles transported by the fluid velocity $\mathbf{u}(\mathbf{x}, t)$ with a superimposed swimming velocity v_s

$$\dot{\mathbf{x}} = \mathbf{u} + v_s \mathbf{p} \quad (2)$$

The gyrotactic model (1-2) has been used to describe mathematically several complex behavior observing in suspensions of bottom-heavy cells, including the formation of thin layers [3] and clustering in turbulence [4, 5].

In this contribution we will discuss the an extension of the gyrotactic model which takes into account the effects of fluid acceleration, its validation in a simple laboratory experiment and numerical predictions for the dynamics of gyrotactic swimmers in turbulent flows.

2. Generalized gyrotactic model

The gyrotactic model (1-2) has been recently generalized by taking into account the effect of fluid acceleration on the orientation of the swimming direction [6]. By introducing the total acceleration on the cell $\mathbf{A} = \mathbf{g} - \mathbf{a}$, where $\mathbf{a} = d\mathbf{u}/dt$, (1) becomes

$$\dot{\mathbf{p}} = -\frac{1}{v_0} [\mathbf{A} - (\mathbf{A} \cdot \mathbf{p})\mathbf{p}] + \frac{1}{2}\omega \times \mathbf{p} + \Gamma_r \quad (3)$$

where $v_0 = Bg$ is the reorientation velocity.

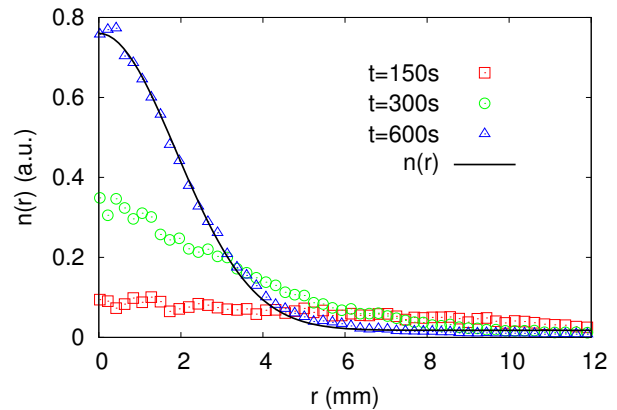


Figure 1: Evolution of the radial population density for the rotating experiment at $\Omega = 7Hz$ at different times. The black solid line represents the theoretical prediction for the total density in stationary conditions based on (2-3).

The model (3) has been validated by laboratory experiments with a suspension of gyrotactic cells (*Chlamydomonas augustae*) in a cylindrical vessel of radius R which rotates with constant angular velocity $\Omega = 2\pi f$ [7]. When rotation is sufficiently fast, centripetal acceleration overcomes gravity and the cells swim towards the axis of the cylinder. The time evolution of cell distribution in the cylinder is measured by fluorescence imaging. Starting from initial uniform concentration, every $\Delta t = 15s$ a blue laser sheet (wavelength $\lambda = 450nm$) illuminates a plane in the cylinder. This induces fluorescence in the cells and a picture is taken by a camera with a high-pass filter at $600nm$. Fluorescence images are converted into cell concentration by a calibrations with uniform suspension of known concentrations.

Figure 1 shows the time evolution of the measured radial cell distribution for an experiment at $f = 7Hz$. The population of swimming cells progressively concentrates around the axis of the cylinder ($r = 0$) and eventually reaches a stationary distribution

in agreement with the theoretical prediction of the model (3) [7].

3. Clustering in turbulence

In order to understand the role of fluid acceleration on the clustering of gyrotactic swimmers, we performed a set of numerical simulations in which we integrate (2-3) together with the Navier-Stokes equations which provides the incompressible velocity field $\mathbf{u}(\mathbf{x}, t)$

$$\partial_t \mathbf{u} + \mathbf{u} \cdot \nabla \mathbf{u} = -\nabla p + \nu \nabla^2 \mathbf{u} + \mathbf{f} \quad (4)$$

where ν is the kinematic viscosity and \mathbf{f} is a random Gaussian forcing which injects kinetic energy at large scales at a rate ε . From the velocity field we compute the vorticity $\boldsymbol{\omega} = \nabla \times \mathbf{u}$ and the acceleration $\mathbf{a} = \partial_t \mathbf{u} + \mathbf{u} \cdot \nabla \mathbf{u}$ needed for integrating (3). Different populations of swimmers, characterized by different values of v_s and v_0 , are considered starting from initial uniform random distribution. The results are presented in term of the two dimensionless parameter, the swimming number $\Phi = v_s/v_k$ and the stability number $\Psi = v_0 \omega_r m s/g$, where $v_k = (\nu \varepsilon)^{1/4}$ is the Kolmogorov velocity.

As for the case of rotating cylinder, we observe that the distribution of does not remain uniform and dynamically concentrate of regions of the space characterized of values of high vorticity, as shown in Figure 2. This is a consequence of the dissipative nature of the system of equations (1,3). Indeed the (\mathbf{x}, \mathbf{p}) phase space contracts at a rate

$$\sum_{i=1}^3 \left(\frac{\partial \dot{x}_i}{\partial x_i} + \frac{\partial \dot{p}_i}{\partial p_i} \right) = \frac{1}{v_0} \mathbf{A} \cdot \mathbf{p} \quad (5)$$

Since the stabilizing torque reorients \mathbf{p} towards $-\mathbf{A}$, the contraction rate is negative on average and the trajectories collapse on a fractal attractor in phase space.

To quantify fractal clustering, we computed the correlation dimension D_2 , defined as the scaling exponent of the probability to find two cells with a separation distance less than r : $P(|\mathbf{x}_2 - \mathbf{x}_1| < r) \sim r^{D_2}$ as $r \rightarrow 0$. Figure 2 shows the fractal dimension D_2 as a function of the stability number Ψ for different Reynolds number Re_λ . Fractal clustering is found to increase with Re_λ as a consequence of the presence of intense vortices in the turbulent flow, in which gyrotactic swimmers accumulate driven by fluid acceleration, as in the rotating cylinder experiment.

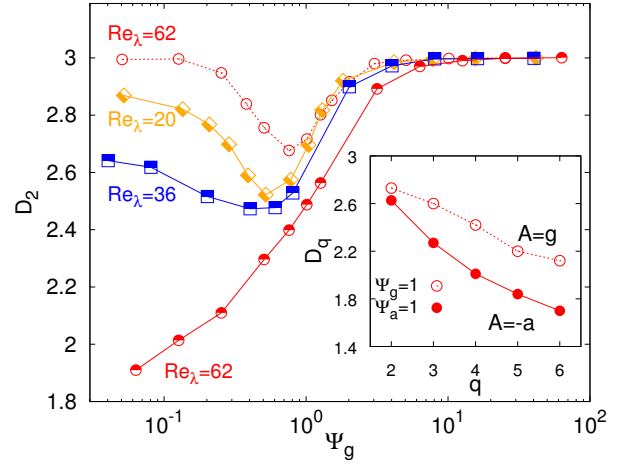


Figure 2: Correlation dimension D_2 versus stability number Ψ for increasing Reynolds numbers at fixed swimming number $\Phi = 3$. Semifilled symbols refer to the complete model with $\mathbf{A} = \mathbf{g} - \mathbf{a}$, open circles denote the case in which $\mathbf{A} = \mathbf{g}$. Inset: generalized dimension D_q as a function of q , for the case $Re_\lambda = 62$.

References

- [1] Kessler, J.O., Hydrodynamic focusing of motile algal cells, *Nature*, 313, pp. 5999, 1985.
- [2] Pedley, T.J., and Kessler, J.O., The orientation of spheroidal microorganisms swimming in a flow field, *Proc. R. Soc. Lond. B*, 231, pp. 47, 1987.
- [3] Durham, W.M., Kessler, J.O., and Stocker, R., Disruption of vertical motility by shear triggers formation of thin phytoplankton layers, *Science*, 323, pp. 1067, 2009.
- [4] Durham, W.M., Climent, E., Barry, M., De Lillo, F., Boffetta, G., Cencini, M., and Stocker, R., Turbulence drives microscale patches of motile phytoplankton, *Nat. Commun.*, 4, pp. 2148, 2013.
- [5] Borgnino, M., De Lillo, F., and Boffetta, G., Scale-dependent colocalization in a population of gyrotactic swimmers, *Phys. Rev. E*, 95, pp. 023108, 2017.
- [6] De Lillo, F., Cencini, M., Durham, W.M., Barry, M., Stocker, R., Climent, E., and Boffetta, G., Turbulent fluid acceleration generates clusters of gyrotactic microorganisms, *Phys. Rev. Lett.*, 112, pp. 044502, 2014.
- [7] Cencini, M., Franchino, M., Santamaria, F., and Boffetta, G., Centripetal focusing of gyrotactic phytoplankton, *J. Theor. Bio.*, 399, pp. 62, 2016.

Enhanced sedimentation of elongated plankton in simple flows

W. Clifton¹ and R. N. Bearon¹ and M. A. Bees²

¹*Department of Mathematical Sciences, University of Liverpool
Liverpool L69 7ZL, UK
rbearon@liverpool.ac.uk*

²*Department of Mathematics, University of York
York YO10 5DD, UK*

Abstract

Negatively buoyant phytoplankton play an important role in the sequestration of CO₂ from the atmosphere and are fundamental to the health of the world's fisheries. However, there is still much to discover on transport mechanisms from the upper photosynthetic regions to the deep ocean. In contrast to intuitive expectations that mixing increases plankton residence time in light-rich regions, recent experimental and computational evidence suggests that turbulence can actually enhance sedimentation of negatively buoyant diatoms. Motivated by these studies we dissect the enhanced sedimentation mechanisms using the simplest possible flows, avoiding expensive computations and obfuscation. In particular, we find that in vertical shear, preferential flow alignment and aggregation in down-welling regions both increase sedimentation, whereas horizontal shear reduces the sedimentation due only to alignment. In simple Kolmogorov flow elongated particles also have an enhanced sedimentation speed as they spend more time in downwelling regions of the flow with vertically aligned orientation, an effect that is dependent on the magnitude of shear. In Taylor-Green flow spatially projected trajectories can intersect and give rise to chaotic dynamics. This is associated with an increase in mean sedimentation speed with aspect ratio and shear strength, and a concomitant depletion of particles within so called retention zones.

Keywords: Plankton, diatoms, enhanced sedimentation, aspect ratio, shear flow, buoyancy

Colonization of moving marine aggregates by bacteria

Ksenia Guseva¹ and Ulrike Feudel²

¹ Theoretical Physics/Complex Systems, ICBM, University of Oldenburg,
26129 Oldenburg, Germany
ksenia.guseva@uni-oldenburg.de

² Theoretical Physics/Complex Systems, ICBM, University of Oldenburg,
26129 Oldenburg, Germany
ulrike.feudel@uni-oldenburg.de

The main objective of this work is to study how the interplay of chemotaxis and different swimming patterns of bacteria influence the colonization of marine aggregates (food particles) advected by a flow. To this extent we develop an individual-based model, which describes how bacteria can detect and follow a moving plume of nutrients in different kinematic flow fields.

Keywords: marine aggregates, marine bacteria, swimming patterns, chemotaxis

1. Introduction

Marine environments are very heterogeneous and turbulent on a small scale. In these highly dynamic conditions there are hot spots for microbial activity, which are related to isolated islands of nutrients. Marine aggregates (a.k.a. marine snow) are one example of such hot spots for microbial colonization, attracting heterotrophic bacteria and flagellates [4]. The local bacterial concentrations around and on marine snow particles exceed the background concentration by several orders of magnitude. However, the aggregates themselves are highly dynamic objects: while advected by the flow field they are subjected to aggregation and fragmentation processes. Efficient motility and food detection is crucial for survival of marine bacteria in such constantly changing environment. In this work we analyse how different types of motility patterns of bacteria [5] can influence the colonization of moving food particles in a flow field.

The best known swimming pattern is that of *E. coli*, which exhibits multiple flagella and uses them to adopt what is known as a *run-and-tumble* motility pattern. It consists of an interchange of persistent forward swimming with fast changes of orientation (turns) by an angle of 70° on average. However, the great majority of marine bacteria have a single flagellum and therefore are characterized by different motion strategies. Some of them adopt a *run-reverse* pattern, where the forward swimming is alternated with turns by approximately 180° . Others have a *run-reverse-flick* motion pattern, where bacteria interchange among forward swimming and turns by 180° and by 90° . Therefore the question arises whether there is an advantage of these swimming patterns developed by marine bacteria for the colonization of a moving food gradient.

2. Model

2.1. Motility patterns and swimming of bacteria

We use an individual based model where the motion of each bacterium is described individually. We also consider that the background flow \mathbf{u} is not affected by swimming of bacteria. Each bacterium is modeled as a spheroid object, small enough to ignore any inertial effects. Furthermore, they are modeled as active particles, which are not only advected by the flow field but are characterized by an intrinsic swimming velocity \mathbf{u}_s . Therefore total velocity of a bacterium is given by a vector sum of the

fluid velocity at its position and the swimming velocity. While the magnitude of the swimming velocity u_s is fixed, its direction \mathbf{p} changes in a way determined by the swimming pattern. The motion consists of periods of persistent swimming followed by instantaneous changes of direction, turns. During these intervals of persistent swimming ("runs"), the motion of bacteria can be described by [3]:

$$\frac{d\mathbf{r}}{dt} = \mathbf{u} + u_s \mathbf{p}, \quad (1)$$

where the unit vector \mathbf{p} is given by

$$\frac{d\mathbf{p}}{dt} = \frac{1}{2} \boldsymbol{\omega} \times \mathbf{p} + \alpha \mathbf{p} \cdot \mathbf{E} \cdot (\mathbf{I} - \mathbf{p}\mathbf{p}), \quad (2)$$

where $\boldsymbol{\omega} = \nabla \times \mathbf{u}$ is the vorticity and \mathbf{E} is the rate of strain tensor of the flow. The first term of the Eq. 2 represents the change of the swimming direction by a coupling to the flow vorticity and the second one due to a coupling with rate of strain. Particle eccentricity is given by the parameter α . In addition to this persistent swimming, each bacterium may also choose to change its swimming direction $\mathbf{p} = [\cos(\theta(t)), \sin(\theta(t))]$, this event is instantaneous and consists of a rotation by an angle θ_m , the new direction of motion becomes $[\cos(\theta(t) + \theta_m), \sin(\theta(t) + \theta_m)]$. After this instantaneous rotation the dynamics returns to Eq. 1, which is followed for another period of time τ . Please note that we assume that the background flow field does not affect the tumbling direction chosen by the bacteria and the angle of rotation θ_m depends only on the motility pattern. It is selected from a probability density $g(\theta_m) = \frac{1}{2} (\delta(\theta_m - \theta_{m0}) + \delta(\theta_m + \theta_{m0}))$. For the three motility patterns we have: run-and-tumble ($\theta_{m0} = 70^\circ$), run-reverse ($\theta_{m0} = 180^\circ$) and run-reverse-flick ($\theta_{m0} = 180^\circ$ or $\theta_{m0} = 90^\circ$) [5]. Small noise may be added to the rotation angle.

2.2. Chemotaxis

As we have described in the previous subsection, the forward swimming motion of bacteria is interrupted by occasional random changes in swimming direction. Organisms search for food along a gradient of chemoattractants released by the food particle indicating its location in space. This behaviour is called chemotaxis, it is modeled considering that each interval of time between a change of direction depends on differences of concentration C that bacteria experience while moving [2]. To our knowledge chemotaxis was not yet described for marine bacteria, therefore

we have used the same modeling approach of *E. coli*. The main idea of the model is to describe that a bacterium when experiencing an increasing concentration of nutrients during a run, has a smaller probability P_t to change its swimming direction. On the contrary, if it senses a decrease of concentration, P_t increases. The model we use is taken from [2] which considers food as a substrate which during the movement of a bacterium activates a receptor on its membrane. The idea is to track the fraction of cellular receptors bound to the substrate $\frac{dP_b}{dt} = \frac{K_d}{(K_d+C)^2} \frac{dC}{dt}$, with a half saturation rate of K_d , along the trajectory:

$$\frac{d\overline{P_b}}{dt} = \frac{1}{T_m} \int_{-\infty}^t \frac{dP_b}{dt'} e^{(t'-t)/T_m} dt' \quad (3)$$

The probability of reorientation for a time step dt is then given by

$$P_t = \frac{\Delta t}{\tau}, \quad \text{where} \quad \tau = \tau_0 e^{\gamma \frac{d\overline{P_b}}{dt}}, \quad (4)$$

and τ_0 gives the average time for swimming in the absence of a food gradient.

3. Results

3.1. Detecting fixed food particles in a flow field

To check how the swimming behaviour in a flow field affects chemotaxis we start with an artificial construction: it consists of a food gradient with a fixed position, which is not affected by the flow movement. We start by comparing the abilities of bacteria with different swimming patterns to locate a fixed food source while swimming in a flow. For a run-and-tumble motility pattern the directions of swimming strongly deviate from the background flow field (independently of α) due to random and frequent reorientation, see Fig. 1 (right). On the other hand, the position of the food source and the particle eccentricity α influence strongly bacteria that adopt the run-reverse strategy. For run-reverse, the alignment with the streamlines of the flow may be strong even at the food source, with deviations due to noise only. As we see in Fig. 1 (left) the back and forth movement together with reorientation implies that the bacterium has to constantly swim against the flow current to get back into the food gradient. As a conclusion the strategy requires high swimming velocity to stay close to the food source at the shown location.

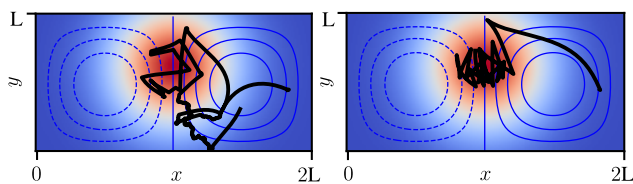


Figure 1: Example of trajectories (in black) of bacteria tracking a fixed food source in a flow (stream lines are indicated by dashed and solid blue lines): (right) Run-and-tumble; (left) Run-reverse. The swimming velocity $u_s = 2u_0$, and $\alpha = 0.9$. The background color indicates the food gradient, with maximum shown in red.

However, a fixed food source is very artificial for a dynamic marine environment. Therefore in the next section we concentrate our analysis on a moving plume.

3.2. Bacteria tracking a plume of nutrients

Our main set up consists of bacteria swimming in a random flow field (also known as synthetic turbulence). In this set-up a

long plume of nutrients rises through the observation area being constantly deformed by the flow field, see Fig. 2. This represents a plume of nutrients left behind a falling marine snow particle. The flow field is constructed to have the statistical properties of homogeneous, isotropic and stationary turbulence, however defined by a single average length of coherent structures (λ_f), by a single correlation time scale (τ_f) and a characteristic velocity u_0 . For details of implementation see [1]. To represent the dynamics from the reference frame of a falling aggregate an additional vertical velocity w_{agg} is added to the flow field.

To keep the number of bacteria constant we set up periodic boundary conditions.

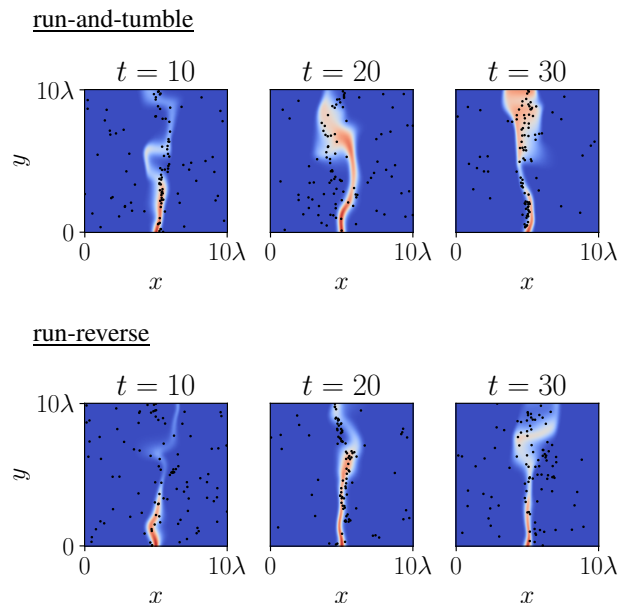


Figure 2: Spatial distribution of 100 bacteria, the flow is characterized by $u_0 = \frac{u_s}{2}$ and $w_{agg} = u_s$.

We analyse the effects of the eccentricity, swimming velocity and the motility pattern on chemotaxis. Our results indicate that the swimming strategies of marine bacteria seem not to bring a considerable advantage in tracking a moving nutrient plume.

References

- [1] A. Careta, F. Sagues, and J. M. Sancho, Stochastic generation of homogeneous isotropic turbulence with well-defined spectra, *Phys. Rev. E*, 48, pp. 2279–2287, 1993.
- [2] G.A. Jackson, Simulating chemosensory responses of marine microorganisms, *Limnol. Oceanogr.*, 32(6), pp.1253–1266, 1987.
- [3] T.J. Pedley, and J.O. Kessler, Hydrodynamic Phenomena in Suspensions of Swimming Microorganisms, *Annu. Rev. Fluid Mech.*, 24, pp. 313–358, 1992.
- [4] R. Stocker and J. R. Seymour, Ecology and Physics of Bacterial Chemotaxis in the Ocean, *Microbiol. Mol. Biol. Rev.*, 76(4), pp. 792–812 (2012).
- [5] J. Taktikos, H. Stark, V. Zaburdaev, How the Motility Pattern of Bacteria Affects Their Dispersal and Chemotaxis, *PLOS ONE*, 8(12): e81936, 2013.

Flow navigation by smart microswimmers via reinforcement learning

Simona Colabrese¹, Kristian Gustavsson², Antonio Celani³ and Luca Biferale^{1*}

¹Department of Physics and INFN, University of Rome "Tor Vergata", Rome, Italy

²Department of Physics, University of Gothenburg, Göteborg, Sweden
kristian.gustafsson@physics.gu.se

³Quantitative Life Sciences, The Abdus Salam International Centre for Theoretical Physics, Trieste, Italy

Abstract

Swimming microorganisms and artificial micro-swimmers can take advantage of environmental stimuli to bias their motility patterns in order to achieve some biologically relevant goal or some engineered task in complex environments. We consider a model for 'smart gravitactic swimmers'. These are active particles suspended in a complex flow, whose task is to reach the highest altitude within some time horizon, given the constraints enforced by fluid mechanics. Sensing partial information about the surrounding flow regions it visits, the smart gravitactic swimmer needs to adapt its swimming behaviour in an appropriate way in order to ultimately maximize its ascent. We use Reinforcement Learning as a framework to develop efficient swimming strategies that allows smart gravitactic swimmers to accomplish their long-term task.

Keywords: microswimmers, swimming strategies, vortex flows, machine learning

1. Introduction

The ability to find efficient navigation strategies of small microswimmers is essential for understanding and predicting the behaviour of biological microorganisms, and for controlling engineered microswimmers. It is believed that engineered microswimmers will become increasingly important in the near future, with uncountable applications, some examples being drug delivery, mixing/unmixing of chemicals, and modification of the rheological properties of fluids. We address the question of how smart particles can learn to escape their hydrodynamical fate in a complex flow by just sensing simple environmental cues and by reacting to these with modification of a few control parameters of their dynamics. We use Reinforcement Learning [1] to develop efficient navigation strategies using a prolonged and continued interaction between the particle and its environment.

2. Model

As an example, we consider a model for 'smart gravitactic swimmers' [2, 3]. These are active particles whose task is to reach the highest altitude within some time horizon, given the constraints enforced by fluid mechanics. We employ a simple model [4, 5] for the position \mathbf{x} and orientation \mathbf{p} of a small, spherical swimming particle:

$$\dot{\mathbf{x}} = \mathbf{u} + v_s \mathbf{p} + \boldsymbol{\eta} \quad (1)$$

$$\dot{\mathbf{p}} = \frac{1}{2B} [\mathbf{k} - (\mathbf{k} \cdot \mathbf{p})\mathbf{p}] + \frac{1}{2} \boldsymbol{\Omega} \times \mathbf{p} + \boldsymbol{\xi} \quad (2)$$

The particle swim with constant speed v_s in its instantaneous direction \mathbf{p} while being carried away by the underlying flow \mathbf{u} . The direction of the swimming velocity is determined by the competition between a stabilizing torque that tries to align the particle with a preferred swimming direction \mathbf{k} on a time scale B , and the rotation induced by the flow vorticity $\boldsymbol{\Omega}$ which could favor or oppose the stabilizing torque (See Fig. 1). Finally, $\boldsymbol{\eta}$ and $\boldsymbol{\xi}$ denote Gaussian white noises with small diffusivity.

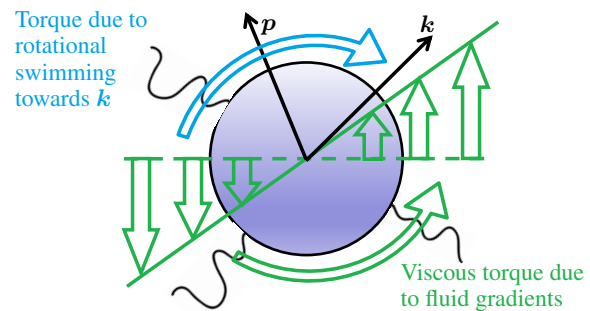


Figure 1: Sketch of the force balance on the body of the microswimmer. The smart microswimmer swims at all times with a constant swimming velocity with amplitude v_s and with variable instantaneous direction \mathbf{p} . The orientation of \mathbf{p} is determined by a competition between the viscous torque due to fluid gradients (green curved arrow), and the torque controlled by the particle itself (blue curved arrow) such that it tries to rotate towards a direction \mathbf{k} .

If the particle has some control on the preferred direction, how should it operate to achieve its goal, that is to obtain, in the long run, the largest possible progression in the upward direction? In a quiescent fluid the optimal choice for the preferred direction is to steadily point upwards, $\mathbf{k} = \hat{z}$. This is realized in *naive gyrotactic particles* by means of an uneven distribution of mass, see for example Ref. [4]. In the presence of an underlying flow this strategy may reveal to be highly ineffective. For example, naive gyrotactic particles in a steady flow with horizontal vortex rolls can aggregate in tight clusters and remain trapped at a given height [5].

Smart gravitactic particles on the contrary, are endowed with the ability of obtaining some partial information about the regions of the flow that they are visiting. They can use this knowledge to

*Partially supported by ERC AdG NewTURB n. 339032.

choose directions $k(t)$ that maximize the total ascent in the long run, which may allow them to escape trapping regions and seek “elevator” regions of the flow. Reinforcement Learning provides a way to construct these efficient strategies just by accumulating experience. This approach takes as input a number of environmental cues the particle can sense, such as crude representations of its current direction and of the vorticity of the underlying flow. Depending on the input signal the particle takes an action by changing its preferred direction. Depending on which action the particle takes for given input signals it receives different reinforcement signals in terms of net increase in altitude. We adopt a Q-learning algorithm [1] in order to find long-term approximately optimal strategies of how the particle should to choose its preferred direction given an input signal. An example of how the smart particle uses experience to develop better and better strategies for ascending in the vertical direction is shown in Fig. 2. The strategies we find are highly nontrivial and cannot be easily guessed in advance.

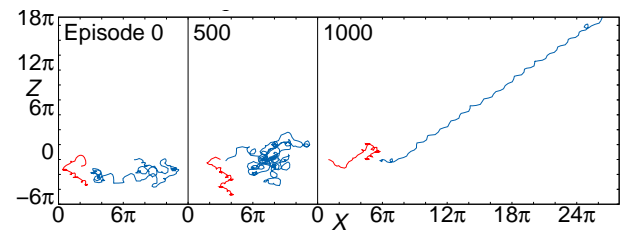


Figure 2: A set of representative trajectories at different stages of learning (episodes) for smart gravitactic particles (blue) compared with typical trajectories for naive gyrotactic particles (red) confined in a trapping dynamics.

References

- [1] Sutton, R.S. and Barto, A.G. *Reinforcement Learning: An Introduction*. MIT Press, Cambridge, 1998.
- [2] Colabrese, S., Gustavsson, K., Celani, A. and Biferale, L., Flow navigation by smart microswimmers via reinforcement learning, *Phys. Rev. Lett.*, 118, 158004, 2017.
- [3] Gustavsson, K., Colabrese, S., Celani, A. and Biferale, L., Finding efficient swimming strategies in a three-dimensional chaotic flow by reinforcement learning, *Eur. Phys. J. E*, 40, 110, 2017.
- [4] Kessler, J.O., Hydrodynamic focusing of motile algal cells, *Nature*, 313, pp. 218–220, 1985.
- [5] Durham, W.M., Climent, E. and Stocker, R., Gyrotaxis in a steady vortical flow. *Phys. Rev. Lett.*, 106, 238102, 2011.

Vertical migration of motile phytoplankton chains through turbulence

E. CLIMENT¹, S. LOVECCHIO¹, W.M. DURHAM², R. STOCKER³

¹ *Institut de Mécanique des Fluides de Toulouse (IMFT), Université de Toulouse, CNRS – Toulouse, France
eric.climent@imft.fr*

² *Department of Physics and Astronomy- Sheffield University, UK
w.m.durham@sheffield.ac.uk*

³ *Department of Civil, Environmental and Geomatic Engineering, ETH Zurich, Zurich 8093, Switzerland
romanstocker@ethz.ch*

Abstract

Motility allows phytoplankton to migrate daily from well-lit surface waters during the day to depth at night, where dissolved nutrients are more abundant and predation risks reduced. Some motile phytoplankton species form multicellular chains, which swim 50-200% more rapidly than single cells of the same species. However, chain formation can also sharply increase the organisms susceptibility to turbulence: destabilizing hydrodynamic torques increase with elongation, potentially suppressing vertical migration by randomizing swimming direction in turbulence. Here, we use direct numerical simulations of turbulence and an individual-based model of phytoplankton motility to understand how chain formation affects the ability of phytoplankton to vertically migrate through a turbulent water column. While chain formation intrinsically destabilizes cells, in turbulent flow chain formation counterintuitively confers enhanced stability, allowing cells to efficiently migrate over depth. In addition, the vertical migration of chains is aided by turbulence because chains are accumulated into regions of the flow moving in the same direction as their migration, whereas single cells are attracted into flows moving in the direction opposite to their migration. Taken together, these mechanisms allow chains to traverse a turbulent water column faster than single cells in weak to moderate turbulence, whereas migration is almost fully suppressed for both single cells and chains in strong turbulence. Our results suggest that chain-forming species have a competitive advantage under conditions that favors rapid vertical migration, and may help explain why turbulence often triggers chain formation.

Keywords: gyrotaxy, turbulence, motility, accumulation, chains

1. Motivation

Turbulence has long been known to exert a powerful control on the composition of phytoplankton communities, yet the underlying mechanisms often remain elusive. A particularly striking adaptation of phytoplankton is chain formation [1], which occurs when cells remain attached to one another after division. Daily, phytoplankton needs to migrate vertically from and towards the ocean surface to find nutrients such as dissolved oxygen. To travel through the water column, they need to fight against gravity (by swimming) and fluid turbulence which can make their journey longer [2]. While chains of motile phytoplankton species swim faster than single cells, their shape can make them less stable to being overturned by turbulence, which disrupts their ability to maintain their bearing as they migrate vertically through the water column.

2. Content

The first benefit to form chains is that micro-organisms sum up their thrust while reducing their drag. Therefore, upwards swimming is faster for chains in a quiescent fluid with steady vertical orientation. However, as chain length increases their tendency to periodically tumble in turbulent structures increases which reduces orientation stability and limits their capacity to swim upwards. The purpose of our study is to elaborate on this apparent contradiction.

Here we investigate the vertical migration of phytoplankton chains in the presence of turbulence using numerical simulations. We carried out direct numerical simulations and physical analysis of the coupled system of homogeneous isotropic turbulence and chain trajectories through Lagrangian tracking [3].

Formation of chains is indeed favorable for vertical migration through the upper layer of the ocean. We find that, counterintuitively, the elongated shape of chains can help them travel through moderate turbulence much more efficiently than single cells and we identify the processes that confer chains this ability. These findings provide new mechanistic understanding of how turbulence affects phytoplankton community structure and potentially offers new insights into how blooms of toxic chain-forming species are initiated.

References

- [1] Bjaerke O, Jonsson PR, Alam A, Selander E (2015) Is chain length in phytoplankton regulated to evade predation? *Journal of Plankton Research* 37(6), 1110-1119.
- [2] Zhan C, Sardina G, Lushi E, Brandt L (2014) Accumulation of motile elongated microorganisms in turbulence. *Journal of Fluid Mechanics* (739), 22-36.
- [3] Turbulence drives microscale patches of motile phytoplankton. (2013) W. M. Durham, E. Climent, M. Barry, F. De Lillo G. Boffetta, M. Cencini and R. Stocker. *Nature Communications* – 4: 2148.

Thermal stratification hinders gyrotactic micro-organism rising in free-surface turbulence

Alfredo Soldati^{1,2}, Salvatore Lovecchio¹, Francesco Zonta², Cristian Marchioli¹

¹Dept. Engineering and Architecture, University of Udine (Italy)
lovecchio.salvo@gmail.com, marchioli@uniud.it

²Institute of Fluid Mechanics and Heat Transfer, TU Wien (Austria)
alfredo.soldati@tuwien.ac.at, francesco.zonta@tuwien.ac.at

Abstract: We examine how different regimes of stable thermal stratification affect the motion of microswimmers (modelled as gyrotactic self-propelling cells) in free-surface turbulent channel flow. This archetypal setup mimics an environmentally-plausible situation that can be found in lakes and oceans. Results from direct numerical simulations of turbulence coupled with Lagrangian tracking reveal that rising of bottom-heavy swimmers depends strongly on the strength of stratification, especially in regions of high temperature and velocity gradients (thermocline): Here hydrodynamic shear may disrupt directional cell motility and hamper near-surface accumulation. For all gyrotactic re-orientation times considered in this study (spanning two orders of magnitude), we observe a reduction of the cell rising speed and temporary confinement under the thermocline: If re-orientation is not fast enough, long-term confinement is observed because cells align in the streamwise direction and their vertical swimming is practically annihilated.

Keywords: Surfacing, Thermal Stratification, Shear Flow, Turbulence, Gyrotaxis, Numerical simulation

1. Introduction

Thermally-stratified turbulence is of crucial importance in many environmental and geophysical flows. At the air-water interface of large water bodies, stable thermal stratification (i.e. fluid density increasing with depth) regulates mixing as well as surface renewal processes produced by turbulent upwashes of fresh water from the bottom boundary layer. For strong enough surface heating, Internal Gravity Waves (IGWs) [1] may arise due to the instability generated by lumps of denser (cold) fluid being lifted upwards into regions of lighter (warm) fluid by turbulence and subsequently driven downwards by buoyancy. IGWs correlate well with regions of the flow characterised by large temperature gradients and low mixing (thermoclines), and can act as thermal barrier for organic and inorganic matter: At sufficiently high levels of stratification, such barrier may prevent vertical mixing and trigger spatial accumulation [1]. One important consequence is the occurrence of thin layers [2, 3], intense assemblages of unicellular photosynthetic organisms that contain high concentrations of marine snow and bacteria, enhance zooplankton growth rates, and are essential for the survival of some fish larvae.

To the best of our knowledge, the interplay between stable thermal stratification and gyrotaxis in turbulent flow has not been examined in detail yet. Therefore, the physical mechanisms that govern the dynamics of motile aquatic micro-organisms (referred to as swimmers hereinafter) in stratified turbulence are not fully understood, and the possibility of observing trapping phenomena in the presence of strong stratification not yet assessed. In an effort to advance current understanding of how gyrotactic swimmers propel themselves through a thermally-stratified fluid, in this paper we investigate their dynamics in the presence of thermocline for the reference case of turbulent open channel flow. In particular, we want to quantify the effect of stratification on the vertical migration of swimmers at varying gyrotaxis (covering a wide range of re-orientation times) and at self-propelling speeds that are typical of the most common phytoplankton species.

2. Physical problem and methodology

We study the dispersion of gyrotactic swimmers in a thermally-stratified turbulent flow in an open channel with a flat

undeformable surface. The size of the channel is $2\pi h \times \pi h \times h$ in the streamwise (x), spanwise (y) and wall-normal (z) directions, respectively (with h the channel height). The fluid dynamics is described by the following three-dimensional time-dependent equations, written in dimensionless vector form:

$$\nabla \cdot \mathbf{u} = 0 \quad (1)$$

$$\dot{\mathbf{u}} + \mathbf{u} \cdot \nabla \mathbf{u} = -\nabla p + Re_\tau^{-1} \nabla^2 \mathbf{u} + Gr \cdot Re_\tau^{-2} \theta \mathbf{k} + \delta_p \quad (2)$$

$$\dot{\theta} + \mathbf{u} \cdot \nabla \theta = (Re_\tau \cdot Pr)^{-1} \nabla^2 \theta - \beta_T, \quad (3)$$

where $\mathbf{u} = (u_x, u_y, u_z)$ is the fluid velocity, ∇p is the gradient of the fluctuating pressure p , δ_p is the imposed pressure gradient, and θ is the fluid temperature. The dimensionless Reynolds, Grashof and Prandtl number are defined as:

$$Re_\tau = \frac{u_\tau h}{\nu}, \quad Gr = \frac{g\beta h^4}{\nu^2} \left. \frac{\partial \theta}{\partial z} \right|_s, \quad Pr = \frac{\mu c_p}{\lambda}; \quad (4)$$

where μ and ν are the dynamic and the kinematic fluid viscosity, β is the thermal expansion coefficient, c_p is the specific heat and λ is the fluid thermal conductivity. Note, that for open channel flow with constant surface heating, we can assume $\beta_T = 1/(Re_\tau Pr)$ in Eq. 3. For the fluid velocity, periodic BC's are applied in x and y , whereas no-slip (resp. no-stress) BC's are enforced at the bottom wall (resp. free surface). For the fluid temperature, a constant heat flux (resp. adiabatic condition) is enforced at the free surface (resp. bottom wall). Swimmers are modelled as spherical particles whose position \mathbf{x}_p and orientation \mathbf{p} evolve in time according to the following equations:

$$\dot{\mathbf{x}}_p = \mathbf{u}_{@p} + \Phi \mathbf{p}, \quad \dot{\mathbf{p}} = \Psi [\mathbf{k} - (\mathbf{k} \cdot \mathbf{p})\mathbf{p}] + (\boldsymbol{\omega}_{@p} \wedge \mathbf{p})/2 \quad (5)$$

where $\Phi = v_s/u_\tau$ is the swimming number (with v_s the swimming speed), $\mathbf{u}_{@p}$ the velocity of fluid in the position of swimmer, $\mathbf{k} = [0, 0, 1]$ is a unit vector pointing upward in the vertical direction, $\boldsymbol{\omega}_{@p}$ is the fluid vorticity at the swimmer's position and $\Psi = \frac{1}{2\mathcal{B}} \frac{\nu}{u_\tau}$ is the stability number, \mathcal{B} being the characteristic time a perturbed gyrotactic swimmer takes to return to the vertical orientation when $\omega = 0$. All variables are in wall units, obtained using u_τ and ν . 10^6 Lagrangian swimmers are tracked using a point-particle approach, and are injected into the flow at a concentration low enough to consider dilute conditions. All

simulations were run at $Re_\tau = 171$ and $Pr = 5$. Three different values of the Grashof number are considered in this study: $Gr = 0, 3.02 \cdot 10^5$ and $9.15 \cdot 10^5$, yielding shear Richardson numbers (measuring the importance of fluid buoyancy compared to fluid inertia) $Ri_\tau = Gr/Re_\tau^2 = 0, 165$ and 500 , respectively.

To simulate the motion of the micro-organisms, we considered $\Phi = 0.048$, corresponding to a dimensional swimming velocity $v_s = 100 \mu\text{m/s}$ typical of *Chlamydomonas augustae* cells, and three different values of the stability number ($\Psi_H = 1.13, \Psi_I = 0.113, \Psi_L = 0.0113$), corresponding to $\mathcal{B} = 0.054, 0.54$ and 5.4 s , respectively. In the present flow configuration, the largest value of the Kolmogorov timescale is $\tau_{K,max}^+ \simeq 13$ at the free-surface. Therefore, the selected values of the stability number correspond to three different physical instances with respect to $\tau_{K,max}^+$. At one extreme, $\Psi_L \cdot \tau_{K,max}^+ \sim \mathcal{O}(0.1)$ represents the case in which the timescale of gravitaxis is large compared to the timescale of the dissipative surface eddies and so the motion of the swimmers is dominated by the destabilising effect of small-scale turbulence. At the opposite extreme, $\Psi_H \cdot \tau_{K,max}^+ \sim \mathcal{O}(10)$ represents the case in which the timescale of gravitaxis is small compared to the timescale of the dissipative surface eddies and so the motion of the swimmers is dominated by the stabilising effect of bottom-heaviness. The case $\Psi_I \cdot \tau_{K,max}^+ \sim \mathcal{O}(1)$ represents the situation in which the motion of the swimmers results from the competition between small-scale turbulence around each cell and bottom-heaviness.

3. Results and Discussion

Swimmers can be significantly destabilized in regions of strong velocity and temperature gradients. To assess how such destabilisation may affect the capability of swimmers to trespass the thermocline, we examine the time evolution of swimmer concentration, $C(z, t)$, along the vertical direction, shown in Fig. 1 for all cases simulated in the (Ri_τ, Ψ) parameter space: Each column (resp. row) corresponds to a specific strength of stratification (resp. gyrotaxis). The concentration $C(z, t)$ represents a volumetric number density, obtained by coarse-graining the instantaneous vertical position of the swimmers on horizontal fluid slabs: Green (resp. blue) indicates high (resp. low) swimmer concentrations; the black line in each panel represents the vertical coordinate of the center of mass of the swimmers distribution, $z_{CM}(t) = \frac{1}{N} \sum_{j=1}^N z_j(t)$, with N the total number of swimmers and $z_j(t)$ the vertical position of the j^{th} swimmer at time t .

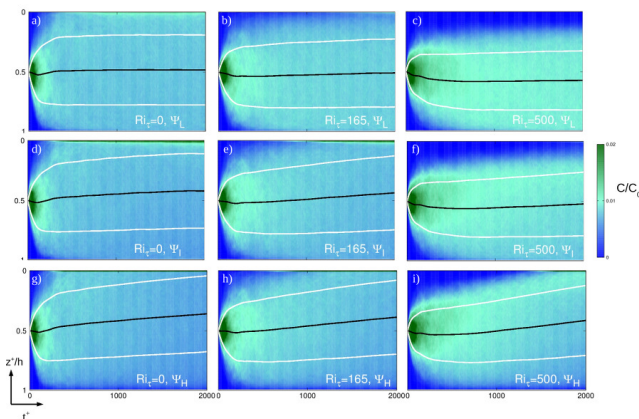


Figure 1: Time evolution of swimmer concentration along the vertical direction, $C(z, t)/C_0$, with $C_0 = C(z, t = 0)$. Rows: a), b) and c) Swimmers with low gyrotaxis, Ψ_L ; d), e) and f) Swimmers with intermediate gyrotaxis, Ψ_I ; g), h) and i) Swimmers with high gyrotaxis, Ψ_H . Columns: a), d) and g) $Ri_\tau = 0$; b), e) and h) $Ri_\tau = 165$; c), f) and i) $Ri_\tau = 500$.

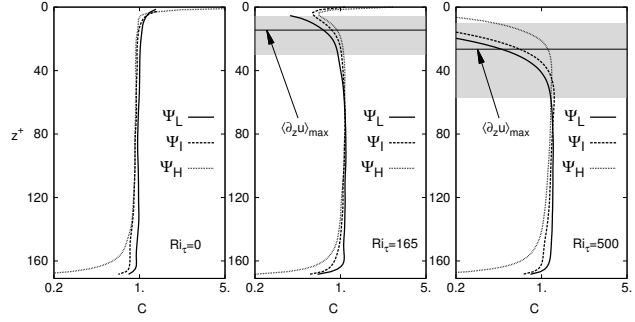


Figure 2: Concentration profiles at $t^+ \simeq 2000$ for Ψ_L (solid line), Ψ_I (dashed line), Ψ_H (dotted line) in the wall normal direction. Panels: (a) $Ri_\tau = 0$, (b) $Ri_\tau = 165$, (c) $Ri_\tau = 500$.

The white lines in each panel represent the positive (resp. negative) standard deviation, $\sigma^\pm = \sqrt{\frac{1}{N} \sum_{j=1}^N [z_j^\pm(t) - z_{CM}]^2}$, of the distribution around the center of mass, with $z_j^+(t)$ (resp. $z_j^-(t)$) the position of swimmers having a vertical coordinate larger (resp. smaller) than z_{CM} . To corroborate these observations, in Fig. 2 the instantaneous wall-normal concentration profiles computed at the end of the simulations, for fixed stratification and varying gyrotaxis, are presented. The unstratified-flow case in panel (a) is shown as reference. The horizontal line in panels (b) and (c) represents the location of maximum mean shear in the upper portion of the domain, whereas the grey areas correspond to regions of higher-than-mean shear. Results demonstrate that the flow region below the free surface becomes more and more depleted of swimmers as stratification levels increase. At $Ri_\tau = 165$, only swimmers with intermediate or high gyrotaxis exhibit a vertical stability sufficient to accumulate at the free surface. In all cases, however, a significant decrease of concentration is found precisely in the region of the thermocline. This correlation is even more evident at $Ri_\tau = 500$ (Fig. 2c): Accumulation is prohibited for all re-orientation times, and the vertical extent of the depletion layer increases as Ψ decreases. This is an obvious effect of the mean shear, and becomes more evident when swimmers react slowly to external fluid velocity fluctuations and gradients. A general conclusion that can be drawn from Fig. 2 is that, differently from the case of unstratified steady shear flows or homogeneous isotropic turbulent flows [2, 4, 5, 6], no gyrotactic trapping occurs and local peaks of concentration do not develop within the thermocline. This happens because our simulations mimic more closely a real physical environment (with stratification levels typical of temperate or tropical regions): In this case, the characteristic timescale of turbulent advection along the vertical direction is much shorter (one order of magnitude at least) than the timescale of self-propelling advection. Therefore, the concentration profiles in the turbulence-dominated region are always smoothed out by turbulent advection mechanisms.

References

- [1] F. Zonta, M. Onorato, A. Soldati. *J. Fluid Mech.*, 697:175–203, 2012.
- [2] W.M. Durham, J.O. Kessler, R. Stocker. *Science*, 323(5917):1067–1070, 2009.
- [3] W.M. Durham, R. Stocker. *Annu. Rev. Mar. Sci.*, 4:177–207, 2012.
- [4] G.J. Thorn, R.N. Bearon. *Phys. Fluids*, 22:041902, 2010.
- [5] F. De Lillo, M. Cencini, et al. *Phys. Rev. Lett.*, 112(4):044502, 2014.
- [6] I. Fouxon, A. Leshansky. *Phys. Rev. E*, 92:013017, 2015.

Buoyancy regulation of non-motile phytoplankton in a turbulent flow

Matteo Borgnino¹, Idan Tuval², Filippo De Lillo¹ and Guido Boffetta¹

¹ University of Turin
via Pietro Giuria 1, 10125, Torino, Italia
matteo.borgnino@unito.it

² UIB-CSIC
C/ Miquel Marquès, 21 - 07190 Esporles - Illes Balears, SPAIN

Abstract

Phytoplankton cells have developed non-trivial strategies to actively respond to environmental signals such as incident light, nutrient concentration or mechanical stresses. All these stimuli affect microorganisms dynamics and distribution over different scales. Starting from this point we investigate by means of direct numerical simulation the influence of turbulence on microorganisms unable to propel themselves, but able to actively respond and consequently to move along the water column.

Keywords: Patchiness, turbulence, buoyancy, strain

1. Introduction

The microscopic distribution of aquatic microorganisms has profound effects on the ecology of the oceans [1,2]. One example is the observed patchiness of phytoplankton at the submeter scale which has a fundamental impact on the rate at which cells encounter each other and their predators [3,4]. Patchiness of phytoplankton at different scales has different origins. While at large scales it is driven by reproduction and/or nutrients [5,6], at scales smaller than one kilometer patchiness is expected to be produced by physical mechanisms, including plankton motility and the interaction with the flow.

In recent years, significant efforts have been devoted to understand the mechanisms underlying the phytoplankton patchiness formation [1], since the latter has profound effects on the ecology of the oceans [3]. These patterns play a fundamental role in microorganisms populations composition, modulating cells activities like the encounter rate, the predation and the reproduction [7].

It was shown that non-motile microorganisms, that comprise ecologically fundamental groups such as diatoms and cyanobacteria, do not behave like simple passive tracers because they are able to modify their buoyancy. The latter is controlled in cyanobacteria by means of gas vesicles, while diatoms regulate density by replacing heavy ions with light ones in the vacuole. These physiological responses have a direct effect on the microorganisms, indeed they represent a mechanism to modify the interaction between the cell and the fluid environment, just like motility does.

Here we focus on mechanical stresses, in particular on how cells behave in turbulence. It is known that motile microorganisms can produce patchiness in presence of a turbulent flow [8], but a largely unanswered question concerns the responses of non-motile cells to environmental signals. Motivated by the physiological regulation of buoyancy prevalent in non-motile phytoplankton species [9], we

investigate, by means of direct numerical simulations (DNS), the dynamics of these cells in a three-dimensional turbulent flow. With our approach we show that, in contrast to passive tracers, the buoyancy regulation strategy leads to clustering formation, we demonstrate how its intensity depends on settling speed and finally we discuss how buoyancy control allow cells to escape from particular flow regions.

2. Mathematical model

Microorganisms are transported by a turbulent velocity field $\mathbf{u}(\mathbf{x},t)$ obtained by direct numerical simulations (DNS) of the incompressible Navier-Stokes equations.

We have considered the classical model for nonmotile phytoplanktonic cells, whose dynamics is described by the Maxey-Riley equation [10].

However by neglecting Basset history term and Faxen corrections, the velocity of a small particle transported by the flow $\mathbf{u} = (u, v, w)$ evolves according to:

$$\frac{d\mathbf{v}_p}{dt} = \beta \frac{d\mathbf{u}}{dt} - \frac{\mathbf{v}_p - \mathbf{u}}{\tau_p} + (1 - \beta)\mathbf{g}$$

where $\beta = 3\rho/(\rho + 2\rho_p)$ is the density ratio and $\tau_p = a^2/3\nu\beta$ is the viscous Stokes time (a is cell's radius). By introducing the co-velocity $\mathbf{W} = \mathbf{v}_p - \mathbf{u}$, by considering that typically $|\mathbf{g}| \gg |d\mathbf{u}/dt|$ and that the Stokes time is much smaller than the Kolmogorov time $\tau_p \ll \tau_\eta$ (with $a = 10^{-4}m$, $\rho = 1030 kg/m^3$ and $\rho_p = 1100 kg/m^3$) we finally obtain:

$$\frac{d\mathbf{x}_p}{dt} = \mathbf{u} - (1 - \beta)\tau_p\mathbf{g}$$

Microorganisms can actively respond to mechanical fluid stresses, by changing their buoyancy as a response to the strain rate of the flow S that comes from $S_{ij} = 1/2 \sum (\partial_i u_j + \partial_j u_i)$.

Since a change in buoyancy is a change in sedimentation velocity we can write the cells dynamics as:

$$\dot{\mathbf{x}}_p = \mathbf{u} - v_s(S)\hat{\mathbf{k}}$$

We will analyze two possible scenarios differing in the sign of the response: we refer to cells whose density decreases (increases) with the mechanical stresses as shear-thinning (shear-thickening) respectively.

3. Results

We have performed a numerical investigation of the spatial distribution of several populations of microorganisms both for shear-thinning and shear-thickening.

Populations differ in both how strong can “answer” to flow cues and which maximum sedimentation velocity can reach. In both cases microorganisms show a patchy distribution in contrast to simple tracers.

In addition to clustering formation we have investigated also the vertical migration by studying the statistics of the time needed to move in the water column.

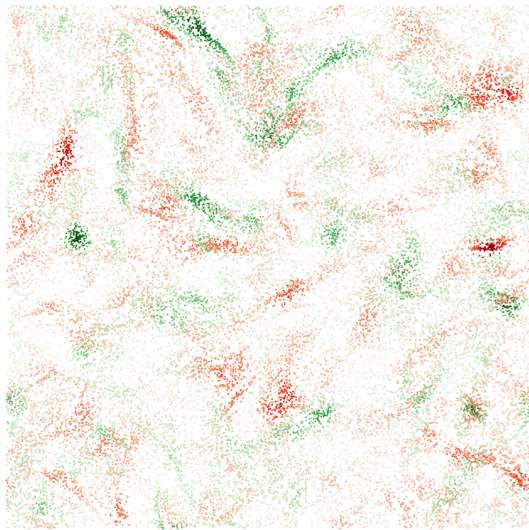


Figure 1: Horizontal section of DNS. Green dots correspond to shear-thickening and red dots to shear-thinning.

References

- [1] R. G. Williams and M. J. Follows, *Ocean Dynamics and the Carbon Cycle: Principles and Mechanisms*, Cambridge University Press, Cambridge, 2011.
- [2] J. Mitchell, H. Yamazaki, L. Seuront, F. Wolk, and H. Li, *J. Mar. Syst.* **69**, 247 (2008).
- [3] T. Kiørboe, *A Mechanistic Approach to Plankton Ecology* Princeton University Press, Princeton, 2008.

- [4] A. W. Visser and T. Kiørboe, *Oecologia* **148**, 538 (2006).
- [5] D. L. Mackas, K. L. Denman, and M. R. Abbott, *Bull. Mar. Science* **37**, 652 (1985).
- [6] J. Mitchell, H. Yamazaki, L. Seuront, F. Wolk, and H. Li, *J. Mar. Syst.* **69**, 247 (2008).
- [7] A. Martin, *Phytoplankton patchiness: the role of lateral stirring and mixing*, *Progr. Ocean.* **57**, 125 (2003)
- [8] W.M. Durham, E. Climent, M. Barry, F. De Lillo, G. Boffetta, M. Cencini, R. Stocker, *Turbulence drives microscale patches of motile phytoplankton*, *Nature Comm.*, **4**, 2148, 2013.
- [9] J. Arrieta, A. Barreira and I. Tuval, *Microscale patches of non-motile phytoplankton*, *Physical Review Letter*, **114**, 128102, 2015.
- [10] M.R. Maxey. and J.J. Riley, *Equation of motion for a small rigid sphere in a nonuniform flow*, *Phys. Fluid*, **26**, 883, 1983.

Preferential sampling and small-scale clustering of gyrotactic microswimmers in turbulence

Kristian Gustavsson¹, Fanny Berglund², Per Jonsson³ and B. Mehlig¹

¹ *Department of Physics, University of Gothenburg, G teborg, Sweden*

² *Department of Mathematical Sciences, University of Gothenburg, G teborg, Sweden*

³ *Department of Marine Sciences, University of Gothenburg, G teborg, Sweden*

Abstract

Recent studies show that spherical motile micro-organisms in turbulence subject to gravitational torques gather in down-welling regions of the turbulent flow. By analysing a statistical model we analytically compute how shape affects the dynamics, preferential sampling, and small-scale spatial clustering. We find that oblong organisms may spend more time in up-welling regions of the flow, and that all organisms are biased to regions of positive fluid-velocity gradients in the upward direction. We analyse small-scale spatial clustering and find that oblong particles may either cluster more or less than spherical ones, depending on the strength of the gravitational torques.

Keywords: clustering, micro-swimmers, gyrotaxis

Role of hydrodynamics in cell motility: Mesoscale hydrodynamic simulations

Roland G. Winkler

Theoretical Soft Matter and Biophysics, Institute for Advanced Simulation, Forschungszentrum Jülich
52425 Jülich, Germany
r.winkler@fz-juelich.de

Abstract

Simulation results are presented for the swimming and swarming properties of an explicit model of flagellated bacteria. Moreover, large-scale collective effects are discussed using the more generic squirmer model for a microswimmer. Thereby, the dynamics is treated by mesoscale hydrodynamic simulations, combining molecular dynamics simulations for microswimmers with the multiparticle collision dynamics method for the embedding fluid. The flow field of an *E. coli*-type bacterium is determined and its swimming properties adjacent to a planar wall are analyzed, with clockwise or counter-clockwise circular trajectories depending on the surface slip. In addition, the flagella-flagella interactions between neighboring, hyper-flagellated, and elongated swarmer cells are addressed. Interestingly, such cells, representative for bacteria in biofilms, exhibit intercellular flagella bundles. The studies of the collective phenomena of squirmers yield a strong dependence on hydrodynamics and shape of the microswimmer. Spherical squirmers exhibit cluster formation, but no motility-induced phase separation (MIPS), contrary to active Brownian particles (no hydrodynamics), which show MIPS. In contrast, spheroidal squirmers exhibit MIPS and, even more, hydrodynamics enhances MIPS. Hence, hydrodynamics and shape determine the phase behavior of active particles.

Keywords: Mesoscale simulation, bacteria swimming and swarming, squirmer, hydrodynamic interactions, collective effects, MIPS

1. Introduction

Many motile bacteria are propelled by helical filaments, which protrude from their cell body and are driven by rotary motors located in the cell membrane [1–3]. Thereby, such bacteria exhibit different modes of locomotion, depending on the environment. In liquid environments, individual (planktonic) cells exhibit the so-called *swimming* motility, with a run-and-tumble motion in response to chemical gradients. Another mode of motion is denoted as bacterial *swarming*, where flagellated bacteria migrate collectively over surfaces and are able to form stable aggregates, which can become highly motile in form of large-scale swirls or streams [1, 2]. Various bacteria strains show distinctly different morphologies in the swarming mode compared to swimmer cells as they are more elongated and their number of flagella is significantly larger. Very little is known about the intercellular interactions, specifically flagella-flagella interactions between adjacent cells. Neither is the reason known why swarming requires multiple flagella nor why a significant cell elongation is required for many bacteria [2].

Collective effects of microswimmers incorporating hydrodynamics can well and efficiently be studied by more generic models, such as the squirmer representation of a microswimmer [1, 5]. From a simulation point of view, similar systems can be studied without hydrodynamics interactions (HIs), so-called active Brownian particles (ABPs). Moreover, spheroidal squirmers and ABPs can be simulated to unravel the influence of shape and HIs on structure formation and collective effects [1, 5].

Mesoscale simulations by, e.g., the multiparticle collision dynamics (MPC) approach for a fluid, provide an efficient way to incorporate the essential aspects of microswimmers such as HIs, details of the bacterium, and geometrical restrictions, if present. Here, results for the swimming and swarming behavior of bacteria cells are presented, using an explicit model, as well as results for the collective behavior of microswimmers exploiting the squirmer approach.

2. Single bacterium – flow field and circular trajectories

Figure 1 shows the flow field created by a model bacterium embedded in a periodic cubic simulation box with MPC fluid. The field of Fig. 1(a) is computed by averaging the velocities of the fluid particles cylindrically symmetrically around the swimming axis. In Fig. 1(c)–(g), the velocities are averaged in the planes perpendicular to the swimming axis at the different locations indicated by the white vertical bars in Fig. 1(a). The flow pattern not too close to the bacterium approximately resembles that of swimming *E. coli* determined from experiments. Closer to the bacterium, the flow field exhibits specific features reflecting the bacterium’s detailed structure. In particular, the flow field reveals a front-back asymmetry, since the cell body and flagellar bundle are physically different units. The streamlines are closed in Fig. 1(a) as a consequence of the applied periodic boundary conditions, which implies differences in the far field compared to experimental observations (cf. Ref. [3] for further details). The flow patterns of Fig. 1 in the planes perpendicular to the swimming axis illustrate the interplay between the rotating flagellar bundle and counterrotating cell body. In Figs. 1(c) and (d), the flow field exhibits two spiral vortices associated with the rotation of the cell body and flagellar bundle, respectively, rotating clockwise and counterclockwise.

Near surfaces, bacteria generically swim on circular trajectories due to the counter-rotation of the body and the flagellar bundle. Figure 1(f) (inset) illustrates simulation trajectories for various surface slip lengths b . The trajectory changes from a clockwise (CW) circle to a counter-clockwise (CCW) circle as b increases [4]. The dependence of the curvature κ of a trajectory of the slip length is very well described by the analytical expression

$$\kappa = \frac{\kappa_0 - \kappa_\infty}{1 + b/h_{\text{eff}}} + \kappa_\infty, \quad (1)$$

where $\kappa_0 = \kappa(b = 0)$ (no slip) and $\kappa_\infty = \kappa(b = \infty)$ (perfect slip). Considering the slip lengths in the range of several ten

nanometers, bacteria cells sense surface slip on the nanoscale.

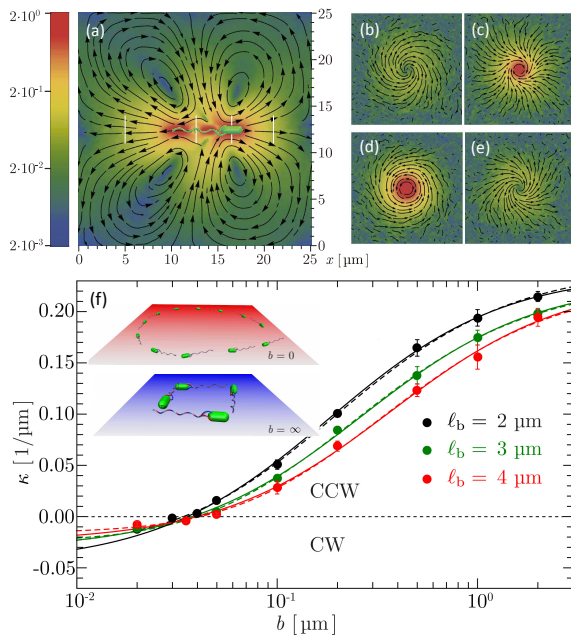


Figure 1: (a) Flow field of a single swimming *E. coli*-type bacterium in the swimming plane [3]. (b)-(e) Flow fields in planes perpendicular to the swimming plane at positions indicated by the white vertical bars in (a). The streamlines indicate the flow direction, and the logarithmic color scheme the magnitude of the flow speed scaled by the bacterial swimming velocity. (f) Average curvature κ of trajectories of cells of various lengths as function of the surface slip length b . The solid line is a least-square fit of simulation data (bullets) by Eq. 1 (for the dashed line, cf. [4]). Inset: CW and CCW trajectories from simulations for the slip lengths $b = 0$ and $b = \infty$, respectively.

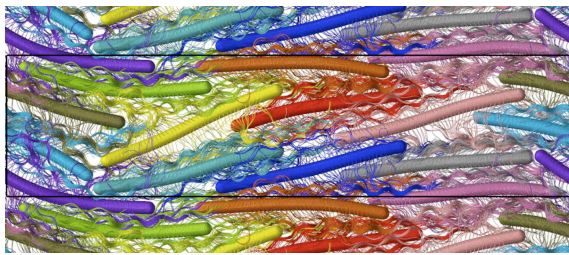


Figure 2: Simulation snapshot of highly elongated and hyper-flagellated bacteria in a thin film. Flagella of adjacent cells form common bundles.

3. Swarming of elongated and hyper-flagellated cells

Bacterial migration is strongly affected by confinement in a thin film (biofilm) [2]. Here, the relatively dense packing of the cells and corresponding steric interactions certainly play a major role. Despite that propulsion is achieved by rotating helical flagella and, most likely, bundle formation. How bundle form and how they arrange is rather unclear at the moment. Figure 2 shows a snapshot of strongly interacting, hyper-flagellated cells. An individual cell is able to from several flagella bundles, which overlap with bundles of adjacent cells. Hence, intercellular bundle formation is possible. At the moment it is not at all clear whether such bundles are efficient in swarming and whether they

are characteristic for swarming cells in biofilms.

4. ABP MIPS and clusters of squirmers

Simulations of squirmers and ABPs in a narrow slit (quasi-2D) yield substantial differences between ABPs and squirmers. An example is presented in Fig. 3. The snapshots indicate MIPS for ABPs, but no such process seems to be present for squirmers. A more detailed analysis of the structural properties in terms of local particle density yields clear evidence for a phase separation of ABPs, where the fraction of the dense phase increases with increasing system size. In contrast, squirmers with the force dipole strengths $\beta = 0, \pm 1$ show clusters, but no phase separation. The different behavior is a consequence of hydrodynamic interactions between squirmers, which gives rise to a faster rotational motion.

Spheroidal squirmers exhibit a qualitatively different behavior. The anisotropic nature of the spheroids leads to shape-induced jamming and alignment, where alignment increases with increasing aspect ratio. We even find that hydrodynamics enhances MIPS compared to ABPs. This result is surprising at first glance. Based on our studies on the cooperative motion of confined elongated squirmers [5], we attribute this enhancement to near-field hydrodynamics and, most importantly, squirmer-surface hydrodynamic interactions. The anisotropic shape leads to shape-induced MIPS for ABPs at considerably smaller Péclet numbers than for spheres. This is related to differences in the clustering mechanisms of isotropic and anisotropic swimmers. For anisotropic swimmers, alignment due to steric interactions is a key mechanism, while isotropic swimmers form clusters due to jamming and blocking.

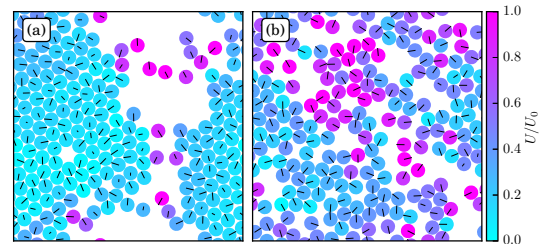


Figure 3: Snapshots of spherical active particles for the two-dimensional packing fraction $\phi^{2D} = 0.6$. (a) Active Brownian particles exhibit MIPS and hexagonal order. (b) Neutral squirmers ($\beta = 0$) exhibit no long-range order, no MIPS, but clusters are formed.

References

- [1] J. Elgeti, R. G. Winkler, and G. Gompper. Physics of microswimmers—single particle motion and collective behavior: a review. *Rep. Prog. Phys.*, 78:056601, 2015.
- [2] T. Eisenstecken, J. Hu, and R. G. Winkler. Bacterial swarmer cells in confinement: a mesoscale hydrodynamic simulation study. *Soft Matter*, 12:8316, 2016.
- [3] J. Hu, M. Yang, G. Gompper, and R. G. Winkler. Modelling the mechanics and hydrodynamics of swimming *e. coli*. *Soft Matter*, 11:7843, 2015.
- [4] J. Hu, A. Wysocki, R. G. Winkler, and G. Gompper. Physical sensing of surface properties by microswimmers – directing bacterial motion via wall slip. *Sci. Rep.*, 5:9586, 2015.
- [5] M. Theers, E. Westphal, G. Gompper, and R. G. Winkler. Modeling a spheroidal microswimmer and cooperative swimming in a narrow slit. *Soft Matter*, 12:7372, 2016.

Oil-microbe interactions: role of chemotaxis and hydrodynamics

Arezoo M. Ardekani^{1*}, Nikhil Desai², Vaseem A. Shaik³

^{1,2,3} School of Mechanical Engineering, Purdue University, West Lafayette, Indiana, USA, 47907.

¹ ardekani@purdue.edu

² desai63@purdue.edu

³ vshaik@purdue.edu

Abstract

We discuss two different approaches that describe the hydrodynamic aspects of bioremediation of soluble and insoluble hydrocarbons (HCs). We first present direct numerical simulations of a continuum framework involving conservation equations for the motile and chemotactic marine bacteria, the soluble HCs that act as a chemoattractant, and the multi-phase fluid flow characteristic of rising oil drops. We investigate the differences in the HC consumption by motile and non-motile bacteria, stemming from the chemotactic ability of the former. A key result of this study is that chemotactic advantage increases linearly with the bacterium's swimming speed. In addition, we show that chemotactic benefit reduces as the volume fraction of the oil drops and/or the diameters of the oil drops increase. Secondly, we investigate a purely hydrodynamics driven attraction of a bacterial cell –modelled as a force dipole– to insoluble oil drops that are either clean, or covered with surfactants. We observe that as the bacterium approaches the drop, it gets hydrodynamically trapped around it, if the drop radius is larger than a critical trapping radius. In cases where the bacterium's diffusive motion is strong, it escapes the drops after some interface-retention time. This time is considerably higher for surfactant-laden drops, as compared to clean drops. The results of our studies are expected to provide vital information and fertile ground for research in the field of bacterial bioremediation in subsurface oil-spills.

Keywords: Biodegradation, Motile microorganisms, Chemotaxis, Hydrodynamic interactions

1. Introduction

The role of micro-organisms in degrading the HCs emanating from the Deepwater Horizon spill in 2010 is well known [1]. The HCs that were released were both soluble and insoluble in water. Soluble hydrocarbons, like methane, dissolved in the water column at a depth of 1100 m, thus facilitating their biodegradation by methanotrophic bacteria. Some insoluble HCs were also trapped in sub-surface plumes due to their dispersion by surfactant addition [2]. In this study, we first model the biodegradation of methane by methanotrophic bacteria—both motile and non-motile—in a swarm of oil droplets rising through the plume (see Fig. 1). We quantify the role of motility on methane consumption, and investigate the effects of various biophysical parameters on bacterial distribution, and the resulting bioremediation rates. Next, we describe, a purely hydrodynamic mechanism of micro-organism attraction to insoluble oil drops. We thus provide two different ways in which hydrodynamics affects microorganism locomotion and the subsequent bioremediation.

2. Mathematical Model

In the first study, we perform fully-resolved direct numerical simulations (DNS) of the equations of fluid flow, chemo-attractant and bacteria transport, and bacterial chemotaxis. The bacteria are modelled as a continuum with an extra chemotactic flux directed along their instantaneous orientation. This orientation changes due to the external flow, and due to the chemo-attractant gradient via a 'chemotactic torque'. The transport equation for the chemo-attractant contains sink terms representing consumption by the motile and non-motile bacteria.

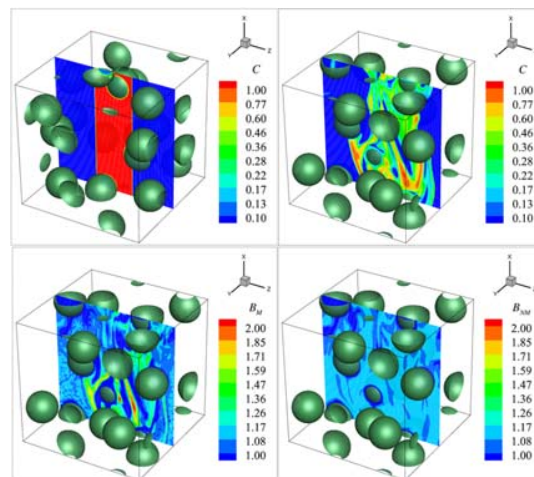


Figure 1: The dispersion of the initial chemo-attractant (C) distribution (top left panel) by the rise of buoyant oil drops. Chemotactic bacteria (B_M) "climb up" the gradients in C to populate the nutrient-rich regions, and thus obtain a motility benefit over the non-motile (also non-chemotactic) bacteria (B_{NM}) that stay uniformly distributed.

In the second study, we utilize the image-singularity system [3] to study the dynamical behaviour of a microorganism, modelled as a force dipole, that is positioned outside a clean, or a surfactant-laden drop (see Fig. 2). The expressions for the micro-organism's translational and rotational velocities are derived by an application of the Faxen's law [3], which allows us to calculate the trajectory of the microorganism.

* To whom correspondence should be addressed. E-mail: ardekani@purdue.edu

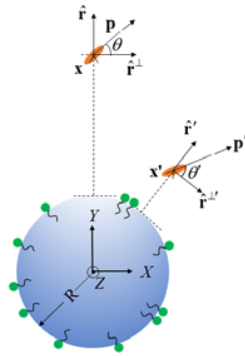


Figure 2: A model micro-swimmer outside a surfactant laden drop. The evolution of the position (\mathbf{x}) and orientation (\mathbf{p}) of the swimmer can be determined by the method discussed briefly in the text. The image is reproduced from N. Desai, V. Shaik, A.M. Ardekani, *Soft Matter*, 2018 with permission from the Royal Society of Chemistry.

3. Results

In the first study, we define an instantaneous motility benefit $\Delta\bar{U}(\bar{t})$ as the difference in the volume-averaged nutrient consumption rates between motile and non-motile bacteria, normalized by a reference consumption rate. Fig. 3 shows that this quantity scales linearly with the swimming speed (V_s) over a wide range of values. This is because all things being identical, chemotactic bacteria that can swim faster reach ‘deeper’ into the nutrient rich regions and thus enhance their nutrient consumption. In addition to this biological parameter, flow parameters like the size and volume fraction of the oil drops also influence the motility benefit. In particular, smaller drops and lower volume fractions offer greater chemotactic advantage. This is because the magnitude of the chemoattractant gradient scales inversely with the characteristic length scale, or the drop diameter. Thus, smaller drops create stronger nutrient gradients which can be climbed easily by the motile bacteria. It is also seen that higher volume fractions mix the initial chemo-attractant distribution thoroughly to destroy any nutrient hot-spots. This reduces the magnitude of the average nutrient gradient in the flow domain, and proves to be disadvantageous to the chemotactic species.

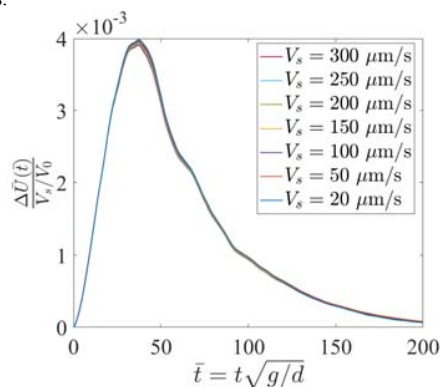


Figure 3: The instantaneous motility benefit scaled by the velocity ratio V_s/V_0 ($V_0 = 100 \mu\text{m/s}$ is the baseline swimming speed). The plots for all V_s values collapse onto a single curve, thus showing the linear dependence of the motility benefit with the bacterial swimming speed.

For the second study, we show 20 sample trajectories of micro-organisms swimming toward a clean drop and a surfactant-laden drop (see Fig. 4). Clearly, most of the swimmers escape the clean drop, while very few can escape the hydrodynamic attraction of the surfactant-laden drop. It is very important to note that the attraction in this case is purely passive, i.e., the swimmers do not actively seek the drop themselves, but are trapped due to their hydrodynamic interactions.

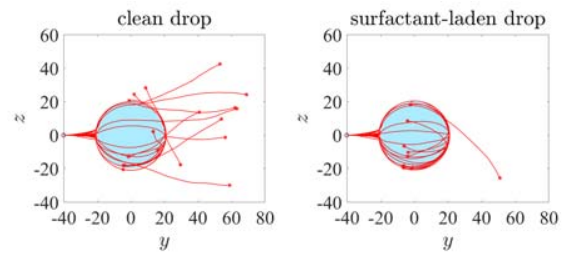


Figure 4: Sample trajectories around a clean and a surfactant-laden drop. Addition of a surfactant greatly enhances the tendency of an approaching swimmer to get hydrodynamically trapped on the surface of the drop. Image reproduced from N. Desai, V. Shaik, A.M. Ardekani, *Soft Matter*, 2018 with permission from the Royal Society of Chemistry.

An interesting result of this study is that surfactant addition benefits the bio-degradation of both soluble and insoluble HC components. In the former case, surfactant addition has an indirect impact, as it can potentially disperse heavier HCs into smaller drops that drive the fluid motion seen in Fig. 1, and generate stronger chemoattractant gradients. In the latter, surfactant addition is directly responsible in increasing the oil drop’s ‘ability’ to attract and trap any oncoming micro-organisms.

4. Acknowledgements

This research was made possible by grants from the Gulf of Mexico Research Initiative and NSF, CBET-1445955-CAREER and CBET1604423. Data are publicly available through the Gulf of Mexico Research Initiative Information & Data Cooperative (GRIIDC) at <https://data.gulfresearchinitiative.org> (DOI: 10.7266/N71Z42VX).

5. References

- [1] E. A. Dubinsky, M. E. Conrad, R. Chakraborty, M. Bill, S. E. Borglin, J. T. Hollibaugh, O. U. Mason, Y. M. Piceno, F. C. Reid, W. T. Stringfellow, L. M. Tom, T. C. Hazen, and G. L. Andersen, *Environ. Sci. Technol.* **47**, 10860 (2013).
- [2] R. M. Atlas and T. C. Hazen, *Environ. Sci. Technol.* **45**, 6709 (2011).
- [3] S. Kim and S. Karrila, *Microhydrodynamics: Principles and Selected Applications* (Butterworth-Heinemann, Boston, 1991).

Distribution of gyrotactic micro-organisms in complex three-dimensional flows: Horizontal shear flow past a vertical circular cylinder

L. Zeng^{1,2} and T. J. Pedley^{2*}

¹State Key Laboratory of Simulation and Regulation of Water Cycle in River Basin, China Institute of Water Resources and Hydropower Research
A-1 Fuxing Road, Haidian District, Beijing 100038, China
e-mail: lizeng@iwhr.com

²Department of Applied Mathematics and Theoretical Physics, University of Cambridge
Centre for Mathematical Sciences, Wilberforce Road, Cambridge CB3 0WA, UK
e-mail: t.j.pedley@damtp.cam.ac.uk

Abstract

Understanding the distribution of swimming micro-organisms in shallow water containing vegetation will make an important contribution to wetland ecology. Here, as a first step, a continuum model is formulated for dilute suspensions of gyrotactic micro-organisms in horizontal shear flow past a single rigid vertical circular cylinder. A numerical platform was developed to solve this problem. It is found that several typical flow patterns occur downstream of the cylinder: parallel vortex shedding, oblique vortex shedding, quasi-steady flow, and secondary (vertical) flow. In the parallel-shedding zone, concentration distribution is very similar for both active and passive particles, except near the top surface where upswimming causes the concentration of active particles to reach values greater than that upstream. In the oblique-shedding zone, the vertical flow dominates the vertical migration of cells in the vortex cores, while outside the cores vertical swimming is comparable to the vertical flow. In the quasi-steady zone, the particle concentration distributions are approximately symmetric with respect to the wake centreplane. Another striking difference between passive and active particles is that a high concentration of the latter occurs in a thin boundary layer on the downstream surface of the cylinder, due to radial swimming.

Keywords: wetland, biological fluid dynamics, complex flow, gyrotactic micro-organisms

1. Introduction

Wetlands, generally populated by various aquatic plants, are among the most significant ecosystems on Earth. Vast numbers of motile micro-organisms are found in wetlands, and many important ecological phenomena, such as harmful algal blooms, occur as such micro-organisms interact with the vegetation. Understanding the distribution of swimming micro-organisms in shallow water containing vegetation, and possibly experiencing a slow horizontal flow (e.g. in tidal marshland), will make an important contribution to understanding the ecology of the whole biological system.

The type of vegetation to be considered here is so-called 'emergent vegetation', in which most of the leafy part of the plants is exposed to the air above the water, and is supported by less leafy stalks beneath the surface. In general the vegetation is flexible, but an obvious simple model of emergent vegetation is an array of rigid vertical circular cylinders; as a first step towards analysing the behaviour of swimming micro-organisms in such an array, this paper will be concerned with flow past a single cylinder.

The type of micro-organisms to be considered are motile algae, such as *Chlamydomonas* or *Dunaliella*, that normally swim upwards on average, in still fluid, because they are bottom-heavy. When the fluid is flowing with non-zero vorticity, however, the cells experience a viscous torque which, when balanced against the gravitational torque induced by their bottom-heaviness, causes them to swim in a non-vertical direction (or, if the vorticity exceeds a critical value, to tumble unsteadily). This

process is termed gyrotaxis [1].

In spite of the probable significance of gyrotactic micro-organisms to the formation and evolution of biological communities, we are not aware of any studies on their distribution in wetland flows. Although there have been extensive investigations of the transport of passive particles in flows associated with vegetation [2], the characteristics and mechanisms of active micro-organisms in such flows remain unclear, due to the complexity of both swimming behaviour and flow pattern. In this paper, therefore, we investigate a very simple proxy for flow through emergent vegetation: horizontal shear flow past a single vertical cylinder that extends from a flat horizontal bed and penetrates the free surface of the fluid. Upstream of the cylinder, the micro-organisms are taken to occupy a narrow vertical strip, of width equal to the cylinder diameter, extending the whole depth of the channel. In all computations, the Reynolds number based on the cylinder diameter and the incoming free-surface velocity is taken to be 100.

2. Results and conclusions

The distribution of gyrotactic micro-organisms is complex, due to the three-dimensionality of the flow and the cell swimming therein. A numerical platform was developed to solve this problem, including a code to solve the three-dimensional concentration distribution of gyrotactic micro-organisms based on OpenFOAM (www.openfoam.org), a code to solve the Fokker-Planck equation [3, 4] based on the finite volume method, and a database to determine the mean swimming velocity V_c and

*This work is supported by the National Key Research and Development Program of China (2016YFC0502202), the National Natural Science Foundation of China (Grant No. 51409272), the IWHR Research and Development Support Program (Grant Nos. HY0145B402016 and HY0145B682017), the Independent Research Project of State Key Laboratory of Simulation and Regulation of Water Cycle in River Basin (Grant Nos. 2015RC01 and 2015ZY04), and China Scholarship Council.

translational diffusivity D in three-dimensional vorticity space. The present parallel computation has been carried out at Tianhe-2 (MilkyWay-2)-TH-IVB-FEP Cluster of National Super Computer Center in Guangzhou, China, which took about 150 h of wall-clock time on 768 processors.

We find that there are three principal flow patterns: parallel vortex shedding in the top region near the water surface, oblique vortex shedding in the middle region, and quasi-steady flow in the bottom region. Secondary (vertical) flow occurs just upstream and downstream of the cylinder as a result of vertical pressure gradients that arise because of the shear in the upstream flow. Frequency spectra of the velocity components in the wake of the cylinder show two dominant frequencies of vortex shedding, in the parallel- and oblique-shedding regions respectively, together with a low frequency, equal to the difference between those two frequencies, that corresponds to a beating modulation.

Corresponding to the flow velocity in the wake of the cylinder, the vorticity ω in the quasi-steady zone remains almost constant, and periodic vorticity occurs in the parallel-shedding and oblique-shedding zones. The spanwise (vertical) vorticity dominates in the parallel-shedding zone, while the magnitudes of the streamwise and spanwise vorticity components are comparable in the oblique-shedding zone. The horizontal vorticity predominates over the spanwise vorticity in the bottom boundary layer. Close to the cylinder, positive circumferential vorticity mainly occurs in the area around the upstream stagnation point at all spanwise positions (except close to the water surface and the bottom bed), while negative circumferential vorticity dominates the remainder of the cylinder surface.

For the case in which $(2BD_r)^{-1} = 2.2$, where B is the time scale for cell reorientation by the gravitational torque, and D_r^{-1} is the time scale for rotational diffusion, the mean swimming velocity and translational diffusivity tensor are given over a three-dimensional vorticity space, based on a combination of the analytical solution [3] and numerical solutions of the steady Fokker-Planck equation. The results were stored in a database of $\mathbf{V}_c - \omega$ and $\mathbf{D} - \omega$, and the mean cell swimming velocity and translational diffusivity tensor in the flow around the cylinder are obtained from that database. In the whole region, with the exception of the bottom bed and the surface of the cylinder, the ambient flow overwhelms cell swimming in the horizontal direction. In the parallel-shedding zone, cells swim almost vertically upwards in the wake of the cylinder due to the weak streamwise and cross-flow vorticity. In the oblique-shedding zone, the vertical flow dominates the vertical migration of cells in the vortex cores, while outside the cores vertical swimming is comparable to the vertical flow. In the quasi-steady zone, the effects of the vertical mean swimming velocity and vertical flow are comparable with each other. The distribution of radial mean swimming velocity is consistent with the distribution of circumferential vorticity. In the wake of the cylinder. The orders of magnitude of the diagonal components of the translational diffusivity tensor are much greater than those of the off-diagonal components, meaning that the cell flux by translational diffusion through a plane is almost proportional to the normal component of the concentration gradient.

The incoming strip of particles, either active or passive, spreads little in the cross-flow direction until the particles are close to the cylinder. In the parallel-shedding zone (except at the very top surface), the general pattern of the concentration distribution is quite similar for both active and passive particles, which means that the horizontal transport of particles in this zone is dominated by advection. However, the maximum concentration of active particles in the wake region occurs at the top surface, and exceeds the initial concentration (Fig. 1 (a)), while that of passive particles does not. This difference is attributable to the cells' ability to swim across streamlines. In the upper part of the oblique-shedding zone, both active and passive

particle clouds travel downstream in the pattern of the oblique vortex street, while in the lower part of this zone, the particle clouds more resemble a fluttering ribbon. The effect of vertical swimming on the concentration distribution is still observed in the oblique-shedding region. In the quasi-steady zone, the particle concentration distribution is approximately symmetric with respect to the wake centreplane. Swimming and translational diffusion of cells smooth out the sharp concentration interface in the rear of the cylinder. Upswimming results in the region of zero cell concentration above the bottom bed being deeper than for passive particles. Another striking difference between passive and active particles is that a high cell concentration occurs in the lee of the cylinder (Fig. 1 (b)), which is caused by the radial swimming velocity rather than the spanwise swimming taking place in the thin layer near the water surface.

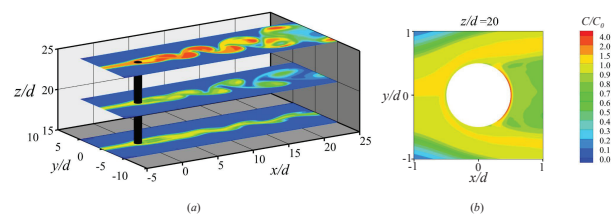


Figure 1: Concentration distribution of active particles: (a) for $z/d = 15, 20$ and 25 , and (b) in the lee of the cylinder. z is the vertical position, and d is the diameter of the cylinder.

A single, rigid, vertical, circular cylinder is clearly a highly idealised model for emergent aquatic vegetation in general. A much more reasonable model would be an array of flexible, and possibly branched, cylindrical stems, in which the flow would be very different and consequently so would the distribution of passive and active (in particular gyrotactic) micro-organisms. However, much of the computational platform that we have developed will be directly applicable to more realistic configurations, since the methods for solving the Fokker-Planck equation and the equation for the particle concentration distribution will not have to be significantly changed; only the flow solver will require substantial modification.

Of the results obtained here, the most relevant to any real vegetation are the predictions of the places where the cell concentration is significantly greater than for passive particles as a result of cell swimming. These are in the vortices at the upper fluid surface and on the leeward surface of the cylinder. The former would be intuitively predictable but the latter would not. Either zone would be potentially profitable for predators; it would be of great interest to investigate such zones in the field to find evidence of enhanced predator-prey interactions.

References

- [1] Kessler, J. O., Hydrodynamic focusing of motile algal cells. *Nature*, 313, pp. 218-220, 1985.
- [2] Nepf, H.M., Flow and transport in regions with aquatic vegetation. *Annu. Rev. Fluid Mech.*, 44, pp. 123-142, 2012.
- [3] Pedley, T. J. and Kessler, J. O., A new continuum model for suspensions of gyrotactic micro-organisms. *J. Fluid Mech.*, 212, pp. 155-182, 1990.
- [4] Pedley, T. J. and Kessler, J. O., Hydrodynamic phenomena in suspensions of swimming micro-organisms. *Annu. Rev. Fluid Mech.*, 24, pp. 313-358, 1992.

Gravitational motion induced by gyrotactic micro-organisms near a vertical wall in a horizontal stagnation point flow

T. J. Pedley^{1*} and L. Zeng²

¹Department of Applied Mathematics and Theoretical Physics, University of Cambridge
Centre for Mathematical Sciences, Wilberforce Road, Cambridge CB3 0WA, UK
e-mail: t.j.pedley@damtp.cam.ac.uk

²State Key Laboratory of Simulation and Regulation of Water Cycle in River Basin, China Institute of Water Resources and Hydropower Research
A-1 Fuxing Road, Haidian District, Beijing 100038, China
e-mail: lizeng@iwhr.com

Abstract

Computation of the distribution of swimming micro-organisms in horizontal shear flow past a vertical cylinder has revealed an accumulation of cells in a thin boundary layer on the lee side of the cylinder. However, the fact that negative buoyancy would generate a flow vertically downwards was ignored. Here we analyse a model problem consisting of horizontal stagnation-point flow against a vertical wall, and write equations for the cell concentration distribution, the vertical velocity component, and the orientation distribution of the swimmers. Numerical solution of these equations will be presented.

Keywords: biological fluid dynamics, complex flow, gyrotactic micro-organisms

1. Introduction

We are interested in the effect of cell swimming on the distribution of gyrotactic micro-organisms in complex flow past aquatic vegetation. A computational study of horizontal shear flow past a vertical circular cylinder has predicted a thin boundary layer of high cell concentration on the downstream surface of the cylinder, at the stagnation point of a separated flow region with closed streamlines [1]. Gravity, acting on the density difference between the cells and the fluid is expected to lead to vertical motion, but gravitational effects were not included in [1]. Here we set up a model problem to investigate such gravity-driven flow.

2. Model

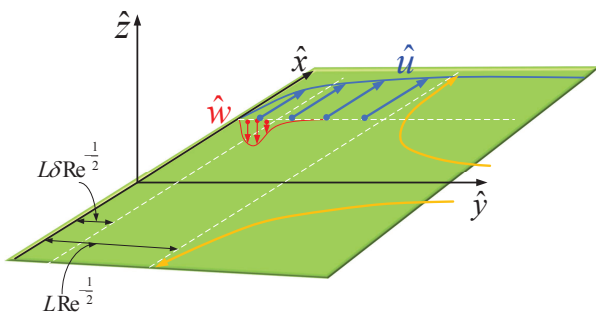


Figure 1: Sketch of a horizontal stagnation point flow, with the viscous and concentration boundary layers.

We take the cells to be suspended in a viscous, incompressible fluid in a semi-infinite domain $-\infty < \hat{x} < \infty, 0 \leq \hat{y} < \infty, -\infty < \hat{z} < \infty$, where carets denote dimensional quantities

and \hat{z} is measured vertically upwards (Fig.1). In the absence of cells, the velocity field $(\hat{u}, \hat{v}, \hat{w})$ is a (Hiemenz) stagnation-point flow:

$$\hat{u} = U_0 x F'(\eta), \quad \hat{v} = -U_0 Re^{-\frac{1}{2}} F(\eta), \quad \hat{w} = 0, \quad (1)$$

where $\eta = Re^{\frac{1}{2}} y$, $(x, y) = (\frac{\hat{x}}{L}, \frac{\hat{y}}{L})$, and $Re = \frac{U_0 L}{\nu}$; U_0 and L are velocity and length scales in the outer flow. $F(\eta)$ satisfies

$$F''' + FF'' - F'^2 + 1 = 0, \quad F(0) = F'(0) = 0, \quad F'(\infty) = 1. \quad (2)$$

The velocity field (1,2) is an exact solution of the Navier-Stokes equations, and represents a viscous boundary layer of thickness $LRe^{-\frac{1}{2}}$. The velocity gradient at the wall is proportional to $F''(0) \equiv \gamma \approx 1.23$ [2].

We assume there is a uniform cell concentration N_0 far from the wall, which is reasonable if the whole region of interest is embedded in an outer region of closed streamlines. We also assume a different concentration $N_0(1+n_1)$ at the wall, to represent possible cell accumulation due to adhesion, for example. As cells are advected towards the wall, they will accumulate in a concentration boundary layer, which we assume has thickness $LRe^{-\frac{1}{2}}\delta$, where $\delta \ll 1$ and, hence, $F \approx \frac{1}{2}\gamma\eta^2$. The cells swim, and in the present continuum model the swimming is represented by the mean swimming velocity relative to the fluid and the effective translational diffusivity:

$$\hat{V} = V_s \langle \mathbf{p} \rangle, \quad \hat{D} = V_s^2 \tau \langle (\mathbf{p} - \langle \mathbf{p} \rangle)(\mathbf{p} - \langle \mathbf{p} \rangle) \rangle, \quad (3)$$

where V_s is the cell swimming speed, assumed the same for all cells, τ is the correlation time and $\langle \dots \rangle$ represents an average over the probability density function $f(\mathbf{p})$ of swimming direction \mathbf{p} , e.g.:

$$\langle \mathbf{p} \rangle = \frac{1}{4\pi} \int \int \mathbf{p} f(\mathbf{p}) d^2 \mathbf{p}, \quad (4)$$

where the integral is over the unit sphere in \mathbf{p} -space. We assume that the cell concentration $N_0 n$ is independent of both x and z , as well as time, so that within the concentration boundary layer the equation for n is

$$-U_0 \cdot \frac{1}{2} \gamma \delta \zeta^2 \frac{dn}{d\zeta} + V_s \frac{Re^{\frac{1}{2}}}{\delta} \frac{d}{d\zeta} (P_y n) = \frac{V_s^2 \tau Re}{L} \frac{d}{d\zeta} (D \frac{dn}{d\zeta}), \quad (5)$$

where $\zeta = \eta/\delta$, $P_y(\zeta)$ is the y -component of $\langle \mathbf{p} \rangle$ and $V_s^2 \tau D(\zeta)$ is the yy component of $\hat{\mathbf{D}}$ (neglecting off-diagonal terms). As in studies of bioconvection [3] the concentration distribution is principally determined by a balance between cell swimming and diffusion perpendicular to the boundary, which gives

$$\delta = \frac{V_s \tau}{L} Re^{\frac{1}{2}}. \quad (6)$$

Equation (5) then becomes

$$-\chi \zeta^2 \frac{dn}{d\zeta} + \frac{d}{d\zeta} (P_y n) = \frac{d}{d\zeta} (D \frac{dn}{d\zeta}), \quad (7)$$

subject to the boundary conditions $n = n_1$ at $\zeta = 0$, $n \rightarrow 1$ as $\zeta \rightarrow \infty$. Here

$$\chi = \frac{U_0 \delta^2}{V_s Re^{\frac{1}{2}}} \cdot \frac{1}{2} \gamma. \quad (8)$$

Accumulation of cells according to (7) will lead to a gravitationally driven vertical velocity $W_0 w(\zeta)$, where we assume that w is also independent of x , z and time. In the vertical component of the momentum equation there must be a balance between the gravitational term and the viscous term, which determines the vertical velocity scale W_0 as

$$W_0 = \tilde{g} N_0 V_s \tau^2 / \nu, \quad (9)$$

where $\tilde{g} = gv\Delta\rho/\rho$ (v being cell volume and $\Delta\rho$ the density difference between cells and water). Thus the vertical momentum equation becomes

$$-\delta^3 \frac{1}{2} \gamma \zeta^2 \frac{dw}{d\zeta} = -(n-1) + \frac{d^2 w}{d\zeta^2}. \quad (10)$$

The first term here represents y -advection by the stagnation point flow, and since $\delta \ll 1$ this is negligible. The boundary conditions on w are $w(0) = w(\infty) = 0$.

Finally we need the Fokker-Planck equation for $f(\mathbf{p})$ which, assuming spherical cells, is

$$\nabla_p^2 f = \lambda [\mathbf{k} \cdot \nabla_p f - 2(\mathbf{k} \cdot \mathbf{p})f] + \Gamma [\frac{1}{2} \omega \cdot (\mathbf{p} \times \nabla_p f)], \quad (11)$$

where \mathbf{k} is a vertical unit vector, $\lambda = (2BD_r)^{-1}$, B is the gyrotactic reorientation time, D_r is the rotational diffusivity, ∇_p is the gradient operator in \mathbf{p} -space, and ω is the dimensionless vorticity $(\frac{d\mathbf{w}}{d\zeta}, 0, 0)$. The parameter Γ is given by

$$\Gamma = \frac{\lambda B Re^{\frac{1}{2}} W_0}{\delta L}. \quad (12)$$

In writing (11) we have assumed that there is no advection term in the equation, i.e. that the time scales B and D_r^{-1} for gyrotactic reorientation are much shorter than the time scale L_0/U_0 for advection by the outer flow, an assumption that is *not* satisfied by the parameter values chosen below. In line with the small vorticity limit of (11) (see[3]) we take $P_y = -A\Gamma \frac{dw}{d\zeta}$ where A is an $O(1)$ constant, not necessarily equal to 1.

The governing equations for the model problem are now complete, comprising (7), (10) and (11). Because of the coupling through the cell-swimming term in (7), the problem is nonlinear and has to be solved numerically. The choice of parameter values is guided by [1] and [2]. We take $L_0 = 10^4 \mu\text{m}$, $U_0 = 10^4 \mu\text{m s}^{-1}$, $\nu = 10^6 \mu\text{m}^2 \text{s}^{-1}$ (so $Re = 100$), $V_s = 63 \mu\text{m s}^{-1}$, $\tau = 5\text{s}$, $\lambda = 2.2$, $B = 3.4\text{s}$. For $N_0 = 10^6$ cells/ml, $\tilde{g}N_0 \approx 500 \mu\text{m s}^{-1}$. Then (6) gives $\delta \approx 0.31$ (small but not very small), (9) gives $W_0 \approx 50 \mu\text{m s}^{-1}$ (comparable with V_s), (8) gives $\chi \approx 1$ and (12) gives $\Gamma \approx 1.2$. We also, arbitrarily, take $n_1 = 0.5$.

3. Results

Numerical results using these parameters will be presented at the Symposium. The predictions for $n(\zeta)$ and $w(\zeta)$ are expected to resemble the graphs shown in Fig.2. The main implication of this work is that the gravitational term should not be neglected in analyses of the distribution of gyrotactic micro-organisms close to a vertical boundary, such as the computations of [1].

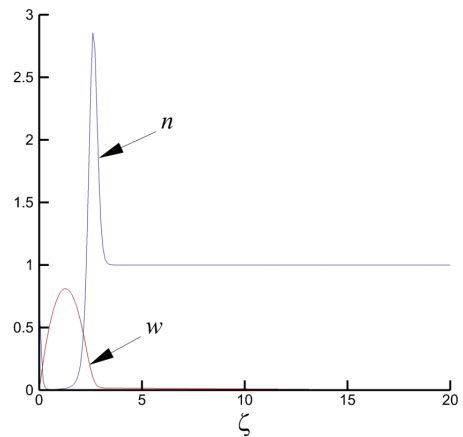


Figure 2: Variation of $w(\zeta)$ and $n(\zeta)$ with ζ .

References

- [1] Zeng, L. and Pedley, T.J., Distribution of gyrotactic micro-organisms in complex three-dimensional flows: I. Horizontal shear flow past a vertical circular cylinder, 2015. (as submitted to JFM)
- [2] Schlichting, H. *Boundary Layer Theory*, 6th ed., McGraw-Hill, New York, 1968.
- [3] Pedley, T. J. and Kessler, J. O., Hydrodynamic phenomena in suspensions of swimming micro-organisms. *Annu. Rev. Fluid Mech.*, 24, pp. 313-358, 1992.

Gyrotactic trapping can be hydrodynamically unstable

Smitha Maretvadakethope¹ and Eric Keaveny² and Yongyun Hwang³

¹Department of Mathematics, Imperial College London
South Kensington, SW7 2AZ, London, UK

Email: smitha.maretvadakethope12@imperial.ac.uk

²Department of Mathematics, Imperial College London
South Kensington, SW7 2AZ, London, UK

Email: e.keaveny@imperial.ac.uk

³Department of Aeronautics, Imperial College London
South Kensington, SW7 2AZ, London, UK

Email: y.hwang@imperial.ac.uk

Abstract

Thin layers of motile phytoplankton are observed in the coastal ocean, meters below the surface, and they often exhibit high ecological activities. In a recent study by Durham et al (2009, *Science*, 323:1067-1070), it was proposed that, for bottom-heavy motile phytoplankton (e.g. *Chlamydomonas*), such thin layers can be formed by ‘gyrotactic trapping’. Here, we perform a linear stability analysis of the layer formed by this mechanism, and show that it can be hydrodynamically unstable if the cell concentration is sufficiently high. The present result implies that the gyrotactic trapping may not be a robust mechanism in the formation of the thin layers of phytoplankton.

Keywords: Gyrotactic trapping, Thin layer, Hydrodynamic instability

1. Introduction

Thin layers of phytoplankton are often found in meters beneath the surface of coastal ocean. These layers typically contain cell concentrations much higher than in the ambient regions, and become important hotspots of ecological activity. Recently, it was proposed that bottom-heavy swimming microalgae such as *Chlamydomonas* can form such a layer in the region where an excessively large gradient of background shear is present [1]. The mechanism, often called ‘gyrotactic trapping’, has been understood as the key process in the formation of such a layer. While the proposed mechanism may be an important process in the formation of thin phytoplankton layers in the coastal ocean, it should also be pointed out that many of the bottom-heavy swimming microalgae species are very often heavier than the ambient fluid. In other words, the layer can be hydrodynamically unstable, especially if the cell concentration of the layer is high enough. The most well-known example of this is bioconvection, which takes place in a shallow stationary suspension due to the highly concentrated thin layer of up-swimming microalgae at the top [2].

This observation now raises the need to examine the robustness of the gyrotactic trapping mechanism especially for a layer with high cell concentration. The purpose of the present study is therefore to address this question by theoretically examining the stability of such a layer formed by the gyrotactic trapping.

2. Problem formulation

2.1. Plane Poiseuille flow of gyrotactic microalgae suspension

We consider the continuum model of randomly swimming bottom-heavy microalgae suspensions in [4, 5]. In this model, the fluid flow is described by the Navier-Stokes equation, while the cell concentration is depicted by an advection-diffusion equation and a quasi-steady and quasi-uniform Fokker-Planck equation that determines the swimming direction of microalgae on average. It has been shown that this model captures most of the known

collective dynamics of the bottom-heavy microalgae suspension with reasonable accuracy, including bioconvection with/without shear flows [3, 5] and blip instability in downward shear flows [5].

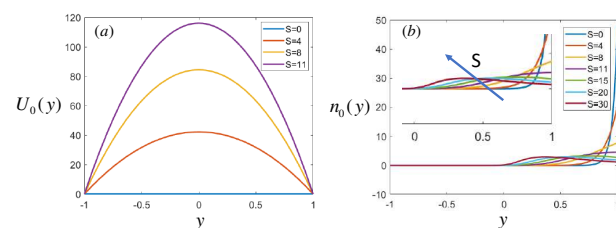


Figure 1: Profiles of basic state with the maximum shear rate S_{max} at the top boundary: (a) base flow; (b) cell concentration.

To create a thin layer formed with the gyrotactic trapping, we introduce a parabolic flow profile as in [1], and this is implemented by considering a plane Poiseuille flow where the dimensionless lower and upper walls are located in $y = -1$ and $y = 1$, respectively. The two most important parameters in the present study are the dimensionless maximum shear rate of the base flow and the Rayleigh number:

$$S_{max} = \frac{dU_0/dy_{max}}{D_R}, \quad Ra = \frac{Nvg'h^3}{D_\nu}, \quad (1)$$

where dU_0/dy_{max} is the maximum shear rate, D_R the rotational diffusivity, N the averaged cell concentration, v the volume of a single cell, g' the reduced gravity, D_ν the nominal translational diffusivity, and h the half-channel height. Note that the maximum shear rate is proportional to the applied pressure gradient. All the parameters here are identical to those in [5].

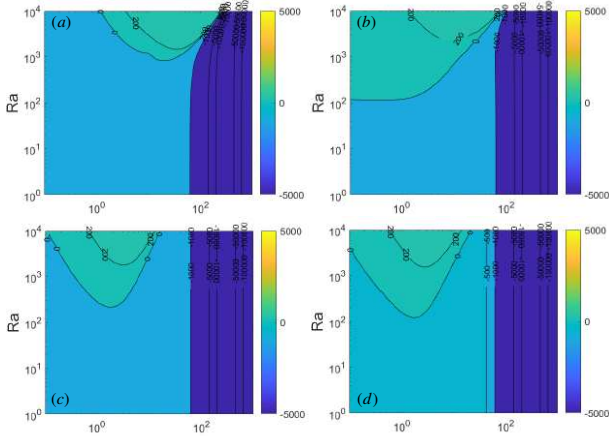


Figure 2: Contour of ω_i of the most unstable mode and its neutral stability curve in the Ra - α plane: (a) $S_{max} = 0$; (b) $S_{max} = 4$; (c) $S_{max} = 11$; (d) $S_{max} = 20$.

3. Results and discussion

3.1. Layer formation by gyrotactic trapping

The basic state is first computed by seeking the steady solution of the continuum model. Figure 1 shows the wall-normal profiles of the basic state (i.e. base flow and cell concentration). At low $S_{max} (\leq 11)$, the up-swimming of the cells is not significantly disturbed, thus the cell concentration is highest at the top boundary ($y = 1$). However, as the shear rate S_{max} increases further, the cell concentration begins to exhibit its maximum below the top boundary and the peak location gradually moves downward. At the highest shear rate considered ($S_{max} = 30$), the formation of a layer of the cells by gyrotactic trapping becomes evident.

3.2. Linear instability

Now, we consider a two-dimensional small perturbation around the basic state. Due to the streamwise homogeneity of the given flow configuration, the small perturbation of the velocity \mathbf{u} and n admits the following normal-mode solution:

$$\mathbf{u}(x, y, t) = \tilde{\mathbf{u}}(y)e^{i(\alpha x - \omega t)}, \quad n(x, y, t) = \tilde{n}(y)e^{i(\alpha x - \omega t)}, \quad (2)$$

where t is the time, ω the complex eigenfrequency, x the streamwise direction, and α the given streamwise wavenumber. The linear eigenvalue problem is subsequently solved numerically.

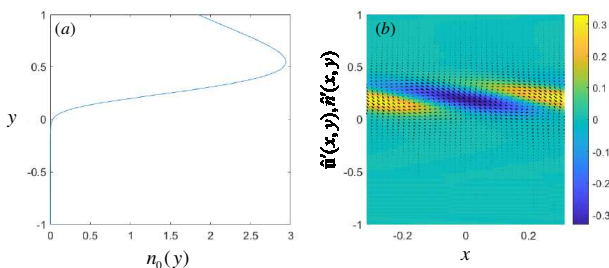


Figure 3: Hydrodynamically unstable layer formed by gyrotactic trapping ($S_{max} = 20$): (a) basic-state cell concentration; (b) the corresponding eigenfunctions. In (b), the vector plot presents $\hat{\mathbf{u}}(x, y) (= \tilde{\mathbf{u}}(y)e^{i\alpha x})$ and the coloured contour indicates $\hat{n}(x, y) (= \tilde{n}(y)e^{i\alpha x})$.

The contour of the temporal growth rate ω_i of the perturbation and the corresponding neutral stability curve are shown in Fig. 2. When $S_{max} = 0$, an instability appears for sufficiently large Ra (fig 2a). This contour is exactly identical to the one in [3, 5] where the emergence of bioconvection is analysed. With a small increase of S_{max} , the growth rate at high wavenumbers becomes reduced, while increased at low wavenumbers (fig 2b). This behaviour is qualitatively identical to that of bioconvective instability in the presence of small uniform shear. The further increase of S appears to stabilise the instability at low wavenumbers a little (fig 2c). However, the instability at low wavenumbers is not suppressed even if the maximum shear rate reaches $S_{max} = 20$. It should be reminded that a deterministic swimming cell with the same gyrotactic time scale starts to tumble if the surrounding dimensionless shear rate becomes $S (= dU/dy/D_R) \geq 4.4$ and that uniform shear with $S \geq 11$ completely stabilizes bioconvective instability [5]. Furthermore, the very high shear rate would strongly inhibit all the instability mechanisms which directly originate from the gyrotactic nature of the cells. In this respect, the emergence of the low wavenumber instability at such high shear rate indicates that there exists a new instability mechanism at play, which does not appear in uniform shear flow.

3.3. Physical mechanism of instability

To understand the origin of the low wavenumber instability at high shear rate, its eigenfunction is visualised in Fig. 3 with the basic-state cell concentration $n_0(y)$. It is evident that the eigenfunction is highly concentrated in the region where the basic-state cell concentration is unstably stratified. This suggests that the mechanism of the low wavenumber instability at high shear rate is gravitational overturning as for the Rayleigh-Taylor instability, and it originates from the unstable stratification in the layer formed by gyrotactic trapping. An additional numerical experiment that artificially suppresses the gravitational instability term also confirms this conclusion. It should be mentioned that this gravitational instability appears when the averaged cell concentration (i.e. Ra in this case) is high enough. However, in the present case, the instability at high shear rate arises only when $Ra \simeq 10^2$, at which the averaged cell concentration is only $N \simeq 10^5 \text{ cells/cm}^3$. This theoretical result indicates that the thin layer observed in [1] might be a feature arising only at very low cell concentrations.

In the final presentation, a further discussion on this issue will be provided with the result of three-dimensional stability analysis.

References

- [1] Durham, W. M., Kessler, J. O. and Stocker, R., Disruption of vertical motility by shear triggers formation of thin phytoplankton layers., *Science*, Vol. 323, pp. 1067-1070, 2009.
- [2] Pedley, T. J. and Kessler, J. O., Hydrodynamic phenomena in suspensions of swimming micro-organisms, *Annu. Rev. Fluid Mech.*, Vol. 24, pp. 313-358, 1992.
- [3] Bees, M. A. and Hill, N. A. Linear bioconvection in a suspension of randomly swimming gyrotactic micro-organisms, *Phys. Fluids*, Vol. 10(8), pp. 1864-1881, 1998.
- [4] Pedley, T. J. Instability of uniform microorganism suspensions revisited *J. Fluid Mech.*, Vol. 647, pp. 335-359, 2010.
- [5] Hwang, Y. and Pedley, T. J. Bioconvection under uniform shear: linear stability analysis. *J. Fluid Mech.*, Vol. 738, pp. 522-562, 2014.

Micro-swimmer dynamics in free-surface turbulence subject to wind stress

Cristian Marchioli¹, Salvatore Lovecchio¹ and Alfredo Soldati^{1,2}

¹Dept. Engineering and Architecture, University of Udine (Italy)
marchioli@uniud.it

²Institute of Fluid Mechanics and Heat Transfer, TU Wien (Austria)
alfredo.soldati@tuwien.ac.at

Abstract: We examine the effect of wind-induced shear on the dynamics of motile micro-swimmers in free-surface turbulence. We focus on gyrotaxis, resulting from the gravitational torque generated by an asymmetric mass distribution within the organism. The combination of such torque with the viscous torque due to shear can reorient swimmers and reduce their vertical migration. Through DNS-based Euler-Lagrangian simulations we investigate the effect of wind-induced shear on swimmers with different reorientation time under different wind directions. We show that wind-induced shear modifies the vertical spread of the swimmers and their orientation with respect to gravity. For all gyrotactic re-orientation times considered (spanning two orders of magnitude of the stability number), we observe a reduction of the rising speed and temporary confinement under the high-shear sub-surface layers.

Keywords: Clustering, Free-surface, Shear Flow, Turbulence, Gyrotaxis, Numerical simulation

1. Introduction

Wind-induced shear has a profound effect on the transport and mixing processes in the upper layers of large water bodies. In oceans, wind shear affects the vertical distribution and residence time of phytoplankton species rising and sinking across the near-surface region. In lakes, where water movement is mainly driven by wind, strong heterogeneities can be induced in the horizontal concentration distribution (patchiness) of phytoplankton cells. One important source of complexity characterizing plankton interaction with wind-forced turbulence is plankton motility. Many phytoplankton species are self-propelled and, even if their swimming speeds are typically smaller than ambient flow speeds, there is well-documented evidence that the interplay between motility and turbulence can result in complex and ecologically important phenomena [2, 3]. In particular, motility can lead to a striking focusing effect known as gyrotaxis when coupled with vertical gradients in horizontal fluid velocity. Gyrotaxis is the directed motility of cells arising from the combination of gravitaxis (which stabilizes cell orientation in the vertical direction, typically through bottom heaviness) and destabilisation by the ambient fluid shear [1]. The balance between the gravitational torque due to the uneven density distribution within the cell, which tends to keep the center of mass below the center of buoyancy, and the hydrodynamic torque exerted by the fluid that surrounds the cell. To the best of our knowledge, the interplay between wind-induced shear and gyrotaxis in a three-dimensional turbulent flow has never been examined in detail. Therefore, the physical mechanisms that govern the dynamics of motile aquatic micro-organisms (swimmers) in wind-sheared turbulence are not fully understood, and the possibility of observing trapping phenomena in the presence of strong wind-induced shear not yet assessed.

2. Physical problem and methodology

We study the dispersion of gyrotactic swimmers in a wind-sheared turbulent flow in an open channel with a flat undeformable surface. The size of the channel is $2\pi h \times \pi h \times h$ in the streamwise (x), spanwise (y) and wall-normal (z) directions, respectively (with h the channel height). The fluid dynamics is described by the following three-dimensional time-dependent equations, written in dimensionless vector form:

$$\nabla \cdot \mathbf{u} = 0, \quad \dot{\mathbf{u}} + \mathbf{u} \cdot \nabla \mathbf{u} = -\nabla p + Re_\tau^{-1} \nabla^2 \mathbf{u} + \delta_p \quad (1)$$

where $\mathbf{u} = (u_x, u_y, u_z)$ is the fluid velocity, ∇p is the gradient of the fluctuating pressure p , δ_p is the imposed pressure gradient that drives the flow in the streamwise direction, and $Re_\tau = u_\tau h / \nu$ is the shear Reynolds number based on the shear velocity u_τ , and on the kinematic fluid viscosity ν . For the fluid velocity, periodic BC's are applied in x and y , whereas no-slip BC's are enforced at the bottom wall. At the free surface, a constant-stress BC is applied to model the wind-induced forcing: The condition $\tau_{xy}(z = h) = \tau_{wind,+}$ is imposed to simulate wind blowing in the streamwise direction (co-current wind), whereas the condition $\tau_{xy}(z = h) = \tau_{wind,-}$ is imposed to simulate wind blowing against the streamwise direction (counter-current wind). Swimmers are modelled as spherical particles whose position \mathbf{x}_p and orientation \mathbf{p} evolve in time according to the following dimensionless equations:

$$\dot{\mathbf{x}}_p = \mathbf{u}_{@p} + \Phi \mathbf{p}, \quad \dot{\mathbf{p}} = \Psi [\mathbf{k} - (\mathbf{k} \cdot \mathbf{p})\mathbf{p}] + (\boldsymbol{\omega}_{@p} \wedge \mathbf{p}) / 2 \quad (2)$$

where $\Phi = v_s / u_\tau$ is the swimming number (with v_s the swimming speed), $\mathbf{u}_{@p}$ the velocity of fluid in the position of swimmer, $\mathbf{k} = [0, 0, 1]$ is a unit vector pointing upward in the vertical direction, $\boldsymbol{\omega}_{@p}$ is the fluid vorticity at the swimmer's position and $\Psi = \frac{1}{2\mathcal{B}} \frac{\nu}{u_\tau^2}$ is the stability number, \mathcal{B} being the characteristic time a perturbed gyrotactic swimmer takes to return to the vertical orientation when $\boldsymbol{\omega} = 0$. All variables are in wall units, obtained using u_τ and ν . 10^6 Lagrangian swimmers are tracked using a point-particle approach, and are injected into the flow at a concentration low enough to consider dilute conditions. All simulations were run at $Re_\tau = 171$. The imposed wind stress was set equal to $\tau_{wind,+} = 0.006 Pa$ (0.7 in wall units) for the counter-current wind simulations, and to $\tau_{wind,-} = -0.003 Pa$ (-0.35 in wall units) for the co-current wind simulations. These values correspond to a mild wind speed of about 1.5 m/s at an altitude of 10 m, which does not generate any wave motion at an air-water interface. To simulate the motion of the micro-organisms, we considered $\Phi = 0.048$, corresponding to a dimensional swimming velocity $v_s = 100 \mu\text{m/s}$ typical of *Chlamydomonas augustae* cells, and three different values of the stability number ($\Psi_H = 1.13$, $\Psi_I = 0.113$, $\Psi_L = 0.0113$), corresponding to $\mathcal{B} = 0.054, 0.54$ and 5.4 s, respectively. In the

present flow configuration, the largest value of the Kolmogorov timescale is $\tau_{K,max}^+ \simeq 13$ at the free-surface. Therefore, the selected values of the stability number correspond to three different physical instances with respect to $\tau_{K,max}^+$. At one extreme, $\Psi_L \cdot \tau_{K,max}^+ \sim \mathcal{O}(0.1)$ represents the case in which the timescale of gravitaxis is large compared to the timescale of the dissipative surface eddies and so the directional motion of the swimmers is dominated by the destabilising effect of small-scale turbulence. At the opposite extreme, $\Psi_H \cdot \tau_{K,max}^+ \sim \mathcal{O}(10)$ represents the case in which the timescale of gravitaxis is small compared to the timescale of the dissipative surface eddies and so the directional motion of the swimmers is dominated by the stabilising effect of bottom-heaviness. The case $\Psi_I \cdot \tau_{K,max}^+ \sim \mathcal{O}(1)$ represents the situation in which the two timescales are comparable and the motion of the swimmers results from the competition between small-scale turbulence around each cell and bottom-heaviness.

3. Results and Discussion

For the flow Reynolds number considered here, turbulence at the free surface is nearly 2D, with surface structures generated and sustained by bursting phenomena that are continuously produced by wall-shear turbulence inside the buffer layer. 2D turbulence can be characterized by the surface divergence of the velocity field $\nabla_{2D} = \frac{\partial u}{\partial x} + \frac{\partial v}{\partial y}$. In the present flow configuration, plankton cells probe a compressible 2D system, where velocity sources are regions of local flow expansion ($\nabla_{2D} > 0$) generated by sub-surface upwellings and velocity sinks are regions of local compression ($\nabla_{2D} < 0$) due to downwellings. As shown in Fig. 1, swimmers that reach the free surface, collect into velocity sinks (visualised in blue) and organize themselves in clusters that are stretched by the fluid forming filamentary structures. Eventually patches of plankton density distribution are produced, which correlate very well with the rapidly changing patches of ∇_{2D} . Fig. 1 shows that the topology of both the velocity sources/sinks and the plankton clusters depend on the wind forcing and on gyrotaxis.

In Fig. 2 we show the the swimmer orientation profiles $\langle p_x \rangle$ and $\langle p_z \rangle$ along the wall-normal direction, for all simulated cases. We focus on the upper portion of the flow domain, where the swimmers interact with wind-induced shear. In the free-slip case (panels (a) and (d) in Fig. 2), $\langle p_x \rangle$ is always small while $\langle p_z \rangle$ increases with Ψ : It is clear that, even without wind forcing, turbulence can disrupt directional swimming for low gyrotaxis.

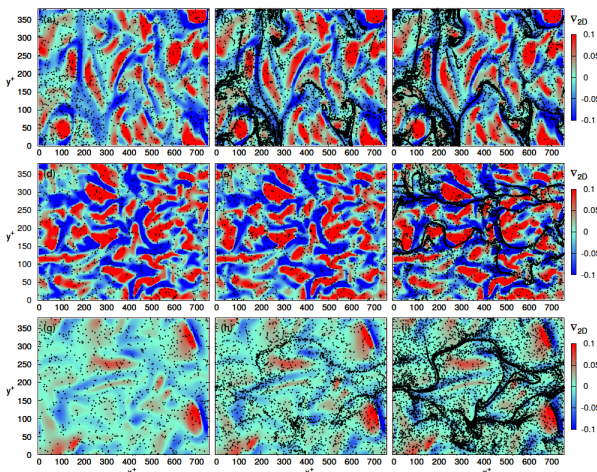


Figure 1: Surface divergence and instantaneous swimmer distribution for the different flow configurations. Rows - Top: Free-slip surface; Middle: Co-current wind; Bottom: Counter-current wind. Columns - Left-hand: Low gyrotaxis, Ψ_L ; Central: Intermediate gyrotaxis, Ψ_I ; Right-hand: High gyrotaxis, Ψ_H .

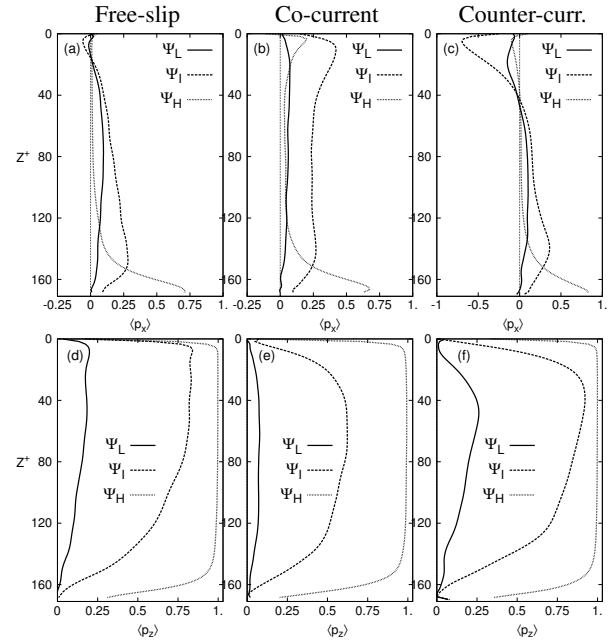


Figure 2: Mean swimmer orientation, $\langle p_i \rangle$, along the wall-normal direction at varying gyrotaxis (Ψ_L : Solid line, Ψ_I : Dashed line, Ψ_H : Dotted line). The free surface is located at $Z^+ = 0$.

As gyrotaxis increases, bottom heaviness becomes predominant and allows swimmers to reach an equilibrium orientation in the direction opposite to gravity. In the co-current case (panels (b) and (e) in Fig. 2), weak (resp. strong) vertical swimming is observed for low (resp. high) gyrotaxis: For the Ψ_L case, this result indicates that local turbulent fluctuations are still strong enough to destabilize the directional motion of the swimmers, being $\Psi_L \cdot \tau_{K,max}^+ \sim \mathcal{O}(10^{-1})$, and wind-induced shear seems to bring minor quantitative changes to the statistics; for the Ψ_H case, it indicates that cell motility is mainly determined by gravitaxis since gravitational acceleration is larger than fluid acceleration and $\Psi_H \cdot \tau_{K,max}^+ \sim \mathcal{O}(10)$. A less trivial behaviour is observed for the Ψ_I case: Compared to the free-slip flow, significantly higher values of $\langle p_x \rangle$ associated to lower values of $\langle p_z \rangle$ are now observed within the wind-induced high-shear surface layer. This is a mean-shear effect, which explains the non-monotonic behaviour of $\langle p_x \rangle$ with Ψ and becomes more evident when $\Psi_I \cdot \tau_{K,max}^+ \sim \mathcal{O}(1)$. In the counter-current case (panels (c) and (f) of Fig. 2), similar considerations can be made yet observing that the direction of wind produces a negative value of $\langle p_x \rangle$ near the surface, this value being maximum ($\langle p_x \rangle \simeq -0.7$) for $\Psi = \Psi_I$: In such situation, swimmers can move against the mean flow aided by wind forcing.

The orientation statistics show that wind may have a significant damping effect on the surfacing of motile micro-organisms, which exhibit a narrower vertical spreading within the flow. Only organisms with high-enough gyrotaxis (namely strong-enough bottom-heaviness) can maintain their ability to swim upwards. This effect may have important consequences for environmental processes such as spring phytoplankton bloom and growth, which are known to occur when turbulent mixing is sufficiently weak.

References

- [1] T.J. Pedley and J.O. Kessler. *Annu. Rev. Fluid Mech.*, 24(1):313–358, 1992.
- [2] W.M. Durham, J.O. Kessler, and R. Stocker. *Science*, 323(5917):1067–1070, 2009.
- [3] J.S. Guasto, R. Rusconi, and R. Stocker. *Annu. Rev. Fluid Mech.*, 44:373–400, 1992.

Confinement and substrate topography control 3D cell migration

Igor Aronson¹, Benjamin Winkler² and Falko Ziebert³

¹ *Pennsylvania State University
218 Hallowell Building, University Park, PA 16802*

² *Albert-Ludwigs-Universität Freiburg
Hermann-Herder-Str. 3, 79104 Freiburg, Germany*

³ *University of Heidelberg
Philosophenweg 19, 69120 Heidelberg, Germany*

Abstract

Cell movement in vivo is typically characterized by strong confinement and very heterogeneous, three-dimensional environments. Such external constraints on cell motility are known to play important roles in many vital processes e.g. during development, differentiation, and the immune response, as well as in threatening pathologies like cancer metastasis. We have developed a physics-driven three-dimensional computational modeling framework, that describes lamellipodium-based motion of cells in arbitrarily shaped topographically structured surroundings. We use it to investigate all the in-vitro model system scenarios that are currently studied experimentally: imposed modulations of surface topography, vertical confinement, confinement in microchannels, as well as motion on fibers. We found that confinement, substrate curvature and topography modulate the cell's speed, shape and actin organization and can induce changes in the direction along axes defined by the constraints. Our model serves as an important benchmark to explore in depth lamellipodium-based motility and its interaction with the environment. It may lead to applications in medicine, tissue engineering, and even in self-healing synthetic materials.

Keywords: surface topography, lamellipodium-based motility, vertical confinement

Painting with bacteria, three ways

Wilson Poon¹

¹ *School of Physics Astronomy, The University of Edinburgh, Edinburgh (UK)*

Abstract

I will compare and contrast three ways of making two-dimensional patterns with bacteria: by making them swim in a near-critical mixture, by projecting static light patterns onto a population that only swims when lit, and by projecting moving light fields onto the same kind of cells. In the first and last case, I will explain the underlying physics in detail (leaving the physics of the second case to a contributed talk by Arlt et al.). Possible applications will be discussed.

Keywords: bacteria, self-assembly, light control

Shear-induced migration and Banding Instabilities in bacterial suspensions

Laxminarsimha Rao, Piyush Garg and Ganesh Subramanian*

Jawaharlal Nehru Centre for Advanced Scientific Research
Bengaluru, Karnataka, India, 560064

Abstract

We analyze the evolution of the concentration field in a sheared bacterial suspension. The analysis is first carried out in the one-way-coupled approximation (flow affects bacteria but the latter do not alter the imposed flow), valid at low bacterial concentrations, to predict the spatially inhomogeneous concentration field that results from a balance between shear-induced migration and diffusion. The method of multiple scales is used to derive a reduced drift-diffusion equation in physical space from the original kinetic equation for the bacterial probability density in position-orientation space. This allows one to map high and low-shear-depletion regions in the parameter space corresponding to a general shearing flow; experimental observations are explained as limiting cases. Next, we go beyond the one-way-coupled approximation, allowing for the bacterial stress to influence the flow field. The back-coupling is crucial in that the tendency of a higher concentration of bacteria to locally reduce the suspension viscosity leads to the homogeneously sheared state being linearly unstable. The unstable modes involve alternating flow-aligned layers of low and high concentration. Extended to an inhomogeneous shear flow, the instability might help explain the intermittent transition to active turbulence in pipe flow.

Keywords: micro-swimmers, pair-correlations

1. Introduction

Recent experiments have highlighted the ability of an ambient shearing to 'manipulate' bacterial populations; bacteria migrate either to high-shear or low-shear regions depending on the particular type of flow. Stocker and co-workers, Ref. [[1]], have shown that bacteria preferentially migrate towards the walls in a pressure-driven flow. In contrast, Sokolov and Aranson, Ref. [[2]], showed that bacteria migrate away from the high-shear regions in the curvilinear shear flow induced by a rotating particle. The microscopic swimming parameters corresponding to the peak spatial inhomogeneity, however, differ substantially in the two experiments. We present a general theoretical framework for analyzing shear-induced migration in active suspensions that explains the aforementioned observations, in addition to anticipating the variation of concentration patterns in a parameter space appropriate to a general curvilinear flow.

The bacterial probability density $\Omega(\mathbf{x}, \mathbf{p}, t)$ satisfies the following equation:

$$\frac{\partial \Omega}{\partial t} + U \mathbf{p} \cdot \nabla_{\mathbf{x}} \Omega - D_r \nabla_{\mathbf{p}}^2 \Omega + \nabla_{\mathbf{p}} \cdot (\dot{\mathbf{p}} \Omega) + \frac{1}{\tau} [\Omega - \int d\mathbf{p}' K(\mathbf{p}|\mathbf{p}') \Omega(\mathbf{p}')] = 0. \quad (1)$$

where U is the swimming speed, and D_r^{-1} and τ (with $\tau D_r \sim O(1)$) characterize the time for return to isotropy due to rotary diffusion and random tumbles, respectively. The shear-induced bacterium rotation, $\dot{\mathbf{p}} = \mathbf{W} \cdot \mathbf{p} + \mathbf{E} \cdot \mathbf{p}(\mathbf{I} - \mathbf{p}\mathbf{p})$, with \mathbf{W} and \mathbf{E} being the vorticity and rate-of-strain tensors, couples Eqn (1) to the equations of motion and continuity given by:

$$-\nabla p + \mu \nabla^2 \mathbf{u} + \nabla \cdot \boldsymbol{\sigma}^B = 0, \quad \nabla \cdot \mathbf{u} = 0. \quad (2)$$

where $\boldsymbol{\sigma}^B = \int (\mathbf{p}\mathbf{p} - \frac{1}{3}) \Omega d\mathbf{p}$ is the bacterial stress. When the scale H of the spatial inhomogeneity significantly exceeds $O(U\tau)$, orientation fluctuations relax more rapidly than concentration fluctuations which evolve on a time scale of $O(H^2/D)$, $D = \frac{1}{3}U^2\tau(1 + \frac{1}{\tau D_r})$ being the swimmer diffusivity. One may

then use the method of multiple scales, Ref. [[4];[3]], treating $U\tau/H$ as a small parameter, to derive a drift-diffusion equation for the slowly evolving bacterial concentration.

2. The one-way-coupled approximation: Shear-induced migration

For rectilinear shear flows, like the one considered by [1], in the one-way-coupled approximation, the concentration is only a function of the transverse coordinate (z), and the drift-diffusion equation reduces to:

$$\frac{\partial n}{\partial t} + \frac{\partial}{\partial z} (d_z(z; Pe)n) = \frac{\partial}{\partial z} (D_{zz}(z; Pe) \frac{\partial n}{\partial z}) \quad (3)$$

where the drift and diffusivity coefficients are defined in terms of moments of the Pe -dependent orientation distribution determined by the imposed shear; here, $Pe = \dot{\gamma}/D_r$ measures the relative importance of flow-induced reorientation and swimmer (rotary) diffusion. The steady state concentration profile is proportional to $\exp[d_z(z; Pe)/D_{zz}(z; Pe)]$. Calculations for a pressure-driven flow show, in contrast to the observations, Ref. [[1]], that shear-induced depletion persists for $Pe \rightarrow \infty$ (see Fig. 2). For a curvilinear flow, of the Taylor-Dean flow type, the spatial inhomogeneity is independent of Pe for $Pe \rightarrow 0$ (in contrast to the $O(Pe^2)$ scaling in the rectilinear case), being proportional to the dimensionless curvature ($U\tau/R$); this arises from persistent swimmer motion across curved streamlines, an effect similar to the one leading to inhomogeneous distributions of finite-Stokes-number particles in turbulence.

3. The two-way-coupled approximation: Banding Instability

With two-way coupling included, the flow-induced bacterium rotation is not known apriori since it depends on the bacterial stress field. As a first step towards understanding the effects of the coupling between velocity and concentration perturbations, we analyze the stability of a homogeneous bacterial suspension

*Address of correspondence: sganesh@jncasr.ac.in

subject to a simple shear flow. The following argument highlights the non-trivial consequence of including the bacterial-stress-induced flow. Since bacterial suspensions exhibit a reduction in the effective viscosity with increasing concentration [5], an initial concentration perturbation in the gradient direction leads to a lower (higher) effective viscosity in regions of high (low) concentration; the lower (higher) viscosity in turn implies locally a high (low) shear rate. In the high-shear region, the bacteria are more effectively aligned with the flow, and consequently, have a lower mean swimming speed (and diffusivity) along the gradient direction. This in turn implies a net flux of bacteria into a high-shear layer from adjacent low-shear layers, providing a mechanism for reinforcement, and thence, an exponential growth of concentration fluctuations (see Fig. ??).

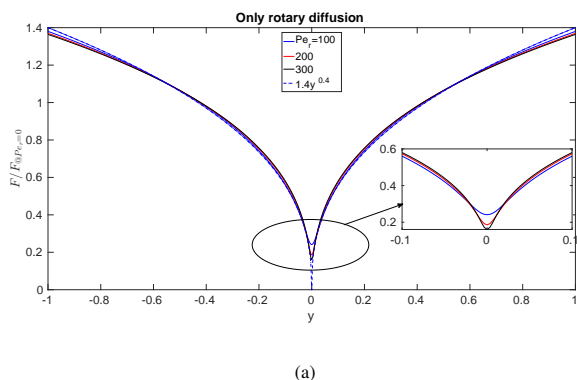


Figure 1: The Pe -dependent bacterial concentration profiles, in pressure-driven channel flow, exhibiting a low-shear depletion.

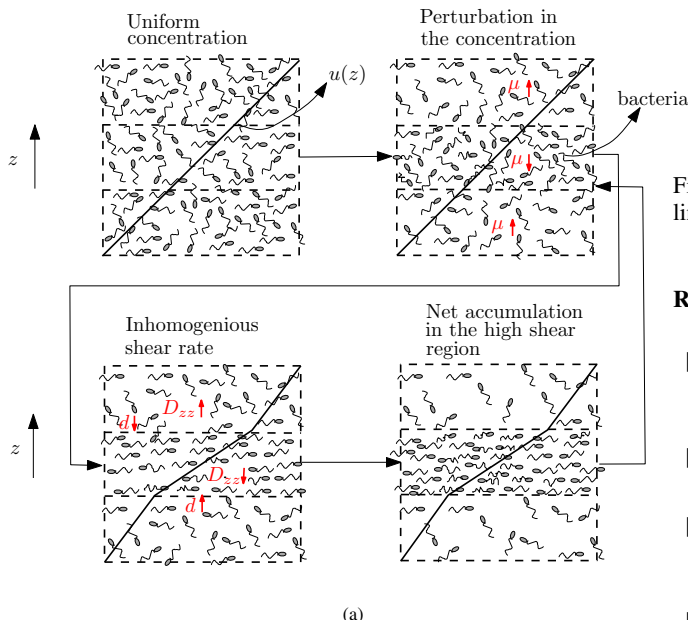


Figure 2: Mechanism for banding instability in a sheared bacterial suspension

A semi-analytical stability calculation, using the method of multiple scales leads again to a drift-diffusion equation, and con-

firms the above physical arguments for banding perturbations with wavelengths much longer than $O(U\tau)$. The full linear stability analysis, carried out without assuming a time scale separation validates the multiple scales analysis. Finally, the governing equations are integrated numerically to study the non-linear banded state that results for long times (see Fig. ??); the inset in the first sub-figure shows that the stress increases linearly with the imposed shear rate, implying a positive effective viscosity in the banded state

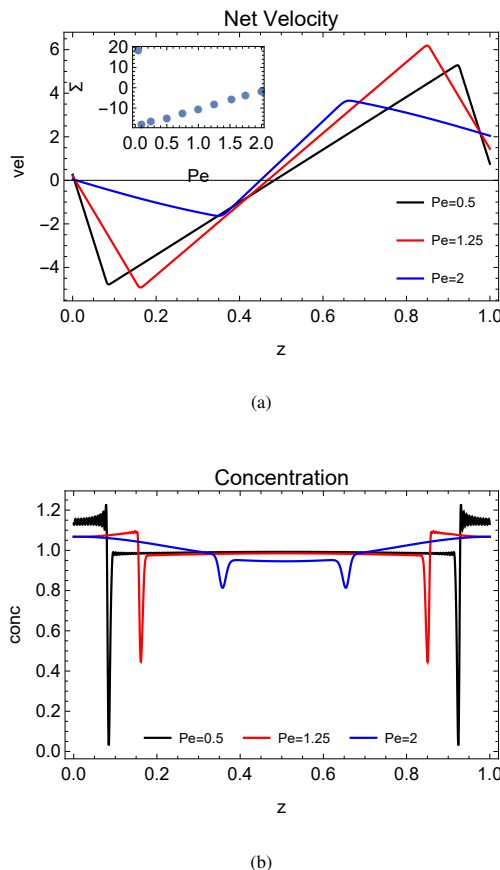


Figure 3: The velocity and concentration profiles in the non-linear banded state for a sheared bacterial suspension

References

- [1] Rusconi R, Guasto JS and Stocker R, Bacterial transport suppressed by fluid shear, *Nat. Phys.*, 10, pp. 212-217, 2014.
- [2] Sokolov A and Aranson IS, Rapid expulsion of microswimmers by a vortical flow, *Nat. Comm.*, 7, pp. 11114, 2016.
- [3] Subramanian G and Brady JF, Multiple scales analysis of the Fokker-Planck equation for simple shear flow, *Physica A*, 334, pp. 343-384, 2004.
- [4] Nitsche LC and Hinch EJ Shear-induced lateral migration of Brownian rigid rods in parabolic channel flow *J. Fluid Mech.*, 332, pp. 1-21, 2004.
- [5] Sokolov A and Aranson IS, Reduction of viscosity in suspension of swimming bacteria, *Physical Review Letters*, 103, pp. 148101, 2009.

Divergence of the velocity variance in interacting swimmer suspensions

Sankalp Nambiar and Ganesh Subramanian*

Engineering Mechanics Unit,
Jawaharlal Nehru Centre for Advanced Scientific Research
Bengaluru, Karnataka, India, 560064

Abstract

In this work we present the fluid velocity covariance ($\langle \mathbf{u}(\mathbf{x}) \cdot \mathbf{u}(\mathbf{x} + \mathbf{r}) \rangle$) for a suspension of hydrodynamically interacting active swimmers. In the absence of interactions, the variance remains finite, and the covariance decays as $O(1/r)$ for large r , being invariant to the particular swimming mechanism (pusher or puller). Interestingly, incorporation of pair-level interactions leads to a divergence of the variance that is logarithmic in the system size, and a non-decaying covariance, for straight swimmers. The divergence arises due to the slow $O(1/r^2)$ decay of the pair-correlation function. For run-and-tumble particles (RTP's) the divergence is cut-off at the large but finite run length ($U\tau$), leading to a variance that scales as $\log(U\tau/L)$, in the limit $U\tau/L \gg 1$. The covariance on the other hand exhibits a weak logarithmic decay post the initial plateau, followed by an $O(1/r)$ decay in the far-field ($r \gg U\tau$). Here, U is the swimming speed, τ is the mean run duration and L is the characteristic swimmer size. Importantly, pair-correlations are crucial to discriminating between tracer diffusivities in dilute pusher and puller suspensions.

Keywords: micro-swimmers, pair-correlations, suspensions

1. Introduction

A suspension of pushers (microscopic swimmers propelled from the rear), a specific realization of active matter that has been extensively investigated in experiments, exhibits several interesting and non-trivial characteristics in relation to those known for passive suspensions. These include, viscosity reduction in a dilute suspension at low imposed shear rates, Ref. [1, 2], shear thickening and negative first normal stress differences, Ref. [3], enhanced tracer particle diffusivities, Ref. [4, 5, 6], long-ranged correlations, Ref. [6, 7, 8, 9] as well as collective motion, Ref. [6, 10], among others. While it is possible to explain some of these phenomena using a mean-field theory for a dilute suspension, effects such as long range order and collective motion require a model that incorporates the specific effects of interactions among swimmers. The fluid velocity (co)variance is one such characteristic that we examine in detail based on an analysis that includes hydrodynamic interactions.

In sedimenting suspensions of dilute non-interacting passive particles (modelled as point monopoles), it is known that the velocity variance diverges linearly with system size in the inertialess limit, Ref. [11, 12, 13]. This is associated with the slowly decaying $O(1/r)$ disturbance velocity fields of point particles. At $O(nL^3)$, when $nL^3 \ll 1$, $\langle \mathbf{u}(\mathbf{x}) \cdot \mathbf{u}(\mathbf{x}) \rangle \sim (nL^3)U^2 \int \frac{1}{r^2} d\mathbf{r} \sim (nL^3)U^2 L_{box}/L$ (n is the number density and L is the characteristic size of the particle). Theoretical analyses have predicted screening of the long-ranged hydrodynamic interactions, leading to a modified long-wavelength limit of the structure factor; nonetheless, in experiments, the divergence is cut-off owing to a container-scale stratification, Ref. [13].

Pushers (or pullers), on the other hand, behave as active force dipoles (with a disturbance velocity field decaying as $O(1/r^2)$) in the far-field and therefore, at $O(nL^3)$, exhibit a fluid velocity variance that remains finite and a covariance that decays away as $O(1/r)$. Herein, we first establish the character of the velocity (co)variance in a suspension of hydrodynamically interacting straight swimmers (that possess no intrinsic orientation decorrelation mechanism such as run-and-tumble dynamics or rotary

diffusion). Interestingly, at $O((nL^3)^2)$, the velocity variance in such a suspension diverges logarithmically with system size. The divergence is attributed to the long ranged orientation correlations that only decay as $O(1/r^2)$ in the far-field. When run-and-tumble particles (RTP's) are considered, the presence of an intrinsic decorrelation mechanism arrests the divergence due to a more rapid decay of the pair-correlation function ($O(1/r^3)$), for distances greater than the run length of $O(U\tau)$. The resulting velocity variance scales as $(\ln(U\tau/L))$ in the limit $U\tau/L \gg 1$. Here, U is the swimming speed, L is the characteristic length and τ is the mean run duration of the swimmer.

2. Fluid Velocity Covariance

For a suspension of swimmers the fluid velocity covariance is defined as:

$$\langle \mathbf{u}(\mathbf{x}) \cdot \mathbf{u}(\mathbf{x}') \rangle = \left\langle \sum_{i,j=1}^N \mathbf{u}_i(\mathbf{x}) \cdot \mathbf{u}_j(\mathbf{x}') \right\rangle, \quad (1)$$

where $\langle \cdot \rangle$ represents the ensemble average over all possible positions ($\mathbf{x}_{i/j}$) and orientations ($\mathbf{p}_{i/j}$) of swimmers i, j . The disturbance velocity field generated by the swimming motion is represented by \mathbf{u}_i for the i th swimmer, and is obtained by solving the Stokes equations with a forcing due to the slender swimmer as:

$$-\nabla P_i + \eta \nabla^2 \mathbf{u}_i = \int_{-L/2}^{L/2} s f(s) \mathbf{p}_i \delta(\mathbf{x} - \mathbf{x}_i - s \mathbf{p}_i) ds, \quad (2)$$

with P_i being the pressure field; the right hand side corresponds to a line distribution of point forces along the swimmer's axis (s), consistent with the force-free constraint. Here, $f(s)$ denotes the linear force density, the magnitude of which is $O(\eta UL/\ln \kappa)$, where η is the suspending fluid viscosity and κ is the aspect ratio of the slender swimmer.

It is convenient to express the covariance in terms of the Fourier transformed velocity field and after some algebra, one

*address of correspondence gsubram@jncasr.ac.in

obtains:

$$\langle \hat{\mathbf{u}}(\mathbf{k}) \cdot \hat{\mathbf{u}}(\mathbf{k}') \rangle = \frac{\delta(\mathbf{k} + \mathbf{k}')}{k^4} \left(\mathbf{I} - \frac{\mathbf{k}\mathbf{k}}{k^2} \right) : \left[(nL^3)C_1 \int d\mathbf{p} \frac{1}{(\mathbf{k} \cdot \mathbf{p})^2} \sin^4\left(\frac{\pi L}{2} \mathbf{k} \cdot \mathbf{p}\right) \mathbf{p}\mathbf{p} + (nL^3)^2 C_2 \int d\mathbf{p} d\mathbf{p}' \frac{1}{\mathbf{k} \cdot \mathbf{p}} \frac{1}{\mathbf{k} \cdot \mathbf{p}'} \sin^2\left(\frac{\pi L}{2} \mathbf{k} \cdot \mathbf{p}\right) \sin^2\left(\frac{\pi L}{2} \mathbf{k} \cdot \mathbf{p}'\right) \mathbf{p}\mathbf{p}' \hat{\Omega}_2 \right]. \quad (3)$$

The first term on right side of Eqn (3) is the $O(nL^3)$ covariance in a suspension of non-interacting swimmers. Note that $C_1 \propto D^2$, with D being the dipole strength and therefore at $O(nL^3)$, the (co)variance is invariant to the particular mechanism of swimming (pusher or puller). The second term accounts for pair-correlations at $O((nL^3)^2)$, with $C_2 \propto D^3$. In Eqn (3), $\hat{\Omega}_2$ is the Fourier transformed pair-correlation function in position-orientation space; $\Omega_2(r, \mathbf{p}, \mathbf{p}')$ denotes the probability density of finding two swimmers with orientations \mathbf{p} and \mathbf{p}' , separated by r .

2.1. Straight Swimmers

For a suspension of straight swimmers, Ω_2 is governed by the following equation at steady state:

$$U(\mathbf{p} - \mathbf{p}') \cdot \nabla_{\mathbf{r}} \Omega_2 + \nabla_{\mathbf{p}} \cdot (\dot{\mathbf{p}} \Omega_2) + \nabla_{\mathbf{p}'} \cdot (\dot{\mathbf{p}}' \Omega_2) = 0, \quad (4)$$

where $\dot{\mathbf{p}}$ represents the rate of rotation of a swimmer due to the disturbance velocity field generated by the other. Since the swimmers are modelled as slender bodies, the disturbance velocity field generated by their motion is $O(1/\ln \kappa)$. On length scales of $O(L)$, we expand Ω_2 as a regular series in $(\ln \kappa)^{-1}$ as $\Omega_2 = \Omega_2^{(0)} + 1/\ln(\kappa) \Omega_2^{(1)} + \dots$, with $\Omega_2^{(0)} = n^2/(4\pi)^2$. $\Omega_2^{(1)}$ captures the first effects of the pair-correlations. From Eqn (4), $\Omega_2^{(1)} \sim \int_{-\infty}^r [\nabla_{\mathbf{p}} \cdot \dot{\mathbf{p}} + \nabla_{\mathbf{p}'} \cdot \dot{\mathbf{p}}'] dz$. Since $\dot{\mathbf{p}}$ scales as the velocity gradient, which is $O(1/r^3)$ in the far-field for a dipolar velocity field, $\Omega_2^{(1)} \sim O(1/r^2)$. The resulting velocity variance is:

$$\langle \mathbf{u}(\mathbf{x}) \cdot \mathbf{u}(\mathbf{x}) \rangle \propto (nL^3) \int r^2 dr \left[\int \frac{1}{r^4} \left(\frac{(nL^3)}{\ln \kappa} \frac{1}{r'^2} \right) r'^2 dr' \right], \quad (5)$$

and therefore exhibits a logarithmic divergence with system size.

The divergence above is resolved by orientation decorrelations, which, for slender swimmers, are driven by weak hydrodynamic interactions that may be modelled in terms of an effective rotary diffusivity, $D_r^h \sim nUL^2/(\ln \kappa)^2$, Ref. [7]. For systems sizes much larger than $O(U/D_r^h)$, the velocity variance must saturate, being given by $c_1(nL^3) + (nL^3)^2 \{c_2 \ln[(\ln \kappa)^2/nL^3] + c_3\}$.

2.2. Run and Tumble Swimmers

Keeping in mind bacteria such as *E.Coli*, we consider a suspension of slender RTP's. The evolution of Ω_2 is now governed by:

$$U(\mathbf{p} - \mathbf{p}') \cdot \nabla_{\mathbf{r}} \Omega_2 + \frac{2}{\tau} \Omega_2 - \frac{1}{4\pi\tau} \int \Omega_2 d\mathbf{p} - \frac{1}{4\pi\tau} \int \Omega_2 d\mathbf{p}' = -\nabla_{\mathbf{p}} \cdot (\dot{\mathbf{p}} \Omega_2) - \nabla_{\mathbf{p}'} \cdot (\dot{\mathbf{p}}' \Omega_2). \quad (6)$$

The additional terms on the left side of Eqn (6) model a random tumbling process, Ref. [7]. Again, expanding Ω_2 as a series in $(\ln \kappa)^{-1}$, one may solve for the pair-correlation function for arbitrary $U\tau/L$. Scaling arguments analogous to those above show that the variance is $O(\ln[U\tau/L])$ for $U\tau/L \gg 1$, and $O(U\tau/L)$ when $U\tau/L \ll 1$. As in §2.1, the resulting variance is again expressible as $c_1(nL^3) + (nL^3)^2 [c_2 \ln[U\tau/L] + c_3]$, when $U\tau/L \gg 1$. Figure 1 shows the variance (green) as a function of $U\tau/L$ for RTP's, and is consistent with the scaling arguments

above. The normalized fluid velocity covariance (black) is plotted as a function of the separation r , for a range of $U\tau/L$. The onset of $O(1/r)$ decay is shifted to larger r , with the appearance of an intermediate regime that scales as $\ln[r/(U\tau)]$, for $U\tau/L \gg 1$.

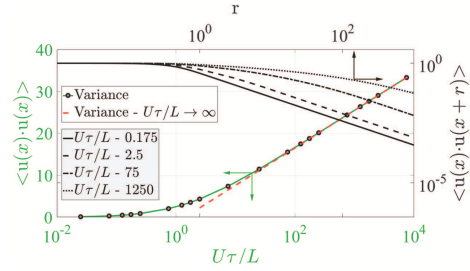


Figure 1: (a) Fluid velocity variance (green) as a function of $U\tau/L$. (b) Fluid velocity covariance (black) as a function of distance (r) for a range of $U\tau/L$.

References

- [1] Sokolov A and Aranson IS, Reduction of viscosity in suspension of swimming bacteria, *Physical Review Letters*, 103, pp. 148101, 2009.
- [2] Lopez HM *et al*, Turning bacteria suspensions into superfluids, *Physical Review Letters*, 115, pp. 028301, 2015.
- [3] Nambiar S *et al*, Stress response in a dilute bacterial suspension II - Active-Passive transition, *Manuscript in preparation*.
- [4] Wu XL and Libchaber A, Particle diffusion in a quasi-two-dimensional bacterial bath, *Physical Review Letters*, 84, pp. 3017, 2000.
- [5] Kasyap TV *et al*, Hydrodynamic tracer diffusion in suspensions of swimming bacteria, *Physics of Fluids*, 26, pp. 081901, 2014.
- [6] Krishnamurthy D and Subramanian G, Collective motion in a suspension of micro-swimmers that run-and-tumble and rotary diffuse, *Journal of Fluid Mechanics*, 781, pp. 422-466, 2015.
- [7] Subramanian G and Koch DL, Critical bacterial concentration for the onset of collective swimming, *Journal of Fluid Mechanics*, 632, pp. 359-400, 2009.
- [8] Subramanian G and Nott PR, The fluid dynamics of swimming microorganisms and cells, *Journal of the Indian Institute of Science*, 91, pp. 283-314, 2011.
- [9] Underhill PT and Graham MD, Correlations and fluctuations of stress and velocity in suspensions of swimming microorganisms, *Physics of Fluids*, 23, pp. 121902, 2011.
- [10] Koch DL and Subramanian G, Collective hydrodynamics of swimming microorganisms: Living fluids, *Annual Review of Fluid Mechanics*, 43, pp. 637-659, 2011.
- [11] Calfisch RE and Luke JHC, Variance in the sedimentation speed of a suspension, *Physics of Fluids*, 28, pp. 759-760, 1985.
- [12] Ladd A, Hydrodynamic Screening in Sedimenting Suspensions of non-Brownian Spheres, *Physical Review Letters*, 76, pp. 1392, 1996.
- [13] Ramaswamy S, Issues in the statistical mechanics of steady sedimentation, *Advances in Physics*, 50, pp. 297-341, 2001.

Optimizing performance of micro-swimmers: the role of hydrodynamic interactions

Nicola Giuliani¹ and Antonio DeSimone²,

¹SISSA — International School for Advanced Studies
Via Bonomea 265, 34136 Trieste, Italy
ngiuliani@sissa.it

²Sant'Anna — Scuola Universitaria Superiore Pisa
Piazza Martiri della Libertà, 56127 Pisa, Italy
antonio.desimone@santannapisa.it

Abstract

The swimming capabilities of unicellular biological organisms is drawing interest in bio-inspired robotic micro-swimmers. The accurate prediction of the swimming performance is a key ingredient for the optimization of such devices. However, hydrodynamic simulations are computational demanding and many simplified models have been developed to ease such demands by neglecting non local interactions. Resistive Force Theory (RFT) is the most notable example, and, given its simplicity, it is extensively used by workers in the field. Unfortunately, RFT cannot correctly reproduce the flagellar motility strategies which are typically employed by biologic organisms, and this lack of accuracy stems from neglecting hydrodynamic interactions. We show through numerical simulation of a model robotic system that the errors introduced by neglecting hydrodynamic interactions between a rotating tail (acting as propeller) and the head to which it is attached are not negligible. Simple correction facotrs can be derived to improve the results obtained using the simplified methods.

Keywords: Hydrodynamic interactions, micro-swimmers, optimization of swimming performance.

1. Introduction

Starting from seminal works of Taylor and Purcell [?, ?] there has been a growing interest in the study of motile cells. On the one hand this research offers insight in the study of complex existing biological problems (from reproductive strategies to disease spreading), on the other hand it can lead to the effective manufacturing of artificial bio-inspired mechanisms. Accurate prediction of the swimming performance is paramount both to understanding the biological motility strategies and to the rational design and performance optimization of artificial robotic micro-swimmers. The present paper addresses the modeling of the swimming problem of motile cells through the introduction of three distinct ingredients: a kinematic model for the position of the swimmer, a dynamic model for the swimmer, and a fluid model for the liquid around the swimmer. Approximations in the hydrodynamics are very common to ease the computational requirements of the simulations needed to optimize swimming performance. Use of Resistive Force Theory (RFT) [?, ?], a simplified theory in which hydrodynamic forces depend only on the local velocity, has become common to address the problem of predicting and optimizing swimming speed. Only recently RFT has been questioned [?], because of its crude approximation of the hydrodynamics around a swimmer. We propose a detailed study of the error introduced by neglecting hydrodynamic interactions between different parts of a model robotic-like swimmer, based on a careful analysis of the associated resistance coefficients. Finally we derive a simple yet effective correction factor to improve the accuracy of the results of the approximated models [?].

2. Methods

Following [?, ?] we consider a swimmer as a time dependent bounded open set $B_t \in \mathbb{R}^d$ with $d = 2, 3$. The map $\psi : \bar{B}_0 \subset \mathbb{R}^d \times [0, T] \rightarrow \mathbb{R}^d$ describes the position x at time

t of a material point X , namely,

$$x(X, t) = \psi(X, t) = q(t) + R(t)s(X, t), \quad (1)$$

where $q(t)$ represents a translation of a point of the swimmer, $R(t)$ is the rotation tensor associated with the rotation of the body frame, and $s(X, t)$ represents the position of all points with respect to the body frame. We focus our analysis on the study of self-propelled micro-swimmers, meaning that only viscous drag forces are acting on the swimmer. Consequently we impose the following dynamic conditions

$$\int_{\Gamma} t(x) d\gamma(x) = 0, \quad (2a)$$

$$\int_{\Gamma} t(x) \wedge (x - x_0) d\gamma(x) = 0, \quad (2b)$$

where x_0 is an arbitrary point of the swimmer and t are the Cauchy stresses acting on the surface Γ of the body. Given the characteristic length scales of the induced flows, the Stokes system is an efficient model for the flow around the swimmer and the associated stresses [?, ?]. Following [?] we obtain the following Boundary Integral Formulation for the problem

$$\alpha(x)u_i(x) - \int_{\Gamma}^{PV} W_{ijk}(x, y)n_k(y)u_j(y)d\gamma_y = \int_{\Gamma} G_{ij}(x, y)t_j(y)d\gamma_y \quad \forall x \in \Gamma, \quad (3)$$

where G, W represent the first two Green tensors associated with the fundamental solution of the Stokes system. We discretize equation (??) using a MPI parallel Boundary Element Method. We impose (??) and (??) as constraints to reconstruct the rigid displacements $q(t), R(t)$ of a generic micro-swimmer starting from the shape variable $s(t)$. In recent years, similar methods have been successfully applied to study motion of bacterium-like swimmers, see e.g. Ramia *et al.* [?]. The resolution of flow fields from full hydrodynamic simulations can be extremely demanding

from a computational point view. For this reason, approximations are often employed and Resistive Force Theory (RFT) [?, ?] is one of the tools most widely used by workers in the field. But while RFT leads to results that are often qualitatively correct, the errors it generates are often too large to be neglected when quantitative accuracy is necessary, and this point has started to emerge only in recent years [?].

In this work we demonstrate that RFT introduces non negligible errors even in cases for which it is generally believed to be accurate. In section ?? we present a rational approach, see [?], to understand the importance of hydrodynamic interaction in a model robotic-like bacterium, and derive expressions for some correction factors to improve the accuracy of the results of the simplified models. It should be emphasized that the correction factors we deduce are model-specific. When more complex flagellar movements and shapes are involved, as in the case of *Euglena Gracilis* in [?], even an optimization of RFT coefficients may be unable to properly recover experimental data. In this case of complex flagellar motility, the full complexity of the complete hydrodynamic interactions may prove necessary.

3. Results

We consider a “robotic” bacterium composed of a rigid spherical head (“body”) and a rotating helical flagellum with fixed shape (“propeller”), we impose the relative angular velocity between head and flagellum to be ω and we assume the motion to be in an unbounded domain. In [?, ?] the author studied the motion of the composite system (head and flagellum) considering the hydrodynamics of the separate components (body and propeller). We call such methodology the “additive approximation” or “additive approach” (AA). Following Purcell’s warning about the actual reliability of such additive technique we compare the results obtained using AA with the complete BEM simulation sketched in Section ??, and we call the latter “global approach” (GA). Following AA we write (??) using the concept of resistive tensors as

$$\begin{bmatrix} A_0 & \\ & C_0 \end{bmatrix} \begin{bmatrix} U \\ \Omega \end{bmatrix} + \begin{bmatrix} A & B \\ B & C \end{bmatrix} \begin{bmatrix} U \\ \Omega - \omega \end{bmatrix} = 0, \quad (4)$$

where A, D are the usual drag and torque coefficients while B represents the coupling coefficient of the propeller. Following GA, instead of invoking AA, we write the velocity field of the swimmer as

$$\underline{v}(x) = U \underline{e} \phi_1(x) + \Omega \underline{e} \wedge (x - x_o) \phi_1(x) + U_2 \underline{e} \phi_2(x) + \Omega_2 \underline{e} \wedge (x - x_o) \phi_2(x), \quad (5)$$

where ϕ_1 and ϕ_2 are the characteristic functions of head and propeller. Requiring $U_2 = U, \Omega_2 = \Omega - \omega$ we write the overall linear and angular momentum balance as

$$\begin{bmatrix} A_1 & \hat{B}_1 \\ \hat{B}_1 & C_1 \end{bmatrix} \begin{bmatrix} U \\ \Omega \end{bmatrix} + \begin{bmatrix} A_2 & \hat{B}_2 \\ \hat{B}_2 & C_2 \end{bmatrix} \begin{bmatrix} U \\ \Omega - \omega \end{bmatrix} = 0. \quad (6)$$

At this point a careful comparison of the solution of (??) and (??) reveals the key importance of hydrodynamic interactions. While the angular velocity Ω is well approximated by AA we see a non negligible error for what concerns the actual swimming speed U . A detailed coefficient analysis reveals that the error caused by neglecting hydrodynamic interaction can be captured by a single coefficient

$$v = \frac{(A_0 + A)(B_1 + B_2)}{(A_1 + A_2)B}, \quad (7)$$

that can be used as a factor to improve the prediction of the swimming speed U obtained by solving (??) for given ω . The factor (??) greatly improves both AA and RFT results, and the error for the swimming velocity U is reduced by almost one order of magnitude for any test case considered.

4. Conclusion

Neglecting hydrodynamic interactions may lead to non negligible errors in the prediction of the swimming performance of micro-swimmers. RFT completely neglects that kind of interactions therefore the errors can be quite dramatic [?], especially when complex flagellar motions are involved [?]. In such cases a full hydrodynamic resolution is necessary. A closer look to the mechanics underlying the swimming strategies shows that it is possible to correct the results coming from RFT and in general from additive approximations as the one described by Purcell in [?]. We have derived a very simple correcting factor for bacteria-like swimmers which has proven to be extremely effective on many different test cases.

Acknowledgement

This work has been supported by the ERC Advanced Grant 340685 MicroMotility. ADS thanks Giancarlo Cicconofri, Giovanni Noselli, and Erik Zorzin for valuable discussions.

References

- [1] Dal Maso, G., DeSimone, A., Morandotti, M., An Existence and Uniqueness Result for the Motion of Self-Propelled Microswimmers, *Society for Industrial {&} Applied Mathematics (SIAM)* vol. 21, pp. 1345–1368, 2011.
- [2] Dal Maso, G., DeSimone, A., Morandotti, M., One-dimensional swimmers in viscous fluids: dynamics, controllability, and existence of optimal controls, *ESAIM: Control, Optimisation and Calculus of Variations*, vol. 21, pp. 190–216, 2015.
- [3] Giuliani, N., Heltai, L., DeSimone, A., Predicting and optimizing micro-swimmer performance from the hydrodynamics of its components: the relevance of interactions, *Soft Robotics*, submitted, 2018.
- [4] Gray, J., Hancock, G. J., The Propulsion of Sea-Urchin Spermatozoa, *Journal of Experimental Biology*, vol. 32, pp. 802–814, 1955.
- [5] Lighthill, J., Flagellar Hydrodynamics, *SIAM Review*, vol. 18, no. 2, pp. 161–230, 1976.
- [6] Pozrikidis, C., Boundary Integral and Singularity Methods for Linearized Viscous Flow, *Cambridge University Press*, 1992.
- [7] Purcell, E. M., Life at low Reynolds number, *American Journal of Physics*, vol. 45, no. 1, pp. 3–11, 1977.
- [8] Purcell, E. M., The efficiency of propulsion by a rotating flagellum, *Proc. Natl. Acad. Sci. USA*, vol. 94, pp. 11307–11311, 1997.
- [9] Ramia, M., Tullock, D. L., Phan-Thien, N., The role of hydrodynamic interaction in the locomotion of microorganisms *Biophysical Journal Volume*, vol. 65, pp. 755–778, 1993.
- [10] Rodenborn, B., Chen, C.H., Swinney, H. L., Liu, B., Zhang, H. P., Propulsion of microorganisms by a helical flagellum, *Proceedings of the National Academy of Sciences of the United States of America*, vol.110, no. 5, pp E338–E347, 2013.

[11] Rossi, M., Cicconofri, G., Beran, A., Noselli, G., DeSimone, A., Kinematics of flagellar swimming in *Euglena gracilis*: Helical trajectories and flagellar shapes, *Proceed-*

ings of the National Academy of Sciences, vol. 114, no. 50, pp. 13085–13090, 2017.

Study of biological and bio-inspired swimming at low Reynolds numbers using an immersed boundary method

Valentina Meschini¹, Giovanni Noselli², Mauro Chinappi³, Roberto Verzicco⁴, Antonio DeSimone⁵

¹SISSA - International School for Advanced Studies
Via Bonomea 265, 34136 Trieste, Italy
vmeschin@sissa.it

²SISSA - International School for Advanced Studies
Via Bonomea 265, 34136 Trieste, Italy
gnoselli@sissa.it

³UniRoma2 - Universita' di Roma Tor Vergata
Via del Politecnico 1, 00133 Roma, Italy
chinappi@uniroma2.it

⁴UniRoma2 - Universita' di Roma Tor Vergata
Via del Politecnico 1, 00133 Roma, Italy
verzicco@uniroma2.it

⁵The BioRobotics Institute. Sant'Anna - Scuola Universitaria Superiore Pisa
Piazza Martiri della Liberta', 56127 Pisa, Italy
antonio.desimone@santannapisa.it

Abstract

The hydrodynamics of flagellated micro-swimmers is investigated by means of numerical solution of the Navier-Stokes equations. We use a fluid-structure interaction algorithm and an immersed boundary method for the time integration in complex geometries, and explore the effects of 3D flow unsteadiness on the system behaviour. Moreover, we analyse the role of the helical tail geometry on the resulting hydrodynamic forces and therefore on the swimmer dynamics. The numerical findings are validated with experimental results from a robotic micro-swimmer realized by means of additive manufacturing (3D printing). Future investigations will also include the analysis of fluid flow by application of Particle Image Velocimetry techniques.

Keywords: Immersed boundary method, fluid-structure interaction, micro-swimmers hydrodynamics

1. Introduction

The study of the physics of locomotion at low Reynolds number from a mathematical and fluid dynamics point of view has a long history, as highlighted in papers [1, 2, 3, 4, 5, 6, 7, 8, 9] where the locomotion properties of different swimmers like *E. coli* or *Euglena* are theoretically and experimentally investigated. The interest for this research field is now increasing because of the potential bio-medical applications of bio-inspired soft robotics, and also due to advances in visualization and experimental techniques leading to better understanding of cell motility. Nevertheless, many relevant issues still need clarification. In terms of computational modelling, the impact of complex and unsteady 3D flows in the interaction between parts of a swimmer, or between a swimmer and the surrounding fluid have yet to be addressed in order to obtain reliable quantitative models [10]. Also the inertial effects due to the pulsatile motion of appendices used for propulsion, pumping, or stirring are often quite important, and need to be resolved accurately. To these aims, the use of Navier-Stokes equation for the fluid model and the inclusion in the model of a Fluid-Structure Interaction (FSI) algorithm which provides the coupling of flow and body dynamics of the swimmers (or of flow and deforming confining walls in a microfluidic device) are unavoidable. It produces a synergistic functioning of flow and structure: the instantaneous configuration of the solid body is given by the fluid dynamics loads and on the other side the flow dynamics is powered by the swimmer's or wall deforma-

tion.

2. Methods

The backbone of the model is a direct numerical simulation (DNS) solver for the time-dependent incompressible viscous flow; it discretizes the Navier-Stokes equations by central second order accurate finite difference schemes that are energy conserving in the inviscid limit. The resulting system of discrete equations is solved by a fractional-step procedure that yields a solenoidal velocity field at each time step. Detailed description of the scheme can be found in [11]. The integration of the Navier Stokes equations on a time dependent domain with moving and deforming boundaries is performed using the Immersed Boundary (IB) method. In this context, forcings in the Navier-Stokes equation can be used to impose a velocity boundary condition over a surface that does not conform to the coordinate lines. This approach is very attractive because it avoids the necessity of body fitted meshes and it handles moving and/or deforming bodies within unsteady three-dimensional flows, [12]. The fluid dynamic solver is two-way-coupled to the structural solver which computes the structure deformations by imposing the local instantaneous balance between the inertia forces, the elastic body forces and the external hydrodynamic loads. The structure dynamics is solved using an interaction potential approach, [13]. The idea is to discretize the micro-swimmer surface with triangular elements and to distribute all the mass on the triangles vertices; all the iner-

tial loads are computed through an interaction potential approach, accounting for the total potential energy of the system, converted into nodal force by applying first derivative in space. Then, knowing the mass and the acceleration at each node and by successive iterations, the velocity and the instantaneous configuration of the structure are obtained. This model allows us to consider both piecewise-rigid structures and deformable ones, which can be a very interesting topic for further studies. The core of the model is the unavoidable coupling of fluid and structure solvers: the fluid equations are advanced first and then, from pressure and viscous stresses, the hydrodynamic loads on the structure are computed. As mentioned above, the whole numerical set-up is accompanied by an ad-hoc experimental set-up suitable for the validation of the numerical results.

3. Conclusion

In this work we study the hydrodynamics of a flagellated micro-swimmer exploiting the hydrodynamics induced by fluid-structure interactions at low Reynolds numbers. We want to assess the effects of 3D flow unsteadiness on the system behaviour. Thus, instead of the usual Stokes equations for the fluid model, the Navier-Stokes one are employed. The effects of the helical tail on the swimmer dynamic and the resulting hydrodynamic forces are evaluated by employing different tail shapes. Moreover the pulsatile motion of the flagellum and its effects in proximity of the swimmer body are analyzed. Finally comparisons between numerical results and experimental measurements by means of hydrodynamics forces and dynamics for a robotic micro-swimmer are discussed.

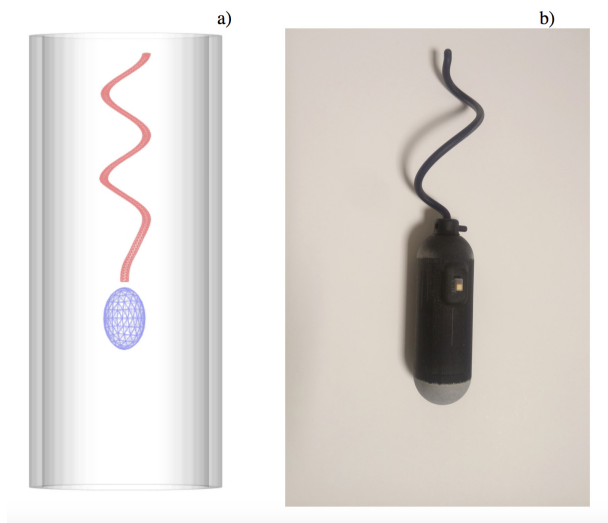


Figure 1: a) Preliminary numerical set-up for the "robotic" swimmer. b) 3D printed robotic swimmer for the experimental set-up.

References

- [1] Pratt, L. A., Kolter, R., Genetic analysis of *E. coli* biofilm formation: roles of flagella, motility, chemotaxis and type I pili, *Mol. Microbiol.*, vol. 30, pp. 285-293, 1998.
- [2] Rusconi, R., Lecuyer, S., Guglielmini, L., Stone, H.A., Laminar flow around corners triggers the formation of biofilm streamers, *J. R. Soc. Interface*, vol. 7, pp. 1293-1299, 2010.
- [3] Squires, T. M., Quake, S., Microfluidics: fluid physics at the nanoliter scale, *Rev. Mod. Phys.*, vol. 77, pp. 977-1026, 2005.
- [4] Purcell, E. M., Life at low Reynolds number, *American Journal Physics*, vol. 45, 1977.
- [5] Fauci, L., Dillon, R., Biofluidmechanics of reproduction, *Ann. Rev. Fluid. Mech.*, vol. 38, 371-394, 2006.
- [6] Lauga, E., Powers, T., The hydrodynamics of swimming microorganisms, *Rep. Prog. Phys.*, vol. 72, 2009.
- [7] Alogues, F., De Simone, A., Heltai, L., Lefebvre-Lepot, A., Merlet, B., Optimally swimming Stokesian robots, *J. Discr. Contin. Dyn. Syst.*, vol. 18, pp.1189-1215, 2013.
- [8] Kwaming, S., Guasto, J. S., Stocker, R., Bacteria can exploit a flagellar buckling instability to change direction, *Nature Physics*, vol. 9, pp. 494-498, 2013.
- [9] Rossi, M., Cicconofri, G., Beran, A., Noselli, G., DeSimone, A., Kinematics of flagellar swimming in *Euglena gracilis*: Helical trajectories and flagellar shapes, *Proceedings of the National Academy of Sciences USA*, vol. 114, pp.13085-13090, 2017.
- [10] Giuliani, L., Heltai, L., DeSimone, A. Predicting and optimizing micro-swimmer performance from the hydrodynamics of its components: the relevance of interactions, *Soft Robotics*, in press, 2018.
- [11] Van der Poel, E. P., Ostilla-Manico, R., Verzicco, R., A pencil distributed finite difference code for strongly turbulent wall-bounded flows, *Computers & Fluids*, vol. 116, pp. 10-16, 2015.
- [12] Spandan, V., Meschini, V., Ostilla-Monico, R., Lohse, D., Querzoli, G., De Tullio, M. D., Verzicco, R., A parallel interaction potential approach coupled with the immersed boundary method for deformable interfaces and membranes, *J. Comp. Phys.*, vol. 348, pp.567-590, 2017.
- [13] Fedosov, D., Multiscale modelling of blood flow and soft matter, *PhD thesis, Brown University*.

Linking individual and collective dynamics of sperm in suspension

Simon F. Schoeller¹ and Eric E. Keaveny^{1*}

¹Imperial College London
Department of Mathematics
South Kensington Campus
London SW7 2AZ, UK
simon.schoeller14@imperial.ac.uk
e.keaveny@imperial.ac.uk

Abstract

Swimming cells are often modelled as simple, rigid objects immersed in a fluid, on which they exert steady, dipolar forces. Such reduced models allow for simulations of large numbers of cells. These simulations predict local alignment, the formation of instabilities and active turbulence. Reduced models, however, do not resolve the time-varying actuation and diverse shapes of cells, such as sperm cells, propelled by undulating, elastic flagella. Here, we explore how time-varying features of cells impact collective motion on a larger scale. We simulate dense suspensions of up to 1000 swimmers. Our model includes elastic, undulating flagella and resolves the resulting Newtonian fluid flow in a quasi-two-dimensional setting. Changing the variability of flagellar undulations gives rise to drastically different collective motion, ranging from cluster formation to active swirls. Quantitative analysis of actively swirling states shows that fluctuations on the length scale and time scale of individual undulations contribute substantially to the fluid's overall energy.

Keywords: sperm locomotion, collective dynamics, fluid-structure interaction, force-coupling method

1. Introduction

Sperm cells across a wide range of species have similar shapes and propulsion mechanisms. Due to the time-averaged far-field of individual sperm cells, induced by flagellar undulations, they are typically classified as *pushers*. At typical separations between sperm cells, however, the temporal fluctuations and higher order force contributions to flows induced by individual sperm cells can get relatively large compared to the dipolar contributions.

Reduced models that approximate cells as pushers predict long-ranged instabilities of polar configurations that result in turbulence-like states with finite velocity correlation lengths (Ref. [1]). Related states can be observed in bacterial baths (Ref. [2]), but also in bull and ram semen (Ref. [3]).

In some species, however, sperm cells form ordered clusters or even remain bundled after ejaculation. Within clusters and bundles, flagella tend to align so as to synchronise their waveforms. Computational studies of up to ~ 100 swimmers show that hydrodynamic interactions can lead to synchronisation and aggregation (Ref. [4]).

Do clustering and turbulence-like states arise for different types of sperm cells, at different densities, or is there a transition between clustering and swirling dynamics? Through simulations we aim at making progress in answering this question.

Focusing on a model of sperm cells propelled by elastic flagella that move in a plane, we simulate the collective dynamics of up to 1000 swimming cells for several hundred undulation periods. We include hydrodynamic interactions through a three dimensional Newtonian fluid and compare the results to a model with local friction only (resistive force theory). We either impose fixed undulation frequencies on all cells or allow for stochastic variability of individual undulation frequencies over time.

We refer to Ref. [5] for details beyond the scope of this abstract.

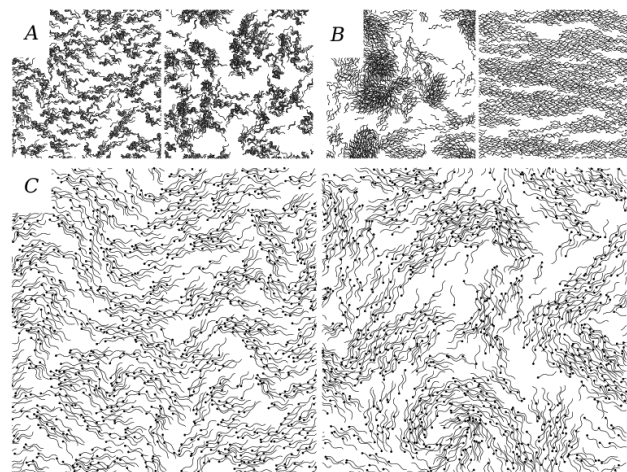


Figure 1: Snapshots of suspensions of 1000 undulating swimmers reveal qualitatively different behaviour. **A** A single, fixed undulation frequency leads to cluster formation. (Here, after 30 and 198 periods.) **B** Randomly varying undulation frequencies, without hydrodynamic interactions (local friction only), yield jamming or laning behaviour. (Here, after 340 periods.) **C** Stochastic undulations and full hydrodynamics, yield a bending instability and active swirls. (Here, after 30 and 198 periods.) Figure adapted from Ref. [5].

* S.F.S. gratefully acknowledges funding by an Imperial College President's PhD scholarship. E.E.K. acknowledges support from EPSRC grant EP/P013651/1.

2. Results

Our simulations reveal that, even on larger scales, a low variability of frequencies results in aggregation and synchronization of flagella (Fig. 1A), whereas a high variability gives rise to bending waves and swirls in initially ordered configurations (Fig. 1C). Both types of collective motion can occur at identical length scales and number densities. They disappear when hydrodynamic interactions are switched off (Fig. 1B). By comparing cases with polar and homogeneous initial configurations to cases with isotropic and homogeneous initial conditions, we find that the swirling state arises independent of the initial configuration.

We quantify both the initial decay of global alignment and the subsequent turbulence-like state. As expected from kinetic theory, systems with higher densities of swimmers show a faster decay of global order, hence, a faster transition to turbulence.

Analysing the swirling states, we find that flows on the time scales and lengths of flagellar undulations dominate the energy injection into the fluid, for the system sizes used. Considering time-scales longer than average undulation periods by applying a low-pass filter to the velocity fields, we find that collective swimming leads to long-range correlations of the swimmers' velocities as well as the fluid's velocity field.

3. Features of the swimmer model

Each cell consist of a head and a flagellum. The head is modelled as a rigid spheroid. The flagellum is treated as an inextensible, elastic beam, governed by the beam equations

$$\frac{d\mathbf{\Lambda}}{ds} + \mathbf{f} = 0, \quad \frac{d\mathbf{M}}{ds} + \hat{\mathbf{t}} \times \mathbf{\Lambda} + \boldsymbol{\tau} = 0. \quad (1)$$

Here, s is an arc-length parametrisation, $\hat{\mathbf{t}}$ the tangent vector, $\mathbf{\Lambda}$ is the tension, and the elastic bending moment is defined as $\mathbf{M} = K\hat{\mathbf{t}} \times d\hat{\mathbf{t}}/ds$ for bending modulus K . The force and torque density, \mathbf{f} and $\boldsymbol{\tau}$, include barrier forces, hydrodynamic forces and torques, as well as internal driving torques based on a preferred curvature model.

In this model, the driving torque density is chosen such that, in the absence of hydrodynamic drag, the preferred curvature $\kappa_\omega(s, t) = \kappa_\omega(s, t + 2\pi/\omega)$ would be attained at time t and arc-length s . Our choice of $\kappa(s, t)$ is approximately sinusoidal, decreasing towards the distal end.

We include stochastic frequency changes by modifying the undulation frequency ω after fixed time intervals, re-drawing it from a log-normal distribution with standard deviation σ_ω for every swimmer. The shape and evolution of the flagellum arises from solving the beam equations.

After discretisation, hydrodynamic forces and torques yield a hydrodynamic mobility problem, which we solve using the force-coupling method (Ref. [6]), to obtain the velocities and angular velocities of hydrodynamically interacting particles. We use a

backward differentiation scheme to integrate the velocities and angular velocities of material points along the flagellum in time. In simulations with resistive force theory, we replace hydrodynamic interactions by anisotropic friction coefficients.

4. Discussion

By varying the undulation frequencies' standard deviation we could see that the same initial state can result in clusters ($\sigma_\omega = 0$, Fig. 1A) or swirls ($\sigma_\omega = \langle \omega \rangle / 5$, Fig. 1C). Both phenomena, clustering and the instability, are determined by hydrodynamic interactions. The frequency standard deviation can be viewed as a proxy for variability across sperm cells.

More generally, we see that not only individual cells' properties, but also their distribution across a suspension can influence the suspension dynamics. Our simulations show that the details of the individual propulsion mechanism, beyond reduced descriptions, have an influence on larger scale dynamics. The different collective modes found suggest that it is worthwhile resolving individual cell's features in large-scale simulations.

Future work will include fully three dimensional dynamics of beating flagella. Active responses to the environment and non-Newtonian rheology could lead to additional diversity in collective behaviour.

References

- [1] Saintillan, D. and Shelley, M.J., Emergence of coherent structures and large-scale flows in motile suspensions. *J. R. Soc. Interface*, 9:571–585, 2011.
- [2] Wensink, H.H., Dunkel, J., Heidenreich, S., Drescher, K., Goldstein, R.E., Löwen, H. and Yeomans, J.M., Meso-scale turbulence in living fluids. *Proc. Natl. Acad. Sci. USA*, 109(36):14308–14313, 2012.
- [3] Creppy, A., Praud, O., Druart, X., Kohnke, P.L., Plouraboué, F., Turbulence of swarming sperm. *Phys. Rev. E* 92(032722), 2015.
- [4] Yang Y., Elgeti J., Gompper G., Cooperation of sperm in two dimensions: Synchronization, attraction, and aggregation through hydrodynamic interactions. *Phys. Rev E* 78(061903), 2008.
- [5] Schoeller, S.F., Keaveny E.E., From flagellar undulations to collective motion: predicting the dynamics of sperm suspensions. *arXiv:1801.08180* [physics.flu-dyn], 2018.
- [6] Maxey, M.R., Patel, B.K., Localized force representations for particles sedimenting in stokes flow. *Int. J. Multiphase Flow* 27:1603–1626, 2001.

E. coli swimming and scattering at surfaces — A mesoscale simulation study

Mahdiyeh Mousavi, Thomas Eisenstecken, Gerhard Gompper, and Roland G Winkler

¹Theoretical Soft Matter and Biophysics, Institute for Advanced Simulation and Institute of Complex Systems
Forschungszentrum Jülich, 52428 Jülich, Germany

m.mousavi@fz-juelich.de, g.gompper@fz-juelich.de, r.winkler@fz-juelich.de

Abstract

Surface effects play a decisive role in the behavior of microorganisms adjacent to surfaces, e.g., in biofilm formation. Thereby, steric as well as hydrodynamic interactions determine the swimming pattern. We present results of mesoscale hydrodynamic simulations combining the multiparticle collision dynamics approach for fluids with molecular dynamics simulations for *E. coli*-type bacteria. The adsorption of a cell at a no-slip surface is determined by steric interactions; hydrodynamic interactions play a minor role in this process. However, swimming at a surface is determined by hydrodynamics, and bacteria swim on clockwise or counterclockwise circular trajectories depending on the surface slip properties.

Keywords: *E. coli*, mesoscale hydrodynamic simulations, wall entrapment, surface swimming

1. Introduction

As is well known by now, microswimmers accumulate at surfaces [1, 2]. Yet, the physical mechanism is still under debate. Two aspects contribute to the swimming behavior next to surfaces. On the one hand, steric effects are important and an approaching and impacting anisotropic microswimmer experience an additional torque leading to parallel alignment of its major axis with the surface. On the other hand, surface hydrodynamic interactions play a role. Depending on the type of microswimmer, such interactions imply either parallel alignment for so-called pushers, e.g., *E. coli*-type bacteria, or perpendicular alignment for pullers, e.g., *Chlamydomonas Reinhardtii*. Here, we show that the alignment of an *E. coli* bacterium is mainly determined by steric interactions. Hydrodynamic interactions play a major role as soon as the cell swims at the surface. Thereby, the trajectory depends on the slip properties of the surface. For no-slip surfaces, clockwise trajectories are obtained, whereas for slip surfaces counterclockwise trajectory appear.

2. Model

A bacterium cell is composed of a spherocylindrical body and five attached helical flagella, which are constructed by point particles of mass M , linked by a harmonic potential

$$U_{bd} = \frac{1}{2} K_{bd} (r - r_e)^2, \quad (1)$$

where r is the distance between two points, r_e the equilibrium bond length, and K_{bd} the spring constant. The filaments are described by the helical wormlike chain model [3], with the elastic energy

$$U_{el} = \frac{1}{2} \sum_{\alpha=1}^3 K_{el}^{\alpha} \sum_{n=1}^{N-1} (\Omega_n^{\alpha} - \Omega_e^{\alpha})^2. \quad (2)$$

Here, $K_{el}^1 = K_{el}^2$ is the bending strength, K_{el}^3 the twist strength, and Ω_n the strain vector [3]. A repulsive Lennard-Jones potential is applied to prevent a flagellum from crossing the cell body or another flagellum. The bacteria cell is then embedded in a fluid which is modelled by multiparticle collision dynamics (MPC)

method, resulting in both hydrodynamic and stochastic interactions. The cell is propelled in the fluid by rotating flagella, where rotation is induced by a motor torque τ acting on each flagellum and an opposite torque $-\tau$ exerted on the body, hence there is no net force and torque on the cell. Further details and the selected parameters can be found in Ref. [3].

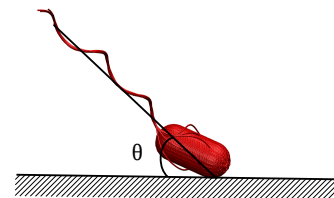


Figure 1: Illustration of an *E. coli* cell touching a wall, and definition of the pitch angle.

3. Results: Surface Scattering

The time evolution of height and pitch angle of a cell with initial orientation angle $\theta = 45^\circ$ (see Fig. 1) swimming toward the wall is depicted in Fig. 2. As already observed experimentally [4], three main stages of wall entrapment (approach, alignment, surface swimming) can be identified in our simulations. Evidently, the pitch angle changes significantly only after the cell sterically interacts with the wall. Hence, far field hydrodynamic interactions contribute very little to the reorientation of the bacterium. However, hydrodynamic interactions manifest themselves during the cell approach by a reduction of the vertical speed as expected from far-field hydrodynamics. As shown in Fig. 3, the vertical velocity decreases by more than a factor of two when cells approach the surface. The velocity change affects the impact angle of the cell with respect to the surface and the angle after impact is somewhat smaller than the starting angle. At the surface swimming stage, the cell swims with a slightly positive angle pointing toward the wall. By using the inertia tensor of the swimming

cell and measuring the main axis of rotation, we obtain the pitch angle of the cell with an average pitch angle of 1.6° which is in-between the prediction from theory (-2.6°) [5] and experiments (approx. 10°) [4]. Furthermore, swimming cells wobble around the swimming direction with particular angle denoted as wobbling angle. The average wobbling angle of our swimming cell is about 6.5° (Fig. 2 the fast oscillations of the red curve). In addition, from the power spectral density of the swimming cell, we find that the bundle rotates five times faster than the body which is consistent with experimental results.

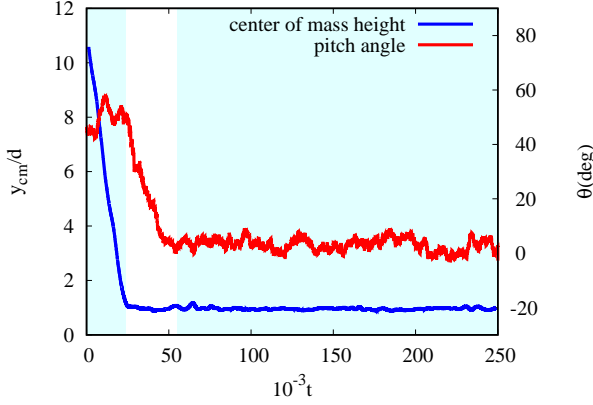


Figure 2: Wall distance (blue) of the center-of-mass of the cell body and pitch angle (cf. Fig. 1) as function of time (MPC time units). d denotes the diameter of the cell body.

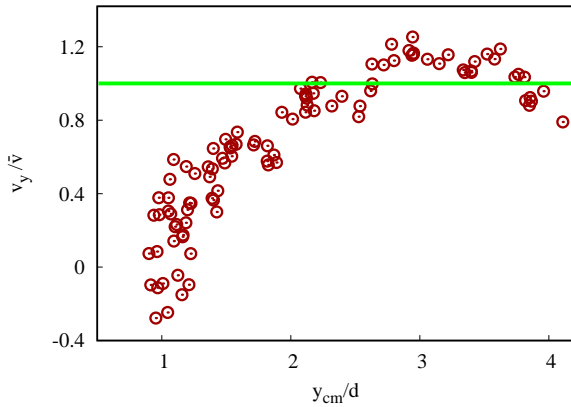


Figure 3: Vertical velocity as function of the the center-of-mass distance of cells from the wall. \bar{v} is the average vertical velocity.

4. Results: Surface Swimming

Hydrodynamic interactions evidently affect the properties of absorbing cells only weakly. However, in the adsorbed stage, hydrodynamics determines the trajectory of a cell. As illustrate in Fig. 4, *E. coli* bacteria swim on clockwise (CW) or counterclockwise (CCW) circle trajectory at no-slip or slip surfaces, respectively [6], as a consequence of a torque appearing by the counter-rotation of the body and the flagellar bundle. Quantitatively, the dependence of the curvature κ of a trajectory of the slip length is very well described by the analytical expression

$$\kappa = \frac{\kappa_0 - \kappa_\infty}{1 + b/h_{\text{eff}}} + \kappa_\infty, \quad (3)$$

where $\kappa_0 = \kappa(b = 0)$ (no slip), $\kappa_\infty = \kappa_\infty(b = \infty)$ (perfect slip), and h_{eff} is the effective height above the surface, as illustrated in Fig. 4. The analytical expression describes the simulation data very well. Considering the range of slip lengths in the range of several ten nanometers, bacteria cells sense surface slip on the nanoscale.

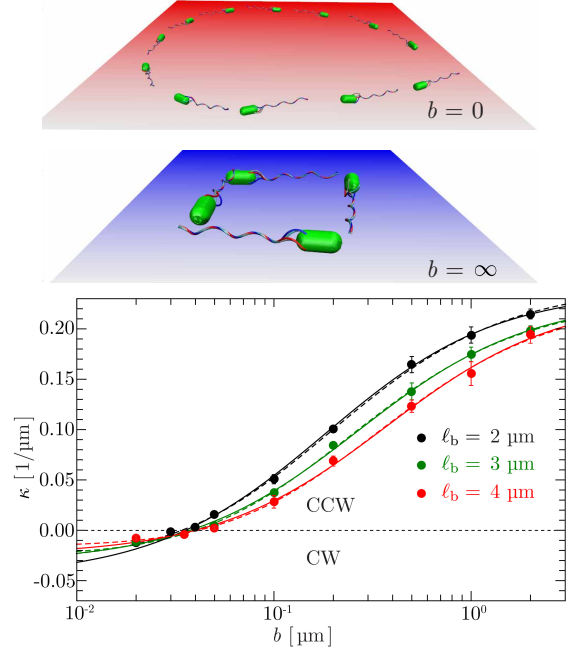


Figure 4: (Top) Clockwise and counterclockwise trajectories of *E. coli* bacteria at no-slip ($b = 0$) and slip ($b = \infty$) surfaces, respectively. (Bottom) Average curvature κ of trajectories of cells of various lengths as function of the surface slip length b . The solid line is a least-square fit of simulation data (bullets) by Eq. 3 (for the dashed line, cf. [6]).

References

- [1] Elgeti, J., Winkler, R. G., and Gompper, G., Physics of microswimmers—single particle motion and collective behavior: a review, *Rep. Prog. Phys.*, 78, 056601, 2015.
- [2] Elgeti, J., and Gompper, G., Microswimmers near surfaces, *Eur. Phys. J. Spec. Top.* 225, 2333, 2016.
- [3] Hu, J., Yang, M., Gompper, G., and Winkler, R. G., Modelling the mechanics and hydrodynamics of swimming *E. coli*, *Soft Matter*, 11, 7867, 2015.
- [4] Bianchi, S., Saglimbeni, F., and Di Leonardo, R., Reynolds number scaling of particle preferential concentration in turbulent channel flow, *Phys. Rev. X*, 7, 011010, 2017.
- [5] Shum, H., Gaffney, E. A., and Smith, D. J., Modelling bacterial behaviour close to a no-slip plane boundary: the influence of bacterial geometry, *Proc. R. Soc. A*, 466, 1725, 2010.
- [6] Hu, J., Wysocki, A., Winkler, R. G., and Gompper, G., Physical sensing of surface properties by microswimmers – directing bacterial motion via wall slip, *Sci. Rep.* 5, 9586, 2015.

Swimming and rafting of *E.coli* microcolonies at air-liquid interfaces

Giorgia Sinibaldi¹, Valerio Iebba² and Mauro Chinappi*

¹Dipartimento di Ingegneria Meccanica e Aerospaziale, Università di Roma La Sapienza
Via Eudossiana 18, 00184 Roma, Italia

²Gustave Roussy Cancer Campus (GRCC), Institut National de la Santé et de la Recherche Médicale (INSERM) U1015 and Equipe Labellisée-Ligue National contre le Cancer, 114 Rue Edouard Vaillant, 94800 Villejuif, France Istituto Pasteur Cenci Bolognetti Foundation, Public Health and Infectious Diseases Dept., Sapienza Università di Roma, Piazzale Aldo Moro 5, 00185 Roma, Italia

³Dipartimento di Ingegneria Industriale, Università di Roma Tor Vergata,
Via del Politecnico 1, Roma 00133, Italia
mauro.chinappi@uniroma2.it

Abstract

The dynamics of active colloidal suspension and swimming microorganisms are strongly affected by the presence of solid-liquid and air-liquid interfaces. In this contribution, we discuss the motion of *E. coli* at air-liquid boundary. We observed and characterized the motion of both single *E. coli* and microcolonies. Both of them follow circular trajectories. Single bacteria preferentially show a counter-clockwise motion, in agreement with previous experimental and theoretical findings. Instead, no preferential rotation direction is observed for microcolonies suggesting that their motion is due to a different physical mechanism. We propose a simple mechanical model where the microcolonies move like rafts constrained to the air-liquid interface to explain the experimental data. Finally, we observed that the microcolony growth is due to the aggregation of colliding single-swimmers, suggesting that the microcolony formation resembles a condensation process where the first nucleus originates by the collision between two single-swimmers.

Keywords: Microswimmers, Microcolonies, *E. coli*

1. Introduction

The swimming of single bacteria and the collective motion of microorganisms have attracted the interest of a varied community. Accumulation at interface (both solid-liquid and air-liquid) was studied with a number of theoretical, computational and experimental approaches, and several puzzling phenomena such as up-stream flowing and oscillatory motion in microchannel emerged when bacteria swim under strong confinement, for a review, see e.g. [1]. Here we kept *Escherichia coli* as a bacterial model to analyze the motion of single swimmer and microcolonies at air-liquid interface.

2. Methods

Details on the *E. coli* culture, on the experimental setting and on the image acquisition protocol can be found in Sinibaldi et al. [2]. In brief, a droplet of the *E. coli* suspension was deposited on a coverslip. Then the coverslip was put upside-down on a concave glass slide to reduce the evaporation rate. Images are acquired through the 40X objective of an inverted optical microscope at 50 fps.

3. Results

Both isolated *E. coli* and microcolonies follow circular trajectories. Single bacteria preferentially show a counter-clockwise motion. In few cases, complete circles are apparent (Fig. 1B) while, the more frequent condition is characterized by circular arcs connected by cusps (Fig. 2A). Each cusp corresponds to a tumbling event where the *E. coli* momentarily stops its motion and changes swimming direction. Clockwise (CW) and counter-clockwise (CCW) motion of flagellated microswimmers close to

an interface can be explained in terms of fluid dynamic interaction between the swimmer and the surface. No-slip boundary condition at the fluid interface gives rise to CW motion, while swimming close to a free-slip interface results in CCW trajectories [3, 4, 5]. Our results show that CW swimmers are slightly slower than CCW ones, while no statistically significant difference is found concerning the radius of curvature R of the trajectories (p -value > 0.05) (Fig. 1C).

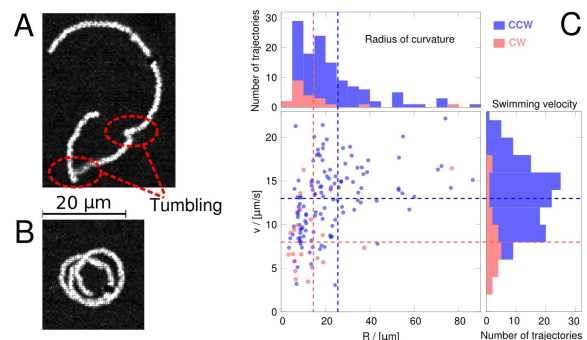


Figure 1: Single *E. coli*. The microswimmer trajectories are constituted by a sequence of circular arcs (A,B). The cusps between two consecutive arcs correspond to tumbling events. C) Radius of curvature R vs swimming velocity v . Red and blue points refer to CW and CCW trajectories, respectively. Horizontal and vertical dashed lines are the mean values. CCW swimmers move significantly faster than CW swimmers (p -value $< 10^{-6}$) while radius of curvature difference are not statistically significant (p -value > 0.05). Image adapted from [2].

*bla blaf

The occurrence of a small percentage of CW swimming bacteria can be ascribed to the presence of molecules in the media that can alter the usual free-slip behavior of an air-liquid interface resulting in region with higher viscosity where no-slip or partial slip conditions hold. Indeed, the local presence of high concentration of molecules secreted by bacteria in specific regions, would result in an increase of the local viscosity [6]. This occurrence can explain also the smaller velocity of the CW swimmer.

Microcolonies. Differently from the single swimmers, microcolonies do not show a preferential direction of rotation. CW (Fig. 2D-F) and CCW (Fig. 2A-C) rotations occur with the same probability. The average speed of microcolonies is lower than single swimmer one and no significant difference in the speed of CW and CCW rotating colonies is observed. These occurrences indicate that the mechanism underlying the microcolony motion is different from the single swimmer. We propose a simple mechanical model where the microcolonies move like rafts constrained to the air-liquid interface to explain the experimental data. In brief, the raft is modeled as a 2D rigid body, hence, three degrees of freedom, namely the position of the center of mass $\mathbf{x}_{cm} = (x_{cm}, y_{cm})$ and the angle θ between the x -axes of the fixed reference system and the unit vector $\hat{\mathbf{e}}_1$ of the body fixed frame of reference, completely describe the motion. The equation of motion are obtained from i) the balance between viscous drag ($\mathbf{F}_\mu = -D \mathbf{v}_{cm}$, with D the translational drag coefficient and $\mathbf{v}_{cm} = \dot{\mathbf{x}}_{cm}$) and external force \mathbf{F}_b resulting from the thrust exerted by the bacteria on the raft and ii) the balance of viscous torque ($T_\mu = -G \omega$ with G the rotational drag coefficient and $\omega = \dot{\theta}$ the angular velocity) and the torque T_b due to the bacteria. After few algebra, we get the following expression for the radius of curvature of the trajectory of the raft center

$$R = \frac{|\mathbf{v}_{cm}|}{\omega} = \frac{|\mathbf{F}_b|G}{T_b D}.$$

A positive R corresponds to CCW motion while negative R to CW. It is worth noting that the sign of R depends only on T_b . If the orientation and the distribution of force exerted by the bacteria are unbiased, positive and negative T_b have the same probability and, consequently, CW or CCW motion occur with the same frequency. Hence, this simple model easily explains the main observations of our work, i.e. the circular motion of the microcolony and the absence of a preferential direction in the microcolony rotation. Finally, we observed that the microcolony growth is due to the aggregation of colliding single-swimmers, suggesting that the microcolony formation resembles a condensation process where the first nucleus originates by the collision between two single-swimmers.

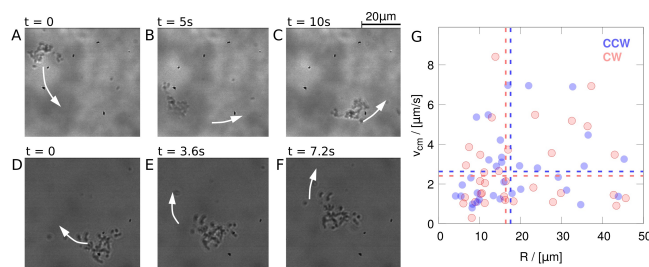


Figure 2: Single *E. coli*. Microcolonies move like 2D rigid raft suspended at the air-liquid interface and exhibit both CCW (A-C) and CW motion (D-F). Panel G reports the scatter plot of the speed $|\mathbf{v}_{cm}|$ vs the radius of curvature R of the trajectory of the microcolony center. Red and blue symbols refer to CW and CCW motion, respectively. Horizontal and vertical lines correspond to the average CW and CCW radius of curvature and speed. No significant difference is observed between CW and CCW for both average speed and radius of curvature. Image adapted from [2].

4. Conclusion

We analyzed experimental data on *E. coli* motion at air-liquid interface. We characterized the motion of both single swimmers and microcolonies and circular trajectories were observed in both cases. For microcolonies motion, we proposed a simple mechanical model where the colony is described as a raft suspended at the air-liquid interface and each bacterial cell at the raft contour exerts a thrust. This toy model allows to qualitatively explain why no preferential rotation direction exists and to predict the scaling of raft velocity, angular velocity on the raft size. We also reported preliminary evidences on aggregation by collision and disgregation phenomena of pre-formed microcolonies. Our data suggest that collision is an important mechanism for microcolony growth, and it could have pitfalls in clinics. We also observed disgregation events where a small portion of large microcolony splits and starts rafting independently. This last phenomenon can potentially play a relevant role in propagation of infections through biofilm dispersal. Future directions of the present work would encompass dynamic experiments to simulate different shear-stress conditions, thus envisioning a broader behavior of microcolonies at air-liquid interface and to develop computational tools able to simulate raft swimming, splitting and aggregation.

References

- [1] Elgeti, J., Winkler, R.G., and Gompper, G., Physics of microswimmers-single particle motion and collective behavior: A review, *Rep. Prog. Phys.*, 78, 056601, 2015.
- [2] Sinibaldi, G., Iebba, V. and Chinappi, M., Swimming and rafting of *E. coli* microcolonies at air-liquid interfaces, *MicrobiologyOpen*, 2017.
- [3] Di Leonardo, R., Dell'Arciprete, D., Angelani, L., and Iebba, V., Swimming with an image, *Phys. Rev. Lett.*, 106, 038101, 2011.
- [4] Lauga, E., DiLuzio, W.R., Whitesides, G.M., and Stone, H.A., Swimming in circles: Motion of bacteria near solid boundaries, *Biophys. J.*, 90, pp 400–412, 2006.
- [5] Pimponi, D., Chinappi, M., Gualtieri, P., and Casciola, C.M., Hydrodynamics of flagellated microswimmers near free-slip interfaces, *J. Fluid. Mech.*, 789, pp 514–533, 2016.
- [6] Morse, M., Huang, A., Li, G., Maxey, M.R., and Tang, J.X., Molecular adsorption steers bacterial swimming at the air/water interface, *Biophys. J.*, 105, pp 21–28, 2013.

Oscillatory surface rheotaxis of swimming *E. coli* bacteria

Arnold J. T. M. Mathijssen¹, Nuris Figueroa-Morales², Gaspard Junot², Eric Clement², Anke Lindner² and Andreas Zöttl³ *

¹Department of Bioengineering, Stanford University
443 Via Ortega, Stanford, CA 94305, USA

²PMMH, UMR 7636 CNRS-ESPCI-Universités Pierre et Marie Curie and Denis Diderot
10, rue Vauquelin, 75231 Paris Cedex 5, France
anke.lindner@espci.fr

³Rudolf Peierls Centre for Theoretical Physics, University of Oxford
1 Keble Road, OX1 3NP, UK

We demonstrate experimentally and theoretically the existence of oscillatory rheotaxis by *E. coli* bacteria at surfaces under flow. Three transitions are identified with increasing shear rate: From circular to straight upstream motion, the emergence of oscillations at tuneable frequencies, and finally coexistence of rheotaxis along the positive and negative vorticity directions. We develop a model to explain these transitions and predict the corresponding critical shear rates. Our results shed new light on bacterial transport in flow networks and strategies for contamination prevention.

Keywords: rheotaxis, *E. coli* bacteria, fluid structure interactions

Swimming microorganisms must respond to flows in complex environments, ranging from open oceans to narrow capillaries. To succeed in such diverse conditions, microbial transport often features surprising dynamics. Microswimmers can accumulate in shear flows, swim along the vorticity direction, exhibit oscillatory trajectories and upstream motion in Poiseuille flows, or align resonantly in oscillatory flows. One at a time, these observations have been explained by the hydrodynamic interactions of complex-shaped swimmers with a viscous flow in bulk. Concurrently, however, the interplay of these properties remains largely unexplored

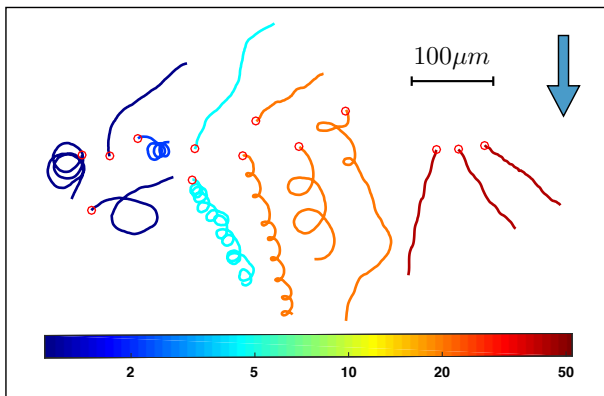


Figure 1: Collage of various surface dynamics types, obtained from 3D tracking of *E. coli* bacteria at shear rates $\dot{\gamma} = 1 - 50 \text{ s}^{-1}$, shown in the lab frame at a distance from 2-5 μm from the bottom surface.

Moreover, in the presence of walls these dynamics become increasingly intricate, but due to boundary accumulation the understanding of surficial locomotion is of particular importance. In quiescent liquids chiral swimmers move in circles, but in flows they can orient with respect to velocity gradients; an effect now baptized as *rheotaxis*. The robustness of upstream swimming has been analysed theoretically, and observed for artificial microswimmers, sperm cells and *E. coli* bacteria. Yet, at higher flow rates *E. coli* orient perpendicular (“to the right”) to the applied flow. The underlying mechanism of rheotaxis, and consequently predictions for optimal upstream swimming, are actively sought after.

To date, bacterial rheotaxis at surfaces has been quantified by measuring instantaneous orientation distributions or average transport velocities. Here, we investigate the time-resolved re-orientation dynamics of *E. coli* bacteria, theoretically and experimentally, as a function of applied shear close to walls. With increasing flow, we identify four regimes separated by critical shear rates [1]: (I) circular swimming with a bias to the right, i.e. along the direction of vorticity; (II) upstream swimming without oscillations; (III) oscillatory motion, increasingly more to the right; (IV) coexistence of swimming to the right and to the left, with dynamical switching between these states. By modelling bacterial rheotaxis comprehensively – accounting for their chiral nature, hydrodynamic and steric interactions, elongation, fore-aft asymmetry and activity – we assess the relative importance of these contributions throughout a trajectory, and explain the full dynamics.

References

- [1] Arnold J. T. M. Mathijssen, Nuris Figueroa-Morales, Gaspard Junot, Eric Clement, Anke Lindner and Andreas Zöttl, submitted, 2018

*AM acknowledges funding from the Human Frontier Science Program (Fellowship LT001670/2017). AL and NFM acknowledge funding from the ERC Consolidator Grant PaDyFlow (Agreement 682367). AZ acknowledges funding from the European Union’s Horizon 2020 research and innovation programme under the Marie Skłodowska-Curie grant (Agreement 653284). EC, GJ and AL acknowledge funding from the ANR BacFlow.

Bacterial chemotaxis during biofilm formation

Nuno M. Oliveira^{1,2,3}, Kevin R. Foster^{1,2*}, William M. Durham^{1,4*}

¹Department of Zoology, University of Oxford
South Parks Road, Oxford, OX1 3PS

²Oxford Centre for Integrative Systems Biology, University of Oxford,
Oxford OX1 3PS, United Kingdom

³Department of Applied Math and Theoretical Physics, University of Cambridge,
Wilberforce Road, Cambridge CB3 0WA, United Kingdom

⁴Department of Physics and Astronomy, University of Sheffield,
Hounsfield Road, Sheffield S3 7RH, United Kingdom

kevin.foster@zoo.ox.ac.uk or w.m.durham@sheffield.ac.uk

Abstract

Bacterial biofilms affect many aspects of our lives, from causing disease to promoting health and shaping many key processes in the environment. Despite this, surface-attached cells in biofilms are often portrayed as static and sluggish, a stark contrast to the energetic swimming they exhibit in liquid. Here we use microfluidic devices and automated cell tracking to challenge this view: we find that individual cells will actively move toward nutrients within a developing biofilm. This ability not only allows cells to seek out favoured positions on a surface but our analyses show that they can regulate their movement with remarkable submicron precision. Our findings suggest we can systematically engineer biofilms by manipulating the movement of the cells from which they are founded.

Keywords: *Pseudomonas aeruginosa*, bacterial chemotaxis, twitching motility, Type IV pili, Pil-Chp system

1. Introduction

Over the past 40 years, bacterial chemotaxis has become a major model system in biology, providing fundamental insights into the molecular basis of signal transduction and microbial behaviour. Efforts have focused on swimming bacteria, namely *Escherichia coli*, which regulate the rotation of their corkscrew shaped flagella to move towards more favourable chemical environments [1]. However, most bacteria actually live in surface attached communities called biofilms, where flagella are largely ineffective at driving movement. Bacterial biofilms affect our lives in myriad ways, from promoting good health and facilitating many important industrial processes, to being a major cause of recalcitrant infections. While cells within biofilms were historically considered to be static and simply grow in place, we now realize that motility often plays a key role in biofilm development. Instead of flagella, many bacterial species use grappling hook like appendages called Type IV pili to pull themselves across surfaces, a process called “twitching” motility. Biofilms harbour steep and diverse chemical gradients, which result from the combined effects of cell metabolism, attenuated diffusion and secretion of a wide variety of compounds. While these chemical gradients can give the bacteria positioned in some regions of a biofilm a tremendous growth advantage over others just tens of microns away, remarkably little is known about how biofilm bacteria might use their pili to navigate towards greener pastures.

2. Individual bacteria can navigate chemical gradients on surfaces

Pseudomonas aeruginosa is an intensely studied opportunistic pathogen and a canonical model for the study of biofilms. After attaching to surfaces, *P. aeruginosa* cells are highly motile and move by pulling themselves along using multiple Type IV pili. In this study we follow the movement of solitary *P. aeruginosa* cells in the early stages of biofilm development so that we can readily calculate each cell’s chemical environment and resolve how it modifies their behavior. To generate stable chemical gradients, we use two inlet microfluidic devices where flow balances the smoothing effect of molecular diffusion (Fig. 1A). We used automated cell tracking to follow surface-attached *P. aeruginosa* cells that are exposed to a stable spatial gradient of a chemoattractant (DMSO). Our method allows us to follow large numbers of attached cells and quantify their individual responses to the presence, or absence, of a chemical gradient.

In a DMSO gradient, we found that cell movement is strongly biased in the direction of increasing DMSO concentration (Fig. 1B), which contrasted with random motility in the absence of chemical gradient. After 2 h of incubation, the chemotactic bias peaks, with more than three times as many cells moving toward the chemoattractant source than moving away from it, but biased motility is maintained even as the surface becomes more crowded with cells. These data show single cells direct their motility along chemical gradients and suggest that surface-attached cells are capable of chemotaxis.

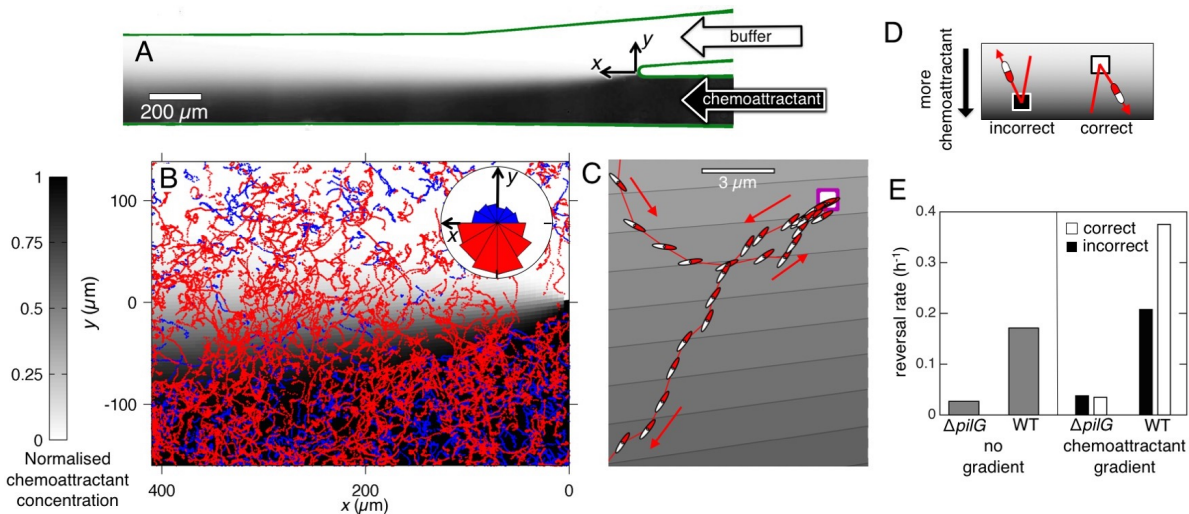


Figure 1: Pili-based chemotaxis in surface attached bacteria. (A) Microfluidic device used to expose a large population of surface attached cells to a steady gradient of a chemoattractant (DMSO). (B) In the presence of a DMSO gradient, *P. aeruginosa* cells preferentially bias their motility up the gradient (trajectories in red), rather than down it (trajectories in blue). Inset: Circular histogram shows the distribution of cell movement direction. (C) Chemotaxis is facilitated by reversals, in which a cell stops and moves back in the opposite direction without turning. Here, a cell initially moving up the gradient veers off course and deploys a reversal (purple square) to send it back up the gradient. Shaded regions in the background show isocontours of the DMSO concentration. Red and white symbols show cell orientation (not to scale). (D) Reversals can be classified as either ‘correct’ or ‘incorrect’. Correct reversals occur when cells initially moving towards lower concentrations of DMSO redirect their motility towards higher concentrations. Incorrect reversals occur in the opposite direction. (E) Automated cell tracking reveals that in the DMSO gradient, wild-type cells generate incorrect reversals at nearly the same rate as those in the absence of a gradient. However, cells perform correct reversals at a much higher rate in the DMSO gradient, indicating they generate chemotaxis via a “pessimistic” response. Mutants lacking the response regulator PilG have a much lower reversal rate in either condition and therefore cannot perform chemotaxis. All images from [2].

3. *P. aeruginosa* uses a “pessimistic” chemotactic strategy on surfaces

We next sought to understand how *P. aeruginosa* cells bias their movement on surfaces. Chemotaxis in swimming *E. coli* cells is achieved by cells performing straight runs interspersed by sharp reorientations (tumbles), where tumbles are delayed when moving up a chemoattractant gradient [1]. Do twitching bacteria use similar movement strategies in our experiments? Although twitching motility gets its name from the jerky motion that cells exhibit over the timescale of minutes, we find that in chemical gradients cells can maintain a consistent movement direction for periods longer than 1 h. Moreover, these twitching runs are interspersed by events where a cell reverses by stopping and then moving back in the opposite direction without turning (Fig. 1C, D). Twitching *P. aeruginosa* cells pull themselves along surfaces with pili that cluster at their poles, which drives movement parallel to their long axis and allows rapid changes in direction if a cell changes the pole that it is pulling from. To follow this process, we developed an automated algorithm that detects when the cell’s movement switches direction such that a cell’s leading pole becomes its trailing pole.

Both WT cells and those lacking the response regulator PilG were found to actively reverse their direction in both the presence and absence of DMSO gradients. However, $\Delta pilG$ cells, which do not show chemotaxis [2], reversed at a much lower rate than WT cells in both of these conditions, indicating that the reversals are indeed important for chemotaxis (Fig. 1E).

To examine the potential link between reversal rate and the ability to perform chemotaxis, we analyzed how the reversal rate changes as a function of the direction that cells are moving (Fig. 1D). This analysis revealed that $\Delta pilG$ cells reverse at nearly the same rate whether they are moving toward or away from the chemoattractant (Fig. 1E). In sharp contrast, WT cells almost double their reversal rate when moving away from the source of a chemoattractant but keep their basal reversal rate when moving toward the source (Fig. 1E). This observation is consistent with a “pessimistic” chemotactic strategy where cells respond to a reduction in the chemoattractant concentration, which contrasts with the “optimistic” strategy used by swimming *E. coli* that chemotax by postponing tumbles when moving toward a chemoattractant source. Put another way, swimming *E. coli* respond “if life gets better” [1] and our data show that twitching *P. aeruginosa* respond if life gets worse [2].

Taken together, our findings indicate swimming and biofilm cells generate chemotaxis in a fundamentally different way, suggesting the markedly different chemical landscapes in their environments present different evolutionary pressures on their respective regulatory systems.

References

- [1] Berg HC. *E. coli* in motion, Springer, New York. 2004.
- [2] Oliveira NM, Foster KR, Durham, WM Single-cell chemotaxis during biofilm formation. *Proceedings of the National Academy of Sciences, USA*. 113, pp. 6532–6537, 2016.

Photoactive Microbes - Light-Switchable Adhesion and Motility in Confinement

Christian Titus Kreis¹, Alexandros Fragkopoulos¹, Tanya Ostapenko¹, Thomas Böddeker¹ and Oliver Bäumchen¹

¹Max Planck Institute for Dynamics and Self-Organization (MPIDS)

Am Fassberg 17, D-37077 Göttingen, Germany

oliver.baumchen@ds.mpg.de

Abstract

Optimization through adaptation to the natural habitat represents a general theme in the evolution of life that can be readily observed for cells, microorganisms and even higher-level animals. For microbial life, the ability to adhere to surfaces is ultimately linked to the formation of dense populations called biofilms, which may help to protect the community of cells against external stimuli. In contrast to marine phytoplankton, many photoactive microalgae live in complex environments, such as liquid-infused soil and moist rocks, where they encounter and colonize a plethora of surfaces. First, we discovered that the adhesion of soil-dwelling microalgae to surfaces can be reversibly switched on and off by light. Our results suggest that light-switchable adhesiveness is a natural functionality to regulate the transition between planktonic and surface-associated state, which yields an adhesive adaptation to optimize the photosynthetic efficiency in conjunction with phototaxis. Second, we studied the swimming behaviour of single photoactive microbes in microfluidic confinement and describe how the wall curvature governs microbial motility in their planktonic state. Finally, we also briefly discuss the light-induced emergence of collective effects in microalgal suspensions beyond phototaxis.

Keywords: Motility, Confinement, Photoactive Microalgae, Chlamydomonas, Cell Adhesion, Biofilm Formation, Collective Phenomena

1. Introduction

Life in complex geometries can manifest itself through the many ways in which microorganisms interact with their environment, e.g. amoebic crawling, directional migration of epithelial cells and fibroblasts, microbial proliferation in space-limited environments and also the motility of biological microswimmers in confinement. In fact, the natural habitats for microbial life are often non-bulk situations, including the interstitial space of porous media, such as rocks and soil. The study of how self-propelled microorganisms in a liquid medium interact with their confining boundaries finds application in physiology, e.g. spermatozoa motility in the reproductive tract and the motion of parasites in the vertebrate bloodstream, and in microbiology in the context of biofilm formation. Microalgae represent biological microswimmers that inherit abundant ecological, environmental and technological relevance, e.g. in photo-bioreactors for the sustainable production of biofuels, in water purification systems and bioremediation scenarios. Although there have been advancements towards the understanding of cellular and bacterial adhesion, in vivo adhesion measurements were lacking for motile microalgae due to conceptual limitations of the conventional techniques. Also the precise ways in which these motile microbes behave in their confined environment remained unclear.

Here, we report on single-cell micropipette force spectroscopy experiments with vegetative wild-type *Chlamydomonas reinhardtii* cells in aqueous environment. The biflagellated microalga *Chlamydomonas* is a model organism in cell biology to study cell metabolism, light-directed motility, photosynthesis, while their flagella represent a model system for cellular appendages. These microalgae propel themselves in a liquid medium by a breaststroke-type beating of their flagella, called the planktonic state. Flagella-surface contacts allow for realizing microalgal adhesion to surfaces. The surface association of microalgae represents the initial state of microalgal biofilm formation. In our work, we reveal that the unspecific adhesion of *Chlamydomonas* to surfaces can be reversibly switched on and off by light [1].

Using experiments and Brownian dynamics simulations, we study the motility of a single *Chlamydomonas* microalga in an isolated microhabitat with controlled geometric properties. We demonstrate how the geometry of the habitat controls the cell's navigation in confinement [2]. The probability of finding the cell swimming near the boundary increases with the wall curvature, as seen for both circular and elliptical chambers. The theory, utilizing an asymmetric dumbbell model of the cell and steric wall interactions, captures this curvature-guided navigation quantitatively with no free parameters.

2. Experimental

2.1. Light-Switchable Adhesion to Surfaces

Micropipette force sensors are used to grabbing a motile microalga in a controlled orientation. The cell is brought into contact with a silicon wafer substrate. Force-distance experiments are performed by moving the substrate and repeatedly recording the deflection of the micropipette during approach and retract cycles. We find that only the flagella of the microalgae adhere to the surface; the cell body does not exhibit any adhesiveness. Light conditions were carefully controlled by using narrow band pass filters for the illumination of the cell during adhesion force measurements.

2.2. Curvature-Guided Motility in Confinement

We employed optical microscopy techniques and particle tracking to study the motility of a single wild-type *Chlamydomonas reinhardtii* cell contained within an isolated quasi-two-dimensional microfluidic compartment. We study precisely a single isolated cell in order to exclude any cell-cell interactions or collective effects. Experiments were performed in circular compartments with radii between 25-500 μm , and elliptical chambers with comparable semi-axes dimensions. The height of all compartments was approximately 20 μm , about one cell diameter (body and flagella); thus, out-of-plane reorientations of the cell are inhibited.

3. Results and Discussion

3.1. Light-Switchable Adhesion to Surfaces

The force spectroscopy experiments yield three main results [1]: First, the adhesion of *Chlamydomonas* to surfaces can be reversibly switched on and off by light. Second, the transition between the planktonic and the surface-associated state in response to light occurs on a timescale of seconds. Third, experiments suggest that the adhesive adaptation to the light conditions is realized by a relocalisation of adhesion-promoting flagella membrane glycoproteins in response to a photoreceptor signal.

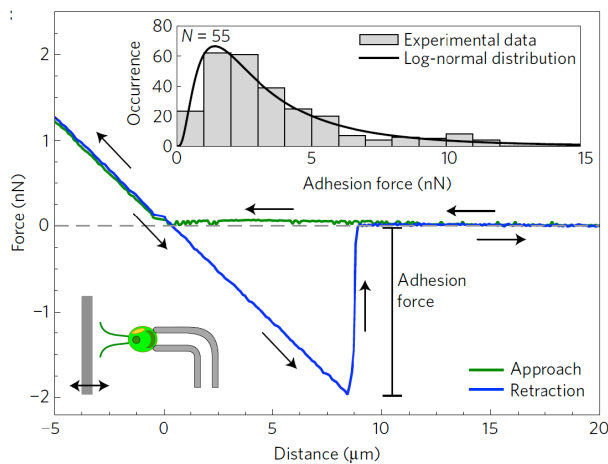


Figure 1: Force-distance measurement consisting of an approach (green) and a retraction (blue) cycle. Typical adhesion forces (inset) are between 1 and 4 nN. Reproduced from Ref. [1].

We found that the cells do not stick in red light, whereas they exhibit significant adhesiveness in blue and white light (see Fig. 1). By gradually decreasing the blue-light intensity for the same cells, a sharp intensity threshold for the adhesion can be identified (see Fig. 2). This threshold value is consistent with other photoreceptor responses, e.g. phototaxis, in *Chlamydomonas*.

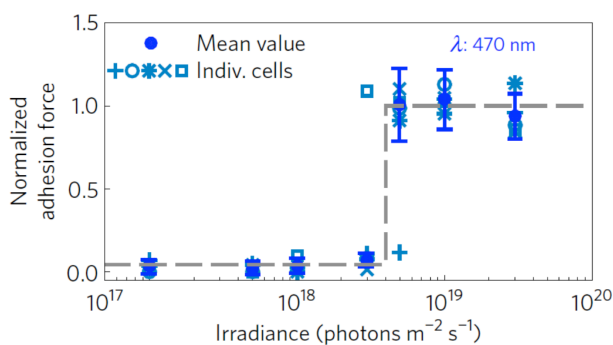


Figure 2: Normalized adhesion force of five cells as a function of the blue-light intensity. The adhesiveness is lost below a sharp threshold value of the irradiance. Reproduced from Ref. [1].

3.2. Curvature-Guided Motility in Confinement

In the absence of external flow, cell-cell interactions, photo- and chemotaxis, we isolated a curvature-guided motility mech-

anism for a single microalga in a confined microfluidic habitat with controlled geometric properties [2]. The concave nature of the confining walls leads to an enhanced probability of near-wall swimming for puller-type microswimmers, as quantified by a statistical analysis of experimental cell trajectories (see Fig. 3). Brownian dynamics simulations based on an active asymmetric dumbbell model quantitatively capture the experiments. The main ingredients of this curvature guidance are the torque that the alga experiences during an interaction event with the wall, the compartment's wall curvature, and the suppression of the alga's diffusive swimming regime in confinement. The fact that we track the motility of a single cell allows for dissecting the fundamental physics of a puller-type microswimmer in confinement. Earlier studies focused on the collective behavior of bacterial suspensions in confinement, which is governed by cell-cell interactions and excluded volume effects.

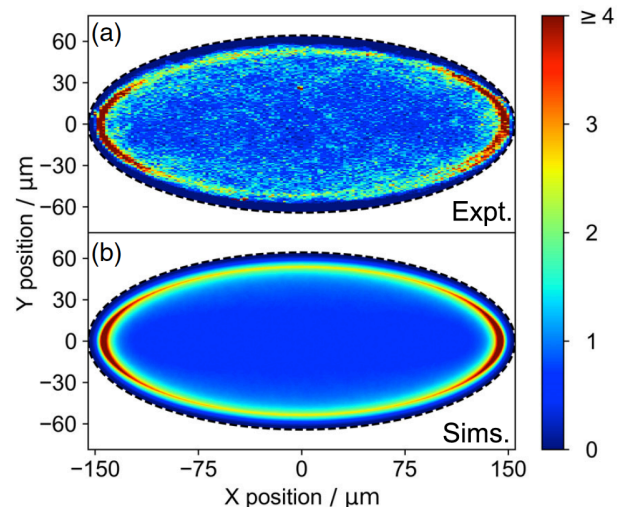


Figure 3: Relative probability density for elliptical compartments (eccentricity: 0.91): (a) experiments and (b) simulations. Reproduced from Ref. [2].

4. Outlook

We also study the adsorption-desorption dynamics of microalgal strains on solid interfaces by using light to reversibly transition between the planktonic and the surface-associated state, which ultimately initiates biofilm formation. Our results reveal physical details of the dynamics on the population level, including the adsorption and desorption rates and the delay time for the organism's adhesive mechanism. Also, we find that for microalgal suspensions in confinement unexpected collective effects may emerge in the absence of light for sufficiently high cell densities.

References

- [1] Kreis C.T., Le Blay M., Linne C., Makowski M. and Bäümchen O., Adhesion of *Chlamydomonas* Microalgae to Surfaces is Switchable by Light, *Nature Physics*, 14, pp. 45-49, 2018.
- [2] Ostapenko T., Schwarzendahl F.J., Böddeker T., Kreis C.T., Cammann J., Mazza M.G. and Bäümchen O., Curvature-Guided Motility of Microalgae in Geometric Confinement, *Phys. Rev. Lett.*, in press, 2018.

Painting with light–powered bacteria: Smart templated self assembly using microswimmers

Jochen Arlt^{1*}, Vincent A Martinez¹, Angela Dawson¹, Teuta Pilizota² and Wilson C K Poon¹

¹School of Physics & Astronomy, The University of Edinburgh, Peter Guthrie Tait Road, Edinburgh EH9 3FD, United Kingdom

²School of Biological Sciences and Centre for Synthetic and Systems Biology, The University of Edinburgh, Alexander Crum Brown Road, Edinburgh EH9 3FF, United Kingdom

Abstract

External control of the swimming speed of ‘active particles’ can be used to self assemble designer structures in situ on the micrometer to millimeter scale. We demonstrate such reconfigurable templated active self assembly in a fluid environment using light powered strains of *Escherichia coli*. The physics and biology controlling the sharpness and formation speed of patterns is investigated using a bespoke fast-responding strain. The fundamental prediction that for active matter the product of density and speed is constant in a system with spatially dependent activity is also verified.

Keywords: IUTAM Symposium, bacteria, light control, self-assembly

1. Introduction

Swimming bacteria in planktonic cultures are one of the most widely studied examples of motile cells and by now can be considered as a model system for ‘active colloids’ [1]. For particular cases, such as the *Escherichia coli* bacteria used here, their versatility can be further enhanced by genetic modifications. Here we use a strain engineered to be powered by green light [2] to control its motility externally. By using spatially and temporally varying light intensity patterns projected on such light powered *E. coli* we can adjust their swimming speed. Changes in speed lead to a change in local bacteria density so that we can use patterned light fields to assemble structures in situ.

2. Results

In order to achieve good external control of the swimming speed we engineered a smooth swimming strain of light-powered *E. coli* that react fast to changes in light intensity. Previously reported mutants [2] only adjust their swimming speed slowly after light intensity is changed and they keep on swimming for minutes after the light is switched off. Our strain AD10 [3] reacts very rapidly to changes in light intensity (fig. 1).

We use a digital mirror device to project patterns of illumination onto a uniform field of cells rendered stationary by O_2 exhaustion. Simple binary patterns such as illustrated in fig. 2 are the easiest to understand, as bacteria only start swimming in the illuminated regions. These swimming cells will eventually reach an edge of the illuminated area and swim out into darkness. There they will stop and therefore accumulate just *outside* the boundary. The cell density within the illuminated areas will drop accordingly while they accumulate in the dark regions. The swimming patterns and thus the bacteria density can be adjusted dynamically by switching between different intensity patterns. And by re-illuminating the sample with uniform light intensity any spatial density variations can be completely removed.

We characterise the time scales governing the pattern formation and elucidate the physics controlling the sharpness and resolution of the patterns formed by our bacteria.

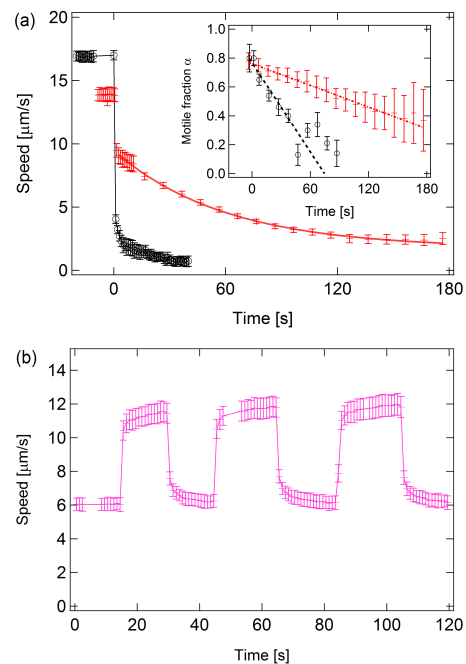


Figure 1: Temporal response of the swimming speed of light controlled *E. coli* to changes in light intensity. (a) Specially engineered fast responding strain AD10 (black symbols) stops swimming within less than 1s after light is switched off, whereas AD57 (red symbols), a strain similar to previously reported mutants, continues swimming more slowly for several minutes. (b) AD10 react fast to changes in light intensity.

*j.arlt@ed.ac.uk

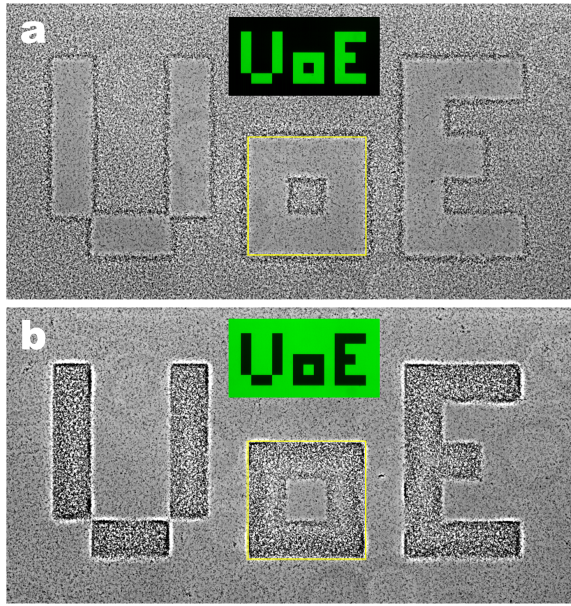


Figure 2: Painting with bacteria: by projecting binary intensity patterns onto suspensions of light controlled bacteria we can induce density variation to assemble structures. Phase contrast images of (a) positive and (b) negative pattern as shown in the insets.

Furthermore we can use our system to experimentally verify the fundamental prediction that for active matter the product of density and speed is constant in a system with spatially dependent activity [4]. By performing carefully controlled experiments using light patterns to impose a spatially varying swimming speed on our bacteria we can confirm this prediction (fig. 3).

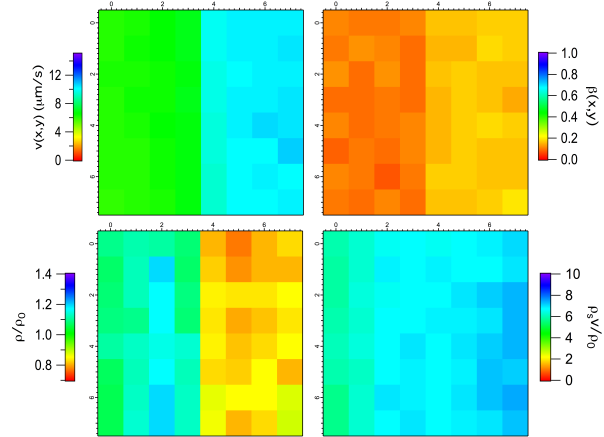


Figure 3: Demonstration of $\rho v = \text{const}$: Spatial maps characterising a dense suspension of light controlled bacteria (OD = 8) near the boundary between a low (left) and high (right) light intensity region after $t \approx 20$ min of illumination: (a) mean speed \bar{v} , (b) mean non-motile fraction β , (c) relative cell density ρ/ρ_0 , and calculated from those (d) $\rho_s v/\rho_0 = \rho(1 - \beta)v/\rho_0$. Each tile corresponds to 64×64 pixel², i.e. $90 \times 90 \mu\text{m}^2$.

References

- [1] Schwarz-Linek, J., Arlt, J., Jepson, A., Dawson, A., Visers, T., Miroli, D., Pilizota, T., Martinez, V.A. and Poon, W.C.K., *Escherichia coli* as a model active colloid: A practical introduction, *Colloids Surf. B*, 137, pp. 2–16, 2016.
- [2] Walter, J. M., Greenfield, D., Bustamante, C. and Liphardt, J., Light-powering *Escherichia coli* with proteorhodopsin, *Proc. Natl. Acad. Sci. USA*, 104, pp. 2408–12, 2007.
- [3] Arlt, J., Martinez, V. A., Dawson, A., Pilizota, T. and Poon, W. C. K., Painting with bacteria: Smart templated self assembly using motile bacteria, *arXiv*, <https://arxiv.org/abs/1710.08188>, 2017.
- [4] Tailleur, J. and Cates, M. E., Sedimentation, trapping and rectification of dilute bacteria, *Europhys. Lett.*, 86, 60002, 2009.

Hydrodynamic genesis of colloidal creatures

Blaise Delmotte¹ and Michelle Driscoll² and Aleksandar Donev¹ and Paul Chaikin³

¹*Courant Institute of Mathematical Sciences, New York University
251 Mercer Street, New York, NY, 10012, USA
delmotte@cims.nyu.edu*

²*Department of Physics and Astronomy, Northwestern University
michelle.driscoll@northwestern.edu
2145 Sheridan Road Evanston, IL 60208*

³*Department of Physics, New York University
726 Broadway, Room 877 New York, NY 10003
chaikin@nyu.edu*

Abstract

When colloidal particles are rotating adjacent to a nearby floor, strong advective flows are generated around them, even quite far away. When a group of these microrollers is driven, the strong hydrodynamic coupling between particles leads to formation of new structures. Our experimental observation show that a suspension of microrollers undergoes a cascade of instabilities: an initially uniform front of microrollers evolves first into a shock-like structure, which then quickly becomes unstable, emitting fingers of a well-defined wavelength; then the fingertips pinch off to form compact motile structures translating at high speed. These colloidal creatures are self-sustained and form a stable state of the system. Combining experiments, large scale numerical simulations and continuum models, we detail the mechanisms involved at each step. We demonstrate that the whole process is primarily controlled by a geometric parameter: the height of the particles above the floor. We also explain the predominant role of hydrodynamic collective effects in the development of these colloidal creatures. To conclude, we show how to use these creatures for particle transport and flow generation in complex environments.

Keywords: collective motion, hydrodynamic instabilities, self-assembly, colloids

1. Introduction

We have uncovered a hydrodynamic instability in a driven system of microrollers: suspensions of colloids rotating parallel to a floor [4]. When driven by a magnetic field rotating about an axis parallel to the floor, these microrollers generate strong advective flows in their vicinity. These flows are responsible for the large-scale collective effects observed in uniform suspensions. When the particle distribution is discontinuous, the microrollers form a shock front which quickly becomes unstable and generates finger-like structures with compact tips. These fingertips can detach to form compact autonomous structures, called colloidal creatures.

2. Experimental setup and simulation tool

Our system consists of magnetically driven colloidal microrollers. These microrollers are suspended in a sealed chamber of depth $H = 200 \mu\text{m}$, width $W = 2 \text{ mm}$, length $L = 50 \text{ mm}$, and are much denser than the surrounding quiescent fluid. As a result they readily sediment, and remain near the chamber floor. They do not rest on the floor, but are suspended by thermal motion at their gravitational height, h , which is set by the balance of thermal energy and their buoyant mass, $h = a + k_B T / mg$, where $a = 0.656 \mu\text{m}$ is the colloid radius, k_B the Boltzmann constant, $T \approx 298 \text{ K}$ the fluid temperature, $m = 1.27 \cdot 10^{-15} \text{ kg}$ their buoyant mass, and g the gravitational acceleration (cf. Fig.1a). The gravitational height, h , of our microrollers is $1 \mu\text{m}$, which we verified by measuring their translational diffusion constant and comparing with the calculated value. In our system, h is two orders of magnitude smaller than the chamber height, H ,

and we only consider particles in a small region ($430 \times 430 \mu\text{m}$) in the middle of the chamber, quite far from any lateral wall. The magnetic microrollers are rotated by a rotating magnetic field, $\mathbf{B} = B_0 [\cos(\omega t)\hat{x} + \sin(\omega t)\hat{z}]$ (cf. Fig.1a). We emphasize that although the colloidal particles are magnetic, the dominant inter-particle interactions in this system are hydrodynamic due to the small magnitude of the particle magnetic moment. Magnetic potential interactions are quite small compared to thermal energy ($\sim 0.1 \text{ kT}$) and viscous forces between particles are quite large compared to magnetic forces (Mason number = 500) [4]. Thus, this system is well-approximated by a system of particles rotating and interacting with steric and hydrodynamic interactions above a floor, i.e. an infinite half-space. The many body simulations are done using an accelerated stresslet-free variant of Stokesian dynamics [5] with Brownian motion parallelized on GPU's [1].

3. Genesis of colloidal creatures

Below we detail each mechanism in the process that leads to the genesis of the colloidal creatures.

3.1. Collective flows

Hydrodynamic coupling plays a crucial role in the dynamics of this system. A sphere rotating near a wall about the \hat{y} -axis will move in the \hat{x} -direction. This motion is a result of the unequal drag force on the top and the bottom of the particle. Its translation speed v_0 is set by the scaled distance to the wall and the rotation rate: $v_0 = \omega a f(h/a)$, and vanishes as the height increases, i.e. $f(h/a) \rightarrow 0$ as $h \rightarrow \infty$. However v_0 is orders of magnitude slower than the fluid velocity at the particle's surface ωa . The velocity field around a particle decays slowly

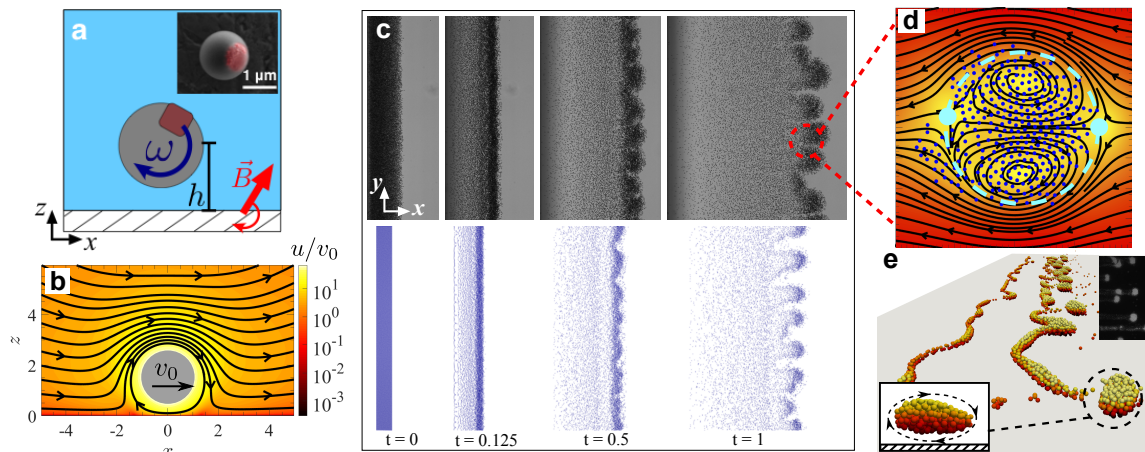


Figure 1: **a**, Sketch of a microroller hovering at a height h from the floor and rotating with angular velocity ω . Red arrow: oscillating magnetic field. Inset: SEM image. **b**, Flow field around a microroller (simulation). Colorbar: flow speed u normalized by the self-induced translational speed of the microroller v_0 . **c**, Development of the fingering instability seen from above: initial strip, formation of the front, transverse instability, fingers. Top: experiments. Bottom: simulation at the same relative times. **d**, Flow field in the frame moving with a fingertip (simulation). Blue dots: microrollers. Cyan dashed line: recirculation zone. Cyan disks: stagnation points. **e**, Detachment and formation of colloidal creatures. Top inset: experimental realization seen from above. Bottom inset: side view of a creature, the arrows indicate the tread-milling motion of the microrollers.

(as $1/r^2$) in the xy -plane, where r is the distance to the particle center (cf. Fig.1b). Thus, even at moderate area fractions, ϕ , particle motion is mainly a result of being advected in the flow of neighbouring particles. In a homogeneous suspension of microrollers, this strong hydrodynamic coupling gives rise to a mean suspension translation velocity which increases linearly with ϕ : i.e. $\bar{v} = \alpha\phi$ [4].

3.2. Hydrodynamic front

We initially localize the particles in a narrow strip on one side of the chamber. After the rotating field is turned on, the particle distribution changes dramatically, organizing into a travelling, shock-like, front with a finite width (cf. Fig.1c). We derived a model which relies on a nonlocal description of the hydrodynamic interactions between microrollers treated as rotlets [3]. The theoretical results and comparisons with experiments and simulations show that the width of the front is controlled by the particle height above the floor.

3.3. Transverse instability

The propagating front quickly becomes unstable in the direction transverse to propagation, leading to the appearance of density fluctuations which continue to grow as fingers. Both the experiments and simulations show a qualitatively similar evolution of the shock, the shock instability, and the fingering, at the same relative times (cf. Fig.1c). We derived the simplest possible model that can capture the fingering instability: two lines of rotlets [2]. Our model directly accounts for the nonlocal hydrodynamic interactions between the particles. Our analytic linear stability analysis confirmed that the fingering instability is linear, that it happens in the plane parallel to the floor and is purely hydrodynamic in origin. The model showed that the transverse flows due to the nearby no-slip surface are responsible for the lengthscale selection.

3.4. Detachment of colloidal creatures

Due to the increased density in the shock region, the fingertips are much denser and, due to collective effects, i.e. $\bar{v} = \alpha\phi$, move much faster than the rest of the suspension. The flow

around the fingertips exhibit a recirculation zone whose size depends on the height of the particles above the floor (cf. Fig.1d). When the microrollers are pushed away from the floor, the fingertips can break off to form self-sustained, compact clusters made of hundreds of particles, which we term colloidal creatures (cf. Fig.1e). These creatures rotate around their centre of mass and translate with a speed up to 15,000 times faster than a single roller would at the same centre of mass height. Creatures form a natural stable state of the system: they move at a constant speed, do not lose particles, and are not observed to dissolve. More recently, we showed that similar structures can be observed in the experiments (cf. Fig.1e, top inset). We are currently exploring how to use these collective effects for various applications such as pumping, guided particle transport and mixing in microfluidic systems.

References

- [1] F. Balboa Usabiaga, B. Delmotte, and A. Donev, "Brownian dynamics of confined suspensions of active microrollers," *The Journal of Chemical Physics*, vol. 146, no. 13, p. 134104, 2017.
- [2] B. Delmotte, A. Donev, M. Driscoll, and P. Chaikin, "Minimal model for a hydrodynamic fingering instability in microroller suspensions," *Phys. Rev. Fluids*, vol. 2, p. 114301, Nov 2017.
- [3] B. Delmotte, M. Driscoll, P. Chaikin, and A. Donev, "Hydrodynamic shocks in microroller suspensions," *Phys. Rev. Fluids*, vol. 2, p. 092301, Sep 2017.
- [4] M. Driscoll, B. Delmotte, M. Youssef, S. Sacanna, A. Donev, and P. Chaikin, "Unstable fronts and motile structures formed by microrollers," *Nature Physics*, vol. 13, no. 4, pp. 375–379, 2017.
- [5] J. W. Swan and J. F. Brady, "Simulation of hydrodynamically interacting particles near a no-slip boundary," *Physics of Fluids (1994-present)*, vol. 19, no. 11, p. 113306, 2007.

Capillary deposition of microorganisms in a microfluidic channel for the study of cells in spatially controlled environments

Roberto Pioli¹, Eleonora Secchi², Lucio Isa³ and Roman Stocker⁴
ETH Zürich

¹pioli@ifu.baug.ethz.ch

²secchi@ifu.baug.ethz.ch

³lucio.isa@mat.ethz.ch

⁴romanstocker@ethz.ch

Controlled and precise deposition of microorganisms into defined spatial arrangements would offer unique and innovative possibilities for the study of microbial physiology and interactions. Full control over the geometrical arrangement is highly desirable because of the crucial importance of distances in microbe-microbe interactions, arising from their dependence on the propagation of chemical signals. Coupling accurate spatial patterning and full control over environmental conditions would provide a powerful and versatile platform for single-cell studies in microbial ecology. We will describe the application of a capillary deposition technique originally developed for colloidal particles called sCAPA (sequential capillary assisted particle assembly) in a microfluidics platform. This technology exploits the capillary forces resulting from the controlled motion of an evaporating droplet inside a microfluidic channel over a microfabricated substrate bearing an array of traps, which each capture an individual microorganism. Sequential depositions allow the generation of the desired spatial layout of single or multiple microorganisms. We successfully calibrated this new technique on colloidal particles and tested it on bacteria. We have shown that the coupling of single cell deposition and microfluidics technology allows both geometric patterning and precise control of environmental conditions, and thus opens a window into the physiology of single microbes and the ecology of microbe-microbe interactions.

Preference: poster presentation.

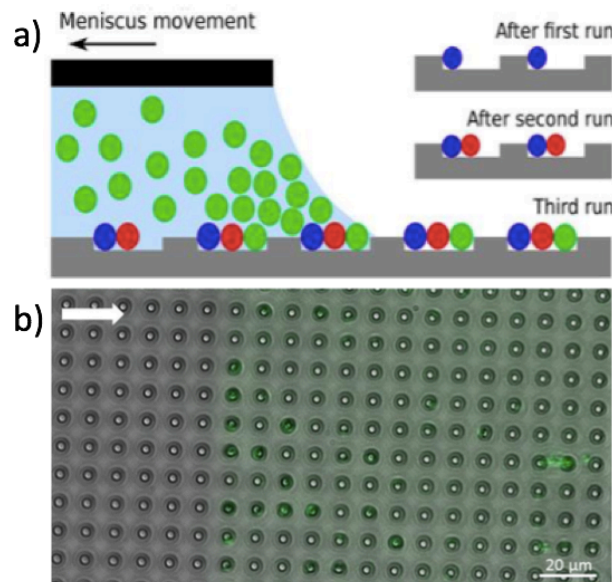


Figure: a) Hybrid particle clusters fabricated by sequential capillary assembly. b) Superposition of a bright-field image and a fluorescent image of a PDMS substrate with 6- μm -diameter circular traps after the evaporation of a suspension of fluorescently labelled *E. coli*. The green color denotes the region where the drop of the bacterial solution was initially placed and is due to the presence of the live/dead stain (LIVE/DEAD BacLight). The white arrow indicates the direction of motion of the contact line.

Numerical design of a T-shaped microfluidic device for the detection of diseased cells through deformability-based separation

Massimiliano M. Villone¹, Marco Trofa¹, Martien A. Hulsen², and Pier Luca Maffettone¹

¹ Department of Chemical, Materials, and Manufacturing Engineering – University of Naples Federico II
Piazzale Tecchio, 80 – 80125 Naples, Italy
massimiliano.villone@unina.it

² Department of Mechanical Engineering, Eindhoven University of Technology
PO Box 513 – 5600 MB Eindhoven, The Netherlands

Abstract

We propose a square cross section asymmetric T-shaped microfluidic channel for the separation of cells suspended in a Newtonian liquid on the basis of their mechanical properties. The design is performed through 3D direct numerical simulations. We show that, when the suspended inclusions start near the inflow channel centerline and the carrier fluid is equally partitioned between the two outflow branches, cell separation can be achieved based on their deformability, with the stiffer ones going ‘straight’ and the softer ones being deviated to the ‘side’ branch. The effects of the geometrical and physical parameters of the system on the phenomenon are investigated. Since cell deformability can be significantly modified by pathology, we give a proof of principle on the possibility of separating diseased cells from healthy ones, thus leading to illness diagnosis.

Keywords: microfluidics, cell separation, cell deformability

1. Introduction

High-throughput characterization of cell mechanical properties is of great interest in biomedical applications, either for analytical or diagnostic purposes [1]. The capability of sorting particles based on their mechanical properties is indeed of primary importance in medicine, since cell deformability is a clinical indicator of a wide range of diseases, e.g., malaria [2] and several tumors [3]. Separation based on the mechanical properties of deformable inclusions can be achieved in microfluidics channels, and, to this end, it has been shown that microfluidic applications can be intelligently designed by treating the cells as elastic capsules or soft beads [3,4]. An effective tool for separating suspended deformable particles is based on bifurcating microchannels [5-7].

We make use of three-dimensional direct numerical simulations to prove the efficacy of a simple microfluidic device for the separation of cells suspended in a Newtonian liquid depending on their mechanical properties.

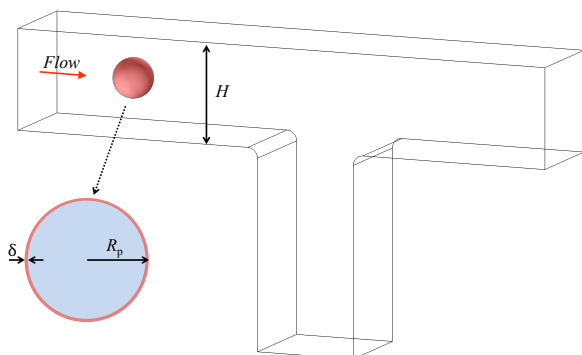


Figure 1: Schematic representation of the T-shaped channel with a capsule suspended on the centerline of the inlet branch. A zoom of the section of the capsule is reported at the bottom on the left.

2. Problem outline and results

As schematically depicted in Fig. 1, the channel is T-shaped, with one inlet branch and two orthogonal outlet branches, and has a square cross-section. By modeling the cells as initially spherical elastic capsules, the geometrical and physical parameters that describe the system are the confinement ratio $\beta = 2R_p/H$, with R_p the cells initial radius and H the side of the channel cross section, and the capillary number $Ca = \eta QR_p/(H^3 G \delta)$, where η is the viscosity of the medium carrying the cells, Q is the flow rate of such medium, G is the shear modulus of the elastic material of which the capsule membrane is made of, and δ is the membrane thickness.

We find that, when the two outlet branches of the microdevice carry the same flow rates, provided that the cells are focused on the centerline of the inlet branch (which spontaneously occurs if such branch is long enough), higher cell deformability (i.e., higher Ca -values) promotes particle deviation toward the side branch (orthogonal to the inlet), whereas stiffer cells (i.e., cells with lower Ca -values) are more prone to follow the main outflow channel (aligned with the inlet).

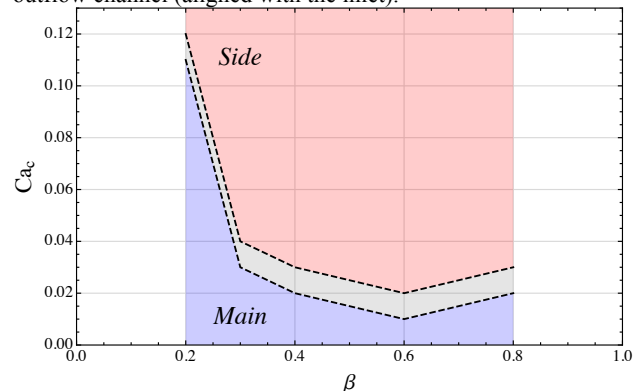


Figure 2: Critical capillary number for an elastic capsule Ca_c as a function of the confinement ratio β .

The critical value of the capillary number for separation Ca_c (i.e., the critical particle deformability) depends on the confinement ratio β as shown in Fig. 2. Consequently, given the confinement ratio, ad-hoc operating conditions can be fixed to separate cells with different mechanical properties.

Since many pathologies can significantly modify cell deformability, e.g., softening cells from three to ten times [3], our numerical results give a proof of principle on the possibility of separating diseased cells from healthy ones, thus leading to illness diagnosis.

References

- [1] Zheng, S., Liu, J.Q., and Tai, Y.C., Streamline-Based Microfluidic Devices for Erythrocytes and Leukocytes Separation, *J. Microelectromech.*, 17, pp. 1029-1038, 2008.
- [2] Diez-Silva, M., Dao, M., Han, J., Lim, C.T., and Suresh, S., Shape and Biomechanical Characteristics of Human Red Blood Cells in Health and Disease, *MRS Bull.*, 35, pp. 382-388, 2010.
- [3] Fraldi, M., Cugno, A., Deseri, L., Dayal, K., and Pugno, N., A frequency-based hypothesis for mechanically targeting and selectively attacking cancer cells, *J. R. Soc. Interface*, 12, 20150656, 2015.
- [4] Pozrikidis, C., *Modeling and simulation of capsules and biological cells*, CRC Press, Boca Raton, 2003.
- [5] Secomb, T.W., Styp-Rekowska, B., and Pries, A.R., Two-Dimensional Simulation of Red Blood Cell Deformation and Lateral Migration in Microvessels, *Ann. Biomed. Eng.*, 35, pp. 755-765, 2007.
- [6] Barber, J.O., Alberding, J.P., Restrepo, J.M., and Secomb, T.W., Simulated Two-dimensional Red Blood Cell Motion, Deformation, and Partitioning in Microvessel Bifurcations, *Ann. Biomed. Eng.*, 36, pp.1690-1698, 2008.
- [7] Woolfenden, H.C., and Blyth, M.G., Motion of a two-dimensional elastic capsule in a branching channel flow, *J. Fluid Mech.*, 669, pp. 3-31, 2011.

Flocking particles with asymmetric obstacles: a model for isolation and sorting motile cells and unicellular organisms

R. Martinez^{1,2}, F. Alarcon¹, D. Rogel-Rodriguez¹, J. Ramirez³, J.L. Aragonés² and C. Valeriani¹

¹*Departamento de Estructura de la Materia, Fisica Termica y Electronica
Facultad de Ciencias Físicas, Universidad Complutense de Madrid, 28040 Madrid, Spain*

²*Condensed Matter Physics Center (IFIMAC)
Universidad Autónoma de Madrid, 28049, Madrid, Spain*

³*Departamento de Ingeniería Química Industrial y Medio Ambiente, Escuela Técnica Superior de Ingenieros Industriales
Universidad Politécnica de Madrid, 28006 Madrid, Spain*

Abstract

In our work we numerically show that it is possible to sort active particles by means of asymmetric obstacles in different ways, depending on the nature of the obstacles and how particles interact with them and with another particles. We have used two types of Vicsek models to represent motile cells, either metric or topological, and two different configurations of funnels, displaced as two infinite walls or in a circle. It has been recently observed both in experiments of bacteria and in computer simulations of run-and-tumble particles, that a higher concentration of particles emerges on the narrow opening of a wall of funnels. However, when particles are Vicsek-like and interacting with an aligning rule with the wall, we demonstrate that, strikingly, particles are trapped on the opposite side, on the wider opening of the wall. Interestingly, when funnels are located on a circular (and not linear) array, trapping depends on the chosen Vicsek model, since the metric Vicsek model forms a clustering state while the topological one rather a polar ordered state.

Keywords: Sorting cells, Vicsek particles, funnels

1. Introduction

Motivated by the experiments with *Escherichia coli* bacteria [1] and cancer cells [2], where motile cells move through asymmetric obstacles, several numerical studies have been performed. In Ref. [3] the authors underlined that pure Brownian motion is not enough to mimic bacteria's rectification at the obstacles, while adding particles' ballistic motion (at least for a short time) is needed. Later on, they also showed that the sorting's direction can be controlled by the flocking parameter, i.e. the exclusion radius of the noise parameter in a system of Vicsek like particles with finite size and repulsive walls [4]. Investigating the interaction of active particles with substrates (barriers), they found that no ratchet effect is present when particles are reflected off the barriers or scattered from the barriers according to Snell's law [5].

One common feature in all research performed so far has been modelling the system as enclosed within solid walls. When considering an array of funnels in a periodic channel, Hu et al. [6] simulated particles moving according to an over-damped Langevin dynamics with finite angular time correlation, finding that not only the time correlation plays a key role in rectifying particles, but also the alignment interaction: purely nematic alignment between particles suppressing the rectification, while polar alignment not always promoting it [7].

In our study, we have first unveiled the effect of trapping Vicsek particles in a two-dimensional infinite walls of funnels (considering periodic boundary conditions). Particles are either Vicsek points or run-and-tumble which interact with the funnels by aligning along the funnel or by an elastic collision. Next, we have considered a circular arrangement of funnels, and compared the different behaviour of a metric versus topological Vicsek model.

2. Methodology

Vicsek particles obey the usual rules: their updated velocity is the mean of their neighbor's ones, plus a white noise. When the amplitude of this noise is small, polar order arises. In determining neighbors, we use two models: metric Vicsek model [8, 9] (taking as neighbours all particles inside a cutoff radius) and topological Vicsek model [10] (taking the Voronoi neighbors of a particle).

The run-and-tumble particles obey the following update rules: at regular time steps they take a random new velocity, which they keep until the next iteration (unless they collide with a funnel).

Besides updating particles' velocities at every time step according to either a Vicsek or a run-and-tumble rule, for the interaction with the funnels, an event-driven dynamics is used: particles follow a straight trajectory until they encounter an obstacle; then, a new velocity is assigned according to a given bouncing rule. In our work, we have considered two possible bouncing rules: one that tends to align particles with the wall of the obstacle, and an elastic one.

3. Results

We have investigated the same geometry with both run-and-tumble and Vicsek particles, as presented in figure 1. Run-and-tumble particles are trapped on the narrow opening of the walls in a system with periodic boundary conditions. However, strikingly, Vicsek particles are trapped on the other side of the funnel wall. Due to periodic boundary conditions, the walls of funnels trap particles in an infinite band.

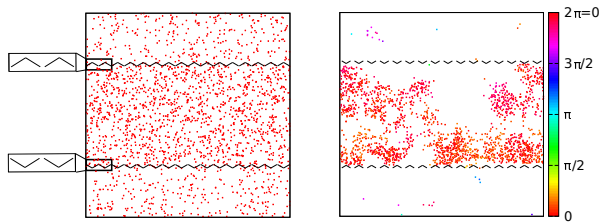


Figure 1: Left: trapping with run-and-tumble particles similar to [1, 3] but with PBC. Right: Vicsek particles trapped at the other side of the funnel wall. In this case color denotes the particle's direction of motion.

In order to have a more local trapping, we have carried out simulations with circular trap: Vicsek particles are efficiently trapped inside the circle. Depending on the Vicsek model trapped particles either form clusters or a polar state, as can be seen in figure 2. For the first time, we detect differences between metric and topological Vicsek model.

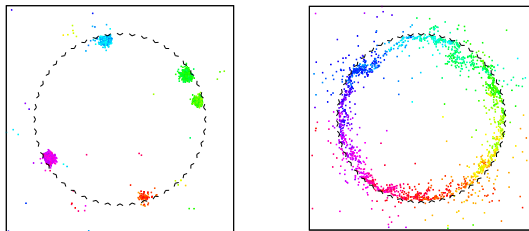


Figure 2: Left, metric Vicsek model, where clusters are present. Right, topological Vicsek model. In both images color denotes the direction of motion.

In the metric Vicsek model we have found that particles are trapped in clusters: from time to time a small flock leaves a trap to later be trapped by another. The rate at which each particle leaves to go to another trap increases when decreasing the number of funnels on the circle and, although no sharp transition of the order parameter as a function of the noise is detected (as in the bulk case), we distinguish states where particles are completely trapped, from states where particles outside traps are not negligible, or where particles are not trapped at all.

However, we have concluded that topological Vicsek particles are found more difficult to trap than metric ones. In this case, we identified states where particles are not trapped from very ordered trapping (polar state). Oppositely to the metric Vicsek, topological Vicsek has a sharp transition between these two states. In the trapping state particles do not leave the traps.

References

- [1] Galajda, P., Keymer, J., Chaikin, P. and Austin, R., A wall of funnels concentrates swimming bacteria, *Journal of bacteriology*, 189, 8704-8707, 2007.
- [2] Mahmud, G., Campbell, C.J., Bishop, K.J.M., Komarova, Y.A., Chaga, O., Soh, S., Huda, S., Kandere-Grzybowski, K. and Grzybowski, B. A., Directing cell motions on micropatterned ratchets *Nature Phys.* 5, 606 (2009)
- [3] Wan, M., Reichhardt, C. O., Nussinov, Z. and Reichhardt, C., Rectification of swimming bacteria and self-driven particle systems by arrays of asymmetric barriers, *Physical review letters*, 101, 018102, 2008.
- [4] Drocco, J.A., Reichhardt, C.O. and Reichhardt, C., Rectification of Swimming Bacteria and Self-Driven Particle Systems by Arrays of Asymmetric Barriers, *Physical Review E*, 85, 056102 (2012).
- [5] Olson Reichhardt, C.J., Drocco, J., Mai, T., Wan, M.B. and Reichhardt, C., Active matter on asymmetric substrates, *Proc. SPIE 8097, Optical Trapping and Optical Micromanipulation VIII*, 8097 (SPIE, Bellingham, WA, 2011).
- [6] Hu, C.T., Wu, J.C. and Ai, B.Q., Memory effects in funnel ratchet of self-propelled particles, *J. Stat. Mech.*, 053206, (2017).
- [7] Zhu, W.J., Li, F.g. and Ai, B.Q., Transport of alignment active particles in funnel structures, *Eur. Phys. J. E*, 40, 59 (2017).
- [8] Vicsek, T., Czirók, A., Ben-Jacob, E., Cohen, I. and Shochet, O., Novel type of phase transition in a system of self-driven particles, *Physical review letters*, 75, 1226, 1995.
- [9] Grégoire, G. and Chaté, H., Onset of collective and cohesive motion, *Physical review letters*, 92, 025702, 2004.
- [10] Ginelli, F. and Chaté, H., Relevance of metric-free interactions in flocking phenomena, *Physical review letters*, 105, 168103, 2010.

A minimal physical model for cell migration in presence of obstacles

Antonio Basoni¹, Giuseppe Gonnella¹, Davide Marenduzzo², Enzo Orlandini³ and Adriano Tiribocchi³

¹Dipartimento di Fisica, Università di Bari
Via Amendola 173, 70126 Bari, Italy

²SUPA, School of Physics and Astronomy, University of Edinburgh
Peter Guthrie Tait Road, Edinburgh, EH9 3FD, UK

³Dipartimento di Fisica e Astronomia and Sezione INFN, Università di Padova
Via Marzolo 8, I-35131 Padova, Italy

Abstract

We present a simplified physical model of cell migration in a complex environment. In the framework of a phase field model we employ a hydrodynamic active polar gel theory to investigate by lattice Boltzmann simulations the cellular mechanical response to steric hindrance, showing its connection with both confining region geometry characteristics and elastic properties of the cell.

Keywords: cell motion, LBM, obstacle, phase-field

1. Introduction

Cell motility in eukaryotes is fundamental to biological functions such as wound healing, immune response and wiring of the brain. On the other side many diseases encompass cell migration, which for example is a pivotal step in metastatic process. Beyond the biological relevance, a motile cell is also an intriguing example of a physical self-driven and organized system. Recent experiments *in vitro* give new insight into motility mechanisms, showing that their differentiation arises from the balance between actin treadmilling (polymerization) and myosin-induced stress (contractility), but cell responsiveness to mechanical external stimuli is still poorly understood.

We present a simplified hydrodynamical model of a cell, consisting of a droplet of active polar fluid. The model predicts a variety of shapes and motility regimes, some closely resembling cases seen experimentally. We show that steric hindrance in a complex environment depends both on obstacle pattern characteristics and on viscoelastic properties and cell size.

2. The model

In [1] it has been shown that cell crawling can be simulated by an active polar fluid droplet with contractility throughout but treadmilling connected to a thin layer near the substrate. This is not the only possible route to motility, cell dynamics can arise solely from the contractile motion of myosin motors [2]. We present a quasi-2d model taking into account the interaction of a droplet with its counterparts or obstacles on its pathway. We introduce a multi-phase field model based on a free-energy functional for polar liquid-crystalline passive droplets that controls the equilibrium physics of the system:

$$\begin{aligned} \mathcal{F}[\phi_i, \mathbf{p}_i] = & \sum_i \int d^3r \left\{ \frac{a}{4\phi_{cr}^4} \phi_i^2 (\phi_i - \phi_0)^2 + \frac{k}{2} |\nabla \phi_i|^2 \right. \\ & - \frac{\alpha}{2} \frac{(\phi_i - \phi_{cr})}{\phi_{cr}} |\mathbf{p}_i|^2 + \frac{\alpha}{4} |\mathbf{p}_i|^4 + \frac{\kappa}{2} (\nabla \mathbf{p}_i)^2 + \beta \mathbf{p}_i \cdot \nabla \phi_i \left. \right\} \\ & + \sum_{i \neq j} \int d^3r \left(\frac{k_{st}}{2} \phi_i^2 \phi_j^2 + k_{ad} \nabla \phi_i \cdot \nabla \phi_j \right), \end{aligned} \quad (1)$$

being ϕ_i and \mathbf{p}_i the order parameters for the i -th droplet, the first defined as local average of actomyosin, the last defined as average orientation of actin filaments. We introduce a steric repulsion that prevents droplets from overlapping and a cell-cell adhesion that can favour the formation of aggregates.

The evolution of $\phi_i(\mathbf{r}; t)$ obeys a convective-diffusion equation

$$\frac{\partial \phi_i}{\partial t} + \nabla \cdot (\phi_i (\mathbf{u} + w \mathbf{p}_i)) = \nabla \cdot \left(M \nabla \frac{\delta \mathcal{F}}{\delta \phi_i} \right), \quad (2)$$

where w is the self-advection parameter. The dynamics of the polarization field $\mathbf{p}_i(\mathbf{r}, t)$ is borrowed from polar liquid crystal theory

$$\frac{\partial \mathbf{p}_i}{\partial t} + (\mathbf{u} + w \mathbf{p}_i) \cdot \nabla \mathbf{p}_i = -\underline{\underline{\Omega}} \cdot \mathbf{p}_i + \xi \underline{\underline{\mathbf{v}}} \cdot \mathbf{p}_i - \frac{1}{\Gamma} \frac{\delta \mathcal{F}}{\delta \mathbf{p}_i}. \quad (3)$$

where $\underline{\underline{\Omega}}$ and $\underline{\underline{\mathbf{v}}}$ are the symmetric and antisymmetric parts of the tensor $\underline{\underline{\nabla}} \mathbf{u}$, ξ is a shape factor related to the geometry of the active particles (actin filaments) and Γ is the rotational viscosity.

The velocity field $\mathbf{u}(\mathbf{r}, t)$ obeys the Navier-Stokes and the continuity equations

$$\begin{aligned} \rho \left(\frac{\partial}{\partial t} + \mathbf{u} \cdot \nabla \right) \mathbf{u} = & -\nabla P + \nabla \cdot (\underline{\underline{\sigma}}^p + \underline{\underline{\sigma}}^a) \\ \nabla \cdot \mathbf{u} = & 0, \end{aligned} \quad (4)$$

here the passive stress tensor $\underline{\underline{\sigma}}^p$ consists of a viscous term, an elastic stress and the contribution due to interfaces [1]. The active stress $\underline{\underline{\sigma}}^a$ comes from the coarse-grained actomyosin contraction process [1]. In this framework we first model the interaction between a cell and a rigid obstacle, where the latter is realized as source of potential energy. Later we consider collision events against cellular fragments or death cells described by a phase field variable with frozen evolution.

3. Simulation results

To solve our model equations we use a hybrid lattice Boltzmann algorithm solving Eqn (2) and Eqn (3) via a finite difference predictor-corrector scheme while the integration of the Navier-Stokes equation is performed by a standard LBM approach. We first study cell migration through narrow channels and observe an increasing cell velocity with decreasing cross section.

The time evolution of velocity in a channel seems to reproduce the experimental trend [3], since the droplet first briefly stall, it accelerates when entering the constriction and reaches a maximum velocity at the end of the channel. We suggest the possibility that the deformation energy stored elastically may have a role in explaining such velocity profile. Then we observe how the surface tension influences both cell morphology and passage time. We find that the model captures some typical cell transit shapes, such as the hourglass shape, and that the passage time increases with interfacial tension.

In Fig.1 and Fig.2 we offer two illustrative situations of a crawling cell on hard substrates. The first one resembles the behavior of a glioma cell crawling on a blood vessel. The second case reproduces a cell migrating through a pattern of obstacles.

Finally, we have performed a first numerical study on collective migration and on the formation of aggregates varying the strength of couplings between droplets, looking for a better comprehension of the polarization mechanism feedback.

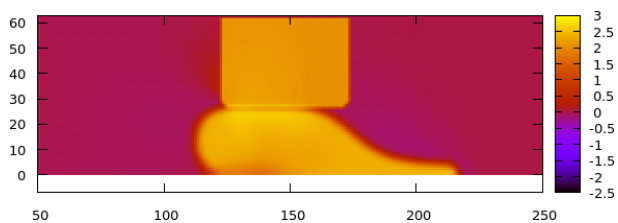


Figure 1: A cell crawling on a substrate encounters an obstructing spatial barrier. We plot the concentration field ϕ of the droplet (side view).

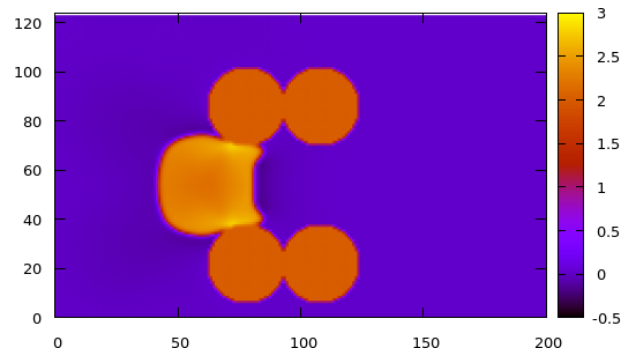


Figure 2: Concentration field ϕ for a cell crawling (top view) through an obstacle pattern of two parallel lines of two disks (in orange).

References

- [1] Tjhung, E., Tiribocchi, A., Marenduzzo, D., Cates, M.E., A minimal physical model captures the shapes of crawling cells. *Nat. Comm.*, 6, 5420, 2015.
- [2] Tjhung, E., Marenduzzo, D., Cates, M.E., Spontaneous symmetry breaking in active droplets provides a generic route to motility. *PNAS*, 109 (31), pp. 12381-12386, 2012.
- [3] Lautscham, L.A., Kämmerer, C., Lange, J.R., Kolb, T., Mark, C., Schilling, A., Strissel, P.L., Strick, R., Gluth, C., Rowat, A.C., Metzner, C., Fabry, B. Migration in confined 3D environments is determined by a combination of adhesiveness, nuclear volume, contractility, and cell stiffness. *Biophys. J.*, 109 (5), pp. 900-913, 2015.

Endocytic reawakening of motility and flocking in jammed epithelia

Fabio Giavazzi¹, Chiara Malinverno², Aldo Ferrari³, Giorgio Scita² and Roberto Cerbino¹

¹ *Università degli Studi di Milano*
Via F.lli Cervi, 93, 20090 Segrate, Italy
fabio.giavazzi@unimi.it

² *IFOM-FIRC Institute of Molecular Oncology*
Via Adamello, 16, 20139 Milano, Italy

³ *ETH Zurich, Laboratory of Thermodynamics in Emerging Technologies*
Sonneggstrasse 3, 8092 Zurich, Switzerland

Abstract

Dynamics of epithelial monolayers has recently been interpreted in terms of a jamming or rigidity transition. How cells control such phase transitions is, however, unknown. Here we show that RAB5A, a key endocytic protein, is sufficient to induce large-scale, coordinated motility over tens of cells, and ballistic motion in otherwise kinetically arrested monolayers. This is linked to increased traction forces and to the extension of cell protrusions, which align with local velocity. Molecularly, impairing endocytosis, macropinocytosis or increasing fluid efflux abrogates RAB5A-induced collective motility. A simple model based on mechanical junctional tension and an active cell reorientation mechanism for the velocity of self-propelled cells identifies regimes of monolayer dynamics that explain endocytic reawakening of locomotion in terms of a combination of large-scale directed migration and local unjamming. These changes in multicellular dynamics enable collectives to migrate under physical constraints and may be exploited by tumours for interstitial dissemination.

Keywords: Endocytosis, collective cell migration, jamming transition

1. Introduction

Collective cell migration is essential for tissue morphogenesis during development and repair, and also for tumour dissemination. Most aspects of multicellular migration are ruled by the physical interactions that cells establish among each other and with their environment. For example, during collective migration within confluent monolayers, cell sheets flow like a fluid yet remain fixed and solid-like at short timescales, with the motion of each cell constrained by the cell crowding due to its neighbours. As cell density rises, neighbouring cells restrict the motion of each cell, forcing them to move in groups, surprisingly similar to what is observed in systems of inert particles that undergo a jamming or rigidity transition at high density [1]. However, while the transition in inert systems invariably occurs at a critical particle packing, epithelial monolayers display limited density fluctuations.

Therefore, material parameters that encode cell properties such as cell-cell adhesion and cortical tension, rather than density alone, have been proposed to govern the rigidity transition in cell monolayers [2,3]. However, the general validity of this theoretical framework remains to be investigated. Even less understood are the molecular determinants and cellular processes that regulate multicellular dynamics by impacting on physical properties.

A cellular process that influences cellular and multicellular motility strategies is membrane trafficking. Here, we report that perturbation of endocytosis by altering the levels of its master regulator RAB5A is sufficient to reawaken the motility of jammed epithelial monolayers. RAB5A causes large,

anisotropic and spatially correlated migratory patterns by globally enhancing endosomal trafficking and macropinocytic internalization [4].

2. Results

To test the role of endocytic trafficking on collective epithelial locomotion, we perturbed the levels of RAB5A by generating doxycycline-inducible, RAB5A-expressing populations of human mammary epithelial MCF-10A cells.

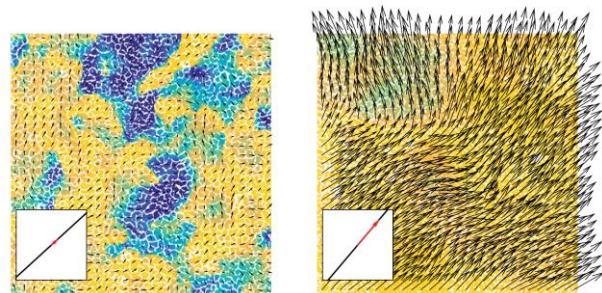


Figure 1: Snapshots of the velocity field obtained from Particle Image Velocimetry (PIV) analysis of doxycycline-treated control (left) and RAB5A-MCF-10A (right) cells seeded at jamming density and monitored by time-lapse microscopy. The size of each field of view is approximately 0.5 mm in real space. The red arrow in each inset is proportional to the mean velocity. The colour map reflects the alignment with respect to the mean velocity. Adapted from Ref. [4].

*Footnotes may appear on the first page only to indicate research grant, sponsoring agency, etc. These should not be numbered but referred to by symbols, e.g. *,+. The footnote text may be produced in a small font.

These cells form polarized monolayers and, upon reaching confluence, display a typical collective locomotion mode characterized by the emergence of large-scale, correlated motility, involving tens of cells. As cells keep on dividing, density increases, causing a near complete kinetic arrest akin to a jamming or rigidity transition [1,2]. Unexpectedly, under these latter conditions, elevation of RAB5A reawakened motility of kinetically arrested monolayer by promoting large multicellular streams (Figure 1). Of note, RAB5A expression did not alter the migration of individual MCF-10A cells in random migration assays. Thus, RAB5A effects on motility are emergent properties of cell collectives.

RAB5 is a master regulator of endocytic processes. Thus, one mechanism through which RAB5A acts is by promoting global alterations in endocytic processes. We showed that these variations impact on junctional tension, topology and dynamics of junctional proteins, facilitating coherent cell motion over long distances. Blockade of endocytosis by pharmacological treatments abrogated RAB5A-dependent collective locomotion and substantially decrease mean cell speed and velocity correlation length.

RAB5A further promotes cell-oriented locomotion through the extension of actin-based polarized protrusions aligned to the local velocity of migratory cohorts.

RAB5A-induced reawakening of motility is associated with a growing length scale of velocity correlation, precluding an understanding of monolayer dynamics simply in terms of an increase in local rearrangements.

To elucidate how these different contributions combine in our experiments, we performed numerical simulations of monolayer dynamics [4,5]. Our simulations are based on a self-propelled Voronoi (SPV) model incorporating the mechanical interaction between the confluent cells, the activity (self-propulsion) at the single-cell level, and a Vicsek-like polar alignment mechanism between the polarization direction of neighbouring cells. The alignment efficiency depends on the characteristic response time that each cell takes to actively align its polarity along the direction of its local velocity.

A study of the phase diagram reveals four different regimes for the monolayer dynamics. When the response time is large, the system behaviour is mainly controlled by the competition between cortical tension and cell-cell adhesion. When the first dominates the monolayer is jammed. Increasing cell-cell adhesion favours local cell rearrangements leading to an unjammed state, as previously described [3].

If the response time is decreased in the presence of a non-negligible single-cell speed, large-scale collective motility is observed in simulations that can be identified either as a “flocking solid” (large velocity correlation length in the absence of local cell rearrangements) or a “flocking liquid” (coordinated directed migration in the presence of local cell rearrangements).

The latter case, in which both local and collective motility are present, captures RAB5A phenotypes. A slow, short-range correlated dynamics without directed motion is instead compatible with the non-flowing liquid-like state of control monolayers (Figure 2).

The main predictions of this model are well verified in the experiments. In particular, while control cells simply slow down in time, the local dynamics in RAB5A monolayers is characterized by faster rearrangements accompanied by a decreasing length scale of dynamic heterogeneities, in the presence of characteristic morphological and structural signatures of fluidization.

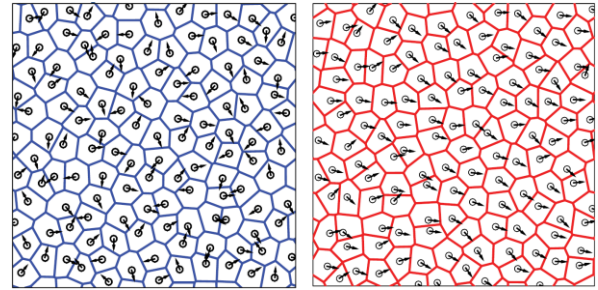


Figure 2: Representative snapshot of the simulated monolayer in a non-flocking state close to the solid–liquid transition (left) and in a “flocking liquid” state, where both directed collective migration is present and cell rearrangements are allowed (right). Each small arrow represents the instantaneous velocity of a cell. Adapted from Ref. [4].

3. Conclusions

We found that RAB5A controls a diverse set of collective motility processes in vitro and in vivo by re-awaking the directional, coordinated locomotion of jammed and kinetically arrested mono-layers. RAB5A exerts this function by promoting the formation of polarized, actin-based, lamellipodia that generate traction forces, which can be efficiently transmitted at long ranges through enhanced junctional contact and stresses. The increased mechanical coupling also enables a cell to obtain directional guidance cues from their neighbours, forcing adjacent cells to align their front-rear polarity, resulting in a positive feedback between polarity and net displacement. This, combined with increased dynamics of junctional E-cadherin to accommodate for cell neighbouring exchange, volume, density and strain fluctuations, collaboratively enable multicellular entities to acquire a fluid-like character. These alterations appear primarily to be the results of mechanical changes caused by global membrane trafficking perturbations. However, given the inextricable link between endocytosis and signalling, we cannot exclude that amplification and rewiring of specific biochemical pathways, particularly those emanating from EGF receptors, underpins some of the altered mechanical properties—a possibility that is currently under investigation. Importantly, these changes of plasticity promote the motility of otherwise jammed and glassy-like monolayers, leading to invasive, collective migration under physical confinement and accelerated multicellular directed migration during embryonic development.

References

- [1] Angelini, T. E., *et al.*, Glass-like dynamics of collective cell migration. *Proc. Natl Acad. Sci. USA* 108, pp. 4714-4719, 2011.
- [2] A Park, J. A., *et al.*, Unjamming and cell shape in the asthmatic airway epithelium, *Nature Materials*, 14, pp. 1040-1048, 2015.
- [3] Bi D., *et al.*, A density-independent rigidity transition in biological tissues, *Nature Physics* 11, pp. 1074–1079, 2015.
- [4] Malinverno, C., Corallino, S., *et al.*, Endocytic reawakening of motility in jammed epithelia, *Nature Materials*, 48, pp. 587-598, 2017.
- [5] Giavazzi, F., Paoluzzi, M., *et al.*, Flocking transitions in confluent tissues, arXiv:1706.01113.

Large speed enhancement of swimming bacteria in dense polymeric fluids

Andreas Zöttl and Julia M. Yeomans

Rudolf Peierls Centre for Theoretical Physics

1 Keble Road, Oxford, OX1 3NP, UK

andreas.zoettl@physics.ox.ac.uk

Abstract

Many cells in the human body have to move through dense complex fluids such as various cells in the extracellular matrix or bacteria in mucus. While the motion of swimming bacteria in simple Newtonian fluids can be well quantified using continuum low Reynolds number hydrodynamics, the presence of supramolecular elements such as biopolymers leads to a much more complex behavior. Although the presence of polymers generally lowers particle mobility, surprisingly, several experiments have shown that bacterial speeds increase in polymeric fluids [1, 2, 3, 4], but there is no clear understanding why. We perform extensive coarse-grained MPCD simulations of a bacterium swimming in explicitly modeled solutions of supramolecular model polymers of different lengths, stiffness and densities. We observe an increase of up to 60% in swimming speed with polymer density and show that this is a consequence of a depletion of polymers in the vicinity of the bacterium leading to an effective slip. However, depletion alone cannot explain the large speed-up, but coupling to the chirality of the bacterial flagellum is essential.

Keywords: swimming, polymeric fluids, hydrodynamic simulations

Microorganisms such as bacteria often move through biological fluids which contain high-molecular weight polymeric material. Prominent examples include the extracellular matrix, mucosal barriers and polymer-aggregated marine snow. Several explanations have been developed to explain the increase of bacterial speed in those fluids, including viscoelastic effects, local shear thinning, local shear-induced viscosity gradients, polymer depletion or modelling the polymers as a gel-forming network or a porous medium. So far experiments do not have the resolution to distinguish between the different theories. The advantage of numerical simulations which resolve some of the microscopic details, at least on a coarse-grained level, is the access to the underlying physical mechanisms depending on the specific swimmer and fluid properties. Here we simulate a model bacterium swimming in different suspensions of polymers at different densities, and reproduce and explain the enhanced swimming speed.

Many swimming bacteria rotate helical flagella attached at the back of their cell body to move forward. We are inspired by biological swimmers such as *E. coli* and build a model bacterium consisting of an elongated cell body of length $2b$ and width $2a$ which is connected to a quasi-stiff helical flagellum of radius R (Fig. 1a) [5]. Depending on the viscosity of the fluid, real bacteria may swim at a constant motor torque regime, or a constant motor angular velocity regime. In our simulations we focus on a constant motor torque \mathbf{T} to the flagellum and an opposing torque $-\mathbf{T}$ to the body. Then the body rotates at angular velocity Ω , and the flagellum counter-rotates at angular velocity ω . This drives the bacterium to swim forwards at an time- and ensemble-average velocity V . Our fluids consist of a Newtonian background fluid such as water at viscosity η_0 and at temperature T which we simulate using multiparticle collision dynamics (MPCD) which is coupled to coarse-grained polymers modelled as N spherical beads of diameter σ connected by quasi-rigid springs of rest length $l_0 = \sigma$ and bending stiffness k_b . We consider solutions of five different types of polymers (Fig. 1d), at different densities ρ . We first measure the fluid viscosities η which increase with density [5]. Fig. 1b shows a typical configuration of a bacterium and surrounding polymers at rather high volume fractions $\rho = 0.2$. Using extensive computer simulations

we simulate the dynamics of $\approx 5.75 \times 10^6$ MPCD fluid particles and of up to $\approx 2.2 \times 10^5$ polymer beads (e.g. $N_p \approx 18300$ polymers of length $N = 12$ at density $\rho = 0.2$). We measure the time- and ensemble-averaged swimmer speeds V and counterintuitively observe that helical microswimmers *increase* their swimming speed for all the fluids considered, by a factor of up to 60% (Fig. 1e).

The large speed-up of the bacterium stems from the fluid structure. For a Newtonian continuum fluid the swimming speed scales inversely with the viscosity and hence would lead to a decrease in speed when adding polymers. Indeed, in the following we explain the increase in speed by determining the flow field around the swimmer. We measure the time- and ensemble-averaged flow field which reads in cylindrical coordinates $\mathbf{v}(r, \phi, z) = v_r \hat{\mathbf{r}} + v_\phi \hat{\boldsymbol{\phi}} + v_z \hat{\mathbf{z}}$. Here $\hat{\mathbf{z}}$ is the symmetry axis of the swimmer. Figure 1c shows the flow field around a swimmer normalized by the swimming speed V in a fluid consisting of water and semiflexible polymer filaments at high density. The leading order far-field flow is a force-dipole field, similar as for bacteria in a Newtonian fluid. Interestingly, the scaled tangential flow field around the rotating cell body, $\bar{v}_\phi(r) = v_\phi(r)/(a\Omega)$, and flagellum, $\bar{v}_\phi(r) = v_\phi(r)/(R\omega)$, are weakened in the presence of polymers [5]. We measure the decay of $\bar{v}_\phi(r)$ near the flagellum for several polymer densities, comparing to the no-polymer case [$\bar{v}_\phi^0(r)$]. Interestingly, for all fluids the velocity fields decay with the same power law. This shows that the hydrodynamic flow fields are not screened, as it would be, for example, in porous media, and that Brinkman theory cannot be used to explain the increase in speed, which has been proposed in the literature as an explanation of swimming enhancement for helical bacteria.

Further we measure the ratio $\bar{v}_\phi(r)/\bar{v}_\phi^0(r)$ which compares the tangential velocity field to the no-polymer case. Very close to the bacterium, the value is close to one, but it decreases rapidly with distance r and levels off to a value I^B (near the cell body) or I^H (near the flagellum). Since the ratio converges to a constant value with increasing distance this again shows that the far-field scaling of the flow field is the same for all fluids, and only the magnitude of the fluid velocity field is decreasing. Very close to the swimmer there exists a thin layer where the flow field de-

cays more quickly with distance r than in the absence of polymers, which is a polymer depletion effect. Polymeric material is less likely to lie near the bacterium than in bulk due to the finite macromolecular size.

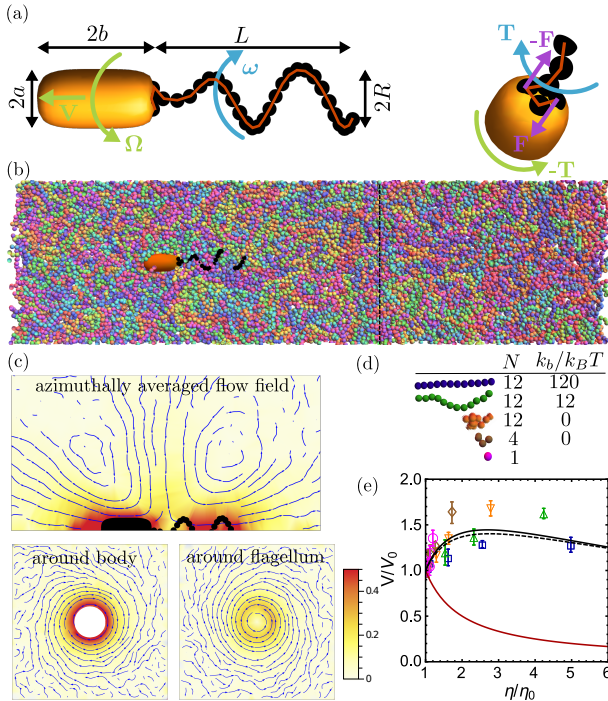


Figure 1: Bacterial swimming in polymeric fluids. (a) swimmer model; (b) snapshot of swimmer in dense fluid consisting of semiflexible polymers; (c) corresponding time- and ensemble-averaged flow field around the swimmer; (d) various polymers; (e) swimming speed depending on scaled viscosity η/η_0 .

We determine an average depletion layer thickness $\delta = 0.35a$ which is comparable to the size of a monomer. Depletion can be quantified by an apparent slip velocity at the surface of the bacterium, $u_s^H = (1 - I^H)R\omega$ and $u_s^B = (1 - I^B)a\Omega$ near the flagellum and the cell body, respectively. The slip velocities increase with polymer density and, interestingly, both collapse to a single curve for all fluids considered when plotted versus η/η_0 [5]. This is well explained by a two-fluid model where the fluid around the swimmer locally has viscosity η_0 in the depletion region and η outside.

However, apparent slip is in itself not sufficient to explain the enhanced swimming speed observed in Fig. 1e because surface-slip of driven spherical or rod-shaped particles does not lead to speed-up. So the depletion layer alone cannot explain why bacteria swim faster in a macromolecular solution. As we show in the following, enhancement in swimming speed is here only possible due to the chirality of the bacterial flagellum and the resulting translation-rotation coupling.

Using Resistive Force Theory (RFT) and locally approximating flagellum segments by a rod, the viscous force per unit length \mathbf{f} opposing the motion of a segment is split into a parallel and a perpendicular component, $\mathbf{f} = -\xi_{||}\mathbf{u}_{||} - \xi_{\perp}\mathbf{u}_{\perp}$, with anisotropic friction coefficients $1 < \xi_{\perp}/\xi_{||} < 2$ and local segment velocity $\mathbf{u} = \mathbf{u}_{||} + \mathbf{u}_{\perp}$. In order to include depletion, the slip velocity u_s^l

is applied tangential to the flagellum [5],

$$\mathbf{f} = -\xi_{||}(u_{||} - u_s^l)\hat{\mathbf{t}} - \xi_{\perp}\mathbf{u}_{\perp}, \quad (1)$$

where $\hat{\mathbf{t}} = \cos\alpha\hat{\mathbf{z}} + \sin\alpha\hat{\phi}$ is the unit vector tangential to the helix and α is its pitch angle. After integration along the flagellum we obtain the total force F and torque T acting on it and we can write its velocity V_H and angular velocity ω_H as

$$V_H = \mu_t F + \mu_{tr} T + R\omega_H \bar{u}_s / \tan\alpha, \quad (2)$$

$$\omega_H = \mu_{tr} F + \mu_r T + \omega_H \bar{u}_s, \quad (3)$$

where $\bar{u}_s = u_s/(R\omega_H) = u_s^l \sin\alpha/(R\omega_H)$ is the normalized apparent slip obtained from the decay of the azimuthal flow field. μ_t , μ_r , and μ_{tr} are the translational, rotational and translation-rotation-coupling mobilities, respectively. For a pure torque-driven helix we have $F = 0$, and eliminating ω_H from Eqs. (2) and (3) results in an expression for its velocity relative to the no-polymer case, $V_H^0 = \mu_{tr}^0 T$:

$$\frac{V_H}{V_H^0} = \frac{\eta_0}{\eta} \left(1 + \frac{1}{\tan\alpha} \frac{\bar{u}_s}{1 - \bar{u}_s} \frac{R\mu_r}{\mu_{tr}} \right) \quad (4)$$

which is a product of two terms. The first factor, η_0/η , decreases with viscosity, as it is the case for swimming in a continuum Newtonian fluid, and the second factor increases with viscosity since the scaled slip velocity \bar{u}_s increase with η . Their competition allows speed enhancement for sufficiently large depletion layer thickness and moderate viscosities, as is the case in our system.

When we include the counterrotating body and solve the full coupled body-flagellum model results in only relatively small corrections to Eq. (4). This is shown in Fig. 1e. We compare the viscosity-dependent swimmer speed from the MPCD simulations to analytic results from (i) the simple torque driven helix model (Eq. (4), black dashed line) and (ii) the full model including the swimmer body (black curve). For comparison we also plot the very different behaviour of the swimmer speed in the absence of any depletion effect (red line). The analytic results, which have no free fit parameters, are in very good qualitative agreement with the MPCD simulation results.

In summary, while swimming in a continuum viscous fluid without a polymer depletion layer always reduces the swimming speed for a constant-torque driven bacterium, a relatively thin polymer-free layer around the swimmer can reverse this effect.

References

- [1] Schneider, W. R., and Doetsch, R. N., Effect of viscosity on bacterial motility, *J. Bacteriol.*, 117, pp. 696–701, 1974.
- [2] Berg, H. C., and Turner, L., Movement of microorganisms in viscous environments, *Nature*, 278, pp. 349–350, 1979.
- [3] Martinez, V. A., Schwarz-Linek, J., Reufer, M., Wilson, L. G., Morozov, A. N., and Poon, W. C. K., Flagellated bacterial motility in polymer solutions, *Proc. Natl. Ac. Sci.*, 111, pp. 17771–17776, 2014.
- [4] Patteson, A. E., Gopinath, A., Goulian, M., and Arratia, P. E., Running and tumbling with *E. coli* in polymeric solutions, *Sci. Rep.*, 5, 15761, 2015.
- [5] Zöttl, A., and Yeomans, J. M., Enhanced bacterial swimming speeds in macromolecular polymer solutions, *arXiv:1710.03505*, 2017.

Scaling of bacteria swimming in polymer solutions

C. Devailly, A. Dawson, J. Arlt, J. Schwarz-Linek, A.N. Morozov, W.C.K. Poon, V.A. Martinez

SUPA and School of Physics and Astronomy, The University of Edinburgh, JCMB, Peter Guthrie Tait Road, Edinburgh EH9 3FD, UK.
vincent.martinez@ed.ac.uk

Abstract

We report experiments of swimming *Escherichia coli* in a range of newtonian and non-newtonian polymer solutions. By using Differential Dynamic Microscopy and Dark Field Microscopy, we measured the swimming speed (V) and body angular velocity (Ω) as a function of low-shear viscosity η_p up to $\approx 100 \times$ the viscosity of water. For the non-newtonian solutions, displaying strong shear-thinning properties, we reveal a remarkable enhancement of swimming speed (V) and precessivity (V/Ω) with increasing η_p compared to the newtonian solution. Additionally, we reveal a striking scaling of both V and Ω as a function of the precessivity for all non-newtonian solutions. We show this scaling is predicted by a 'toy' model for which body and flagella see two effective viscosities.

Keywords: bacterial motility, polymer, active matter, swimming

1. Introduction

Escherichia coli has become a model swimmer in the active matter field [1]. Numerous studies focus on the swimming in water but *E. coli* often live in viscoelastic media such as mucus in intestinal tract. Mucus is a strong viscoelastic material with shear-thinning properties containing long polymer chains as proteins and DNA. It has been suggested recently [2] that in a solution of PolyVinylpyrrolidone (PVP 360kDa), small and fast rotating flagella create a local high shear rate resulting in a polymer-free channel from its surrounding, while the slow rotating body of the bacterium 'feels' the low-shear viscosity of the polymer solution. Thus bacterial body and flagella observe two different environments. Here, we characterised the motility of wild-type *E. coli* in a range of polymer solutions, either biologically relevant (DNA) or model systems (Ficoll, PVP, PAAM and CMC), with distinct properties, i.e. size, stiffness, viscoelasticity, and shear-thinning.

2. Results

We measured the mean swimming speed V and mean body angular velocity Ω of a population of *E. coli* averaged over $\approx 10^4$ cells, using Differential Dynamic Microscopy [3] and Dark-Field Microscopy [2], respectively, over a range of polymer concentration. We dialysed each polymer to remove small-molecular impurities that can be metabolised by the cells and consequently increase their speeds [3]. We characterised independently the low-shear viscosity η_p of the solutions by measuring the diffusion coefficient D of non-motile bacteria. We show in Fig 1, typical results of V , Ω , as a function of η_p for solutions of λ -DNA and Ficoll. We found two distinctive responses over a similar range of η_p . Bacteria swimming in Ficoll display a strong slowing down up to $\times 5$ in both V and Ω , while surprisingly little η_p -dependency (within 5-10%) is observed in λ -DNA solutions. In Ficoll, V is proportional to Ω , as expected for swimmers in newtonian solution at low Reynolds number, and monotonically decreases with two apparent regimes as η_p is increased. We have recently shown that *E. coli* swimming in Ficoll can be quantitatively described by newtonian hydrodynamic theory when considering the low and high load regimes of the motor characteristic through the torque-motor speed relationship [2]. At high viscosity, $v \propto 1/\eta$ as predicted for a motor operating at a constant torque (see dotted line). In DNA, the remarkable

swimming enhancement compared to the newtonian solution, i.e. $V_{\text{DNA}} \approx 5 \times V_{\text{Ficoll}}$ at $\eta \approx 10$ cP, is puzzling and suggests a non-newtonian response in DNA solutions. Subsequent results and analysis will be presented and discussed.

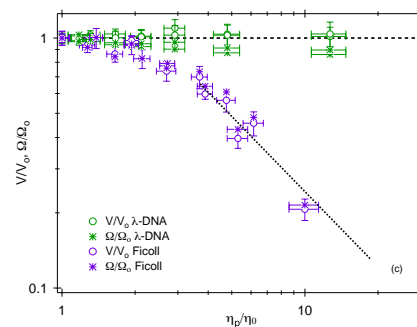


Figure 1: V and Ω of *E. coli* swimming in λ -DNA and Ficoll as a function of η_p . All parameters are normalised to their respective value in buffer with $V_0 \approx 9 - 12 \mu\text{m/s}$, $\Omega_0/2\pi \approx 11 - 15\text{Hz}$, and $D_0 \approx 0.32 - 34 \mu\text{m}^2/\text{s}$. Dotted line represents a slope of -1.

References

- [1] Schwarz-Linek, J., Arlt, J., Jepson, A., Dawson, A., Visers, T., Miroli, D., Pilizota, T., Martinez, V.A., and Poon, W.C.K., *Escherichia coli* as a model active colloid: A practical introduction, *Colloids and Surfaces B: Biointerfaces*, 137, pp. 2-16, 2016.
- [2] Martinez, V.A., Schwarz-Linek, J., Reufer, M., Wilson, L.G., Morozov, A.N., and Poon, W.C.K., Flagellated bacterial motility in polymer solutions, *Proc Natl Acad Sci USA*, 111, pp. 17771-17776, 2014.
- [3] Martinez, V.A., Besseling, R., Croze, A., Tailleur, J., Reufer, M., Schwarz-Linek, J., Wilson, L.G., Bees, M., Poon, W.C.K. Differential Dynamic Microscopy: A High-Throughput Method for Characterizing the Motility of Microorganisms, *Biophys. J.*, 103, pp. 1637-1647, 2012.

Bacteria push the limits of sensory precision to navigate dynamic seascapes

Douglas R. Brumley^{1*}, Francesco Carrara^{2*}, Andrew M. Hein^{3,4}, Yutaka Yawata^{2,5}, Simon A. Levin⁶, Roman Stocker²

¹*School of Mathematics and Statistics, The University of Melbourne, Parkville, Victoria 3010, Australia
d.brumley@unimelb.edu.au*

²*Department of Civil, Environmental and Geomatic Engineering, ETH Zurich, 8093 Zurich, Switzerland*

³*Southwest Fisheries Science Center, National Oceanographic and Atmospheric Administration, Santa Cruz, CA 95060*

⁴*Institute of Marine Sciences, University of California, Santa Cruz, CA 95060*

⁵*Graduate School of Life and Environmental Sciences, University of Tsukuba, Japan*

⁶*Department of Ecology and Evolutionary Biology, Princeton University, Princeton, NJ 08544, USA*

Abstract

The limited precision of sensory organs places fundamental constraints on organismal performance. An open question, however, is whether organisms are routinely pushed to these limits, and how limits might influence interactions between populations of organisms and the environment. Here, we show that marine bacteria operate near the theoretical limit of chemosensory precision when navigating the kinds of chemical landscapes they encounter in the ocean. By combining a method to generate dynamic, replicable resource landscapes, high-speed tracking of freely moving bacteria, a new mathematical theory, and agent-based numerical simulations, we show that sensory noise ultimately limits when and where bacteria can detect and climb chemical gradients. Our results suggest that bacteria inhabit chemical landscapes that are typically dominated by noise that masks shallow chemical gradients, and that the spatiotemporal dynamics of bacterial aggregations can be predicted by mapping the region where chemical gradients rise above noise.

Keywords: chemotaxis, motility, sensing noise, microfluidics, microbial ecology

Motile bacteria in the ocean survive by consuming ephemeral sources of dissolved organic matter (DOM) produced, for example, by phytoplankton lysis and exudation, or sloppy feeding and excretion by larger organisms [1, 2]. Past experiments on bacterial chemotaxis and aggregation using *Escherichia coli* and other model bacteria have generally focused on intermediate to high-concentration conditions, where bacteria can readily detect chemical gradients [3, 4]. However, the natural environments bacteria navigate are often characterized by complex, short-lived, microscale chemical gradients where background conditions are highly dilute [5]. In such diffusing chemical fields, bacteria experience the spreading pulse as a noisy, dynamic signal, rather than as a steady gradient.

Owing to their small size, motile bacterial cells like *E. coli* and marine bacteria, must rely on temporal gradient sensing to bias their swimming behaviour according to whether a chemical concentration is rising or falling over time. Theoretically, the relationship between the magnitude of a gradient signal and the noise associated with a cell's measurement of that signal – the signal to noise ratio (SNR) of the chemical gradient measurement – determines when and where cells can perform chemotaxis. Recent theoretical work has explored the physical limits on the accuracy and precision of cellular gradient sensing [6, 7, 8], expanding on the work of Berg and Purcell [3], which derived the physical limits of concentration sensing. In natural environments, gradients are often noisy, in part due to low concentrations and local fluctuations, and can change over timescales comparable to the chemotactic response [9, 10]. Understanding what governs bacterial chemotaxis and aggregation under such conditions requires a method for quantifying the behaviour of individual bacteria at the onset of gradient detection. Such a method has remained elusive.

We engineered a microfluidic system (Fig. 1A) to introduce an instantaneously available nutrient source of glutamate of

known concentration, in order to determine what triggers chemotactic behaviour of marine bacteria and what governs the dynamics of bacterial aggregations. In the seconds and minutes following release of a glutamate pulse, cells of the bacterium species *Vibrio ordalii* are exposed to a dynamic, yet reproducible chemical microenvironment that evolves in time as the amino acid molecules diffuse (Fig. 1D-E). Through high-resolution tracking [11] of over one million bacterial trajectories (Fig. 1B), we characterize single cell responses to the nutrient pulse, extract instantaneous individual swimming characteristics and reconcile these with the nutrient profile.

We find that there are dynamic regions of space around a spreading pulse where bacteria exhibit strong motion up the chemical gradient (Fig. 1F). Outside of these zones, bacterial motion is unbiased. We show that the locations and spatiotemporal evolution of these chemotaxis zones are governed by the relationship between the chemoattractant gradient and sensory noise (Fig. 2A). The sensing regions across different pulse sizes are time-dependent annuli predicted by the theory of sensory noise. Using this theory, we show that the chemotactic machinery of *Vibrio ordalii* allows this bacterium to operate close to the theoretical limit of chemotactic sensitivity. More generally, we suggest that the relationship between gradient signals and noise is likely to govern bacterial aggregations in the ocean, and that this relationship can be used to predict the spatiotemporal “footprint” of chemoattractant sources. The ability to partition complex nutrient landscapes into discrete zones of active chemotaxis will facilitate the conceptual scaling-up from single hotspots to larger chemical domains such as the intricate turbulence-induced network of dissolved nutrients in the ocean.

*D.R.B. and F.C. contributed equally to this work

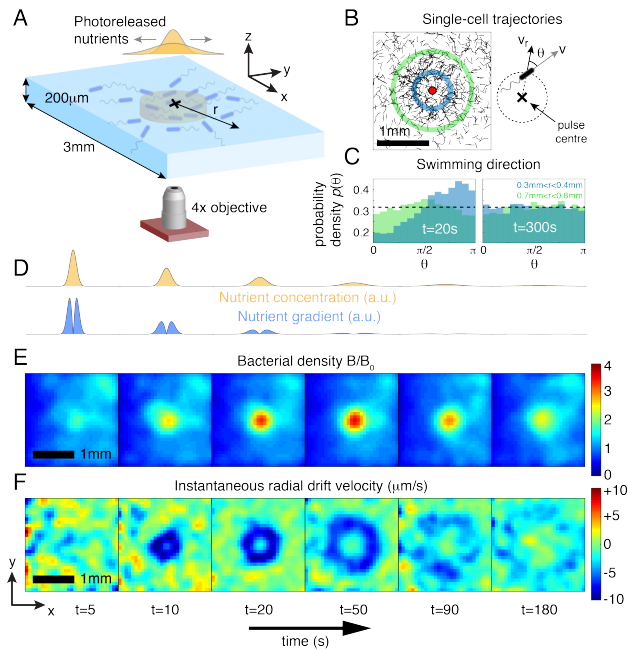


Figure 1: Time-dependent bacterial response to transient nutrient source. (A) Localised chemoattractant becomes available at the centre of the chamber through photorelease of caged glutamate (orange), which subsequently diffuses and attracts chemotactic bacteria (blue). (B) Single-cell trajectories in the first 60 s following pulse release. The swimming velocity makes an angle θ relative to the radial vector from the pulse centre. (C) Probability density functions, $p(\theta)$, showing swimming angle at $t=20$ s and 300 s for bacteria within different regions of space. The blue and green distributions correspond to the shaded regions in B, respectively. The dotted lines correspond to isotropic distributions (random swimming). A strong inward bias, $E[p(\theta)] > \pi/2$, is observed at $t=20$ s for cells in $r \in [300\mu\text{m}, 400\mu\text{m}]$. (D) Time-dependent nutrient profile (orange) and its corresponding spatial gradient (blue), (E) bacterial cell density and (F) instantaneous radial drift velocity v_{drift} at various times following the pulse release at $t=0$. The region of active chemotaxis is defined by the blue sensing annulus, which expands and eventually dissipates.

References

- [1] N. Blackburn, T. Fenchel, and J. Mitchell. Microscale nutrient patches in planktonic habitats shown by chemotactic bacteria. *Science*, 282(5397):2254–2256, 1998.
- [2] R. Stocker and J.R. Seymour. Ecology and physics of bacterial chemotaxis in the ocean. *Microbiology and Molecular Biology Reviews*, 76(4):792–812, 2012.
- [3] H.C. Berg and E.M. Purcell. Physics of chemoreception. *Biophysical Journal*, 20(2):193–219, 1977.
- [4] H.C. Berg. *E. coli in Motion*. Springer, 2008.
- [5] R. Stocker. Marine microbes see a sea of gradients. *Science*, 338(6107):628–633, 2012.
- [6] R.G. Endres and N.S. Wingreen. Accuracy of direct gradient sensing by single cells. *Proceedings of the National Academy of Sciences USA*, 105(41):15749–15754, 2008.

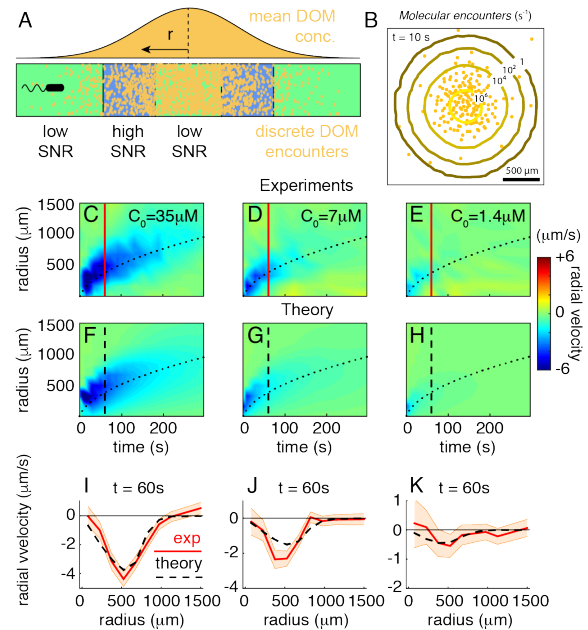


Figure 2: Effects of noise on chemotactic behaviour. (A) Schematic of mean DOM concentration as a function of the distance from the centre of a pulse. Far from and near to the pulse centre, the signal-to-noise ratio (SNR) is low. At an intermediate distance, around the flexus point of the spreading gaussian at $r = \sqrt{4D_C t}$, concentration gradients are strong and the gradient signal can emerge above noise. (B) Contours showing the instantaneous rate of encounter with glutamate molecules experienced by bacteria (calculated at $t=10$ s). (C) Experimentally measured average radial drift velocity of bacteria, v_{drift} , as a function of time and distance from the pulse centre, for an initial pulse of concentration $C_0 = 35 \mu\text{M}$ (LED exposure time $E = 500$ ms). (D, E) Same as C but with $C_0 = 7 \mu\text{M}$ ($E = 100$ ms) and $C_0 = 1.4 \mu\text{M}$ ($E = 20$ ms) respectively. Black dotted lines show $r = \sqrt{4D_C t}$ at the flexus point of the gaussian. (F-H) Theoretical predictions by fitting the model with the precision factor and gain parameters, δ and w (same nutrient parameters as panel C-E). (I-K) Radial velocity profiles from experiments (red) at $t=60$ s together with the theoretical predictions (black dashed) for three different pulse concentrations ($C_0 = 35 \mu\text{M}$, $C_0 = 7 \mu\text{M}$, $C_0 = 1.4 \mu\text{M}$ respectively).

- [7] T. Mora and N.S. Wingreen. Limits of sensing temporal concentration changes by single cells. *Physical Review Letters*, 104(24):248101, 2010.
- [8] A.M. Hein, F. Carrara, D.R. Brumley, R. Stocker, and S.A. Levin. Natural search algorithms as a bridge between organisms, evolution, and ecology. *Proceedings of the National Academy of Sciences*, 2016.
- [9] N.W. Frankel, W. Pontius, Y.S. Dufour, J. Long, L. Hernandez-Nunez, and T. Emonet. Adaptability of non-genetic diversity in bacterial chemotaxis. *eLife*, 3:e03526, 2014.
- [10] A.M. Hein, D.R. Brumley, F. Carrara, R. Stocker, and S.A. Levin. Physical limits on bacterial navigation in dynamic environments. *Journal of The Royal Society Interface*, 13:20150844, 2016.
- [11] K. Son, D.R. Brumley, and R. Stocker. Live from under the lens: exploring microbial motility with dynamic imaging and microfluidics. *Nature Reviews Microbiology*, 13(12):761–775, 2015.

Simulating Bacterial Motility in Confined Environments

John LaGrone¹, Lisa Fauci², and Ricardo Cortez³

¹Tulane University

6823 St. Charles Avenue New Orleans, LA 70118, USA
jlagrone@tulane.edu

²Tulane University

6823 St. Charles Avenue New Orleans, LA 70118, USA
fauci@tulane.edu

³Tulane University

6823 St. Charles Avenue New Orleans, LA 70118, USA
rcortez@tulane.edu

Abstract

We are interested in the propulsion dynamics of bacteria in porous materials such as soil, specifically with applications related to environmental remediation. In order to characterize bacterial swimming in confined environments, we present a computational model of flagellar driven bacteria and their hydrodynamic interactions. We construct an elastic body and flagella using networks of springs and drive the motion using a flagellar motor modeled by placing torques and the base of each flagella. The interaction with the surrounding fluid is modeled using the method of regularized Stokeslets. By placing the modeled flagella in narrow tubes, we investigate how confinement influences the swimming properties. We observe self centering behavior in some cases and a propensity to swim toward and into the wall in other cases. Additionally, we observe increased swimming speed in tubes of smaller radii and are investigating how the confinement influences the tumbling dynamics of the swimming bacteria.

Keywords: Flagella, Bacteria, Stokes flow, Regularized Stokeslets

1. Flagella Model

We begin by constructing a helical flagellum following the parameterization given in [2], we define the centerline of the helix as

$$\begin{aligned} x(s) &= \alpha(s), \\ y(s) &= -R(s) \cos\left(2\pi n_p \frac{s}{l}\right), \\ z(s) &= R(s) \sin\left(2\pi n_p \frac{s}{l}\right), \end{aligned} \quad (1)$$

where l is the total arc length, n_p is the number of turns in the helix, and the radius

$$R(s) = R_m \left[\frac{1}{\pi} \arctan\left(\beta \left(\frac{s}{l} - \gamma\right)\right) + \frac{1}{2} \right], \quad (2)$$

with $\alpha(s)$ is chosen such that the tangent vector $[x'(s), y'(s), z'(s)]$ has unit length.

Introducing a parameter to describe the radius of the flagella, r_F , we define the points, \mathbf{p} , on the cross sections as

$$\mathbf{p}_j(s_i) = \mathbf{x}(s_i) + r_F \left(\cos\left(\frac{2\pi j}{n_s}\right) \mathbf{u} + \sin\left(\frac{2\pi j}{n_s}\right) \mathbf{v} \right), \quad (3)$$

where j ranges from 0 to 5 to form hexagonal cross sections and \mathbf{u} and \mathbf{v} are the normal and binormal vectors to the helix centerline.

Finally, we connect each pair of points on the current cross-section and its immediate neighboring cross-sections with springs governed by the equation of force

$$\mathbf{F}_i = \sum_{j \in C(i)} k \left(\frac{\|\mathbf{x}_i - \mathbf{x}_j\|}{l_j} - 1 \right) \frac{\mathbf{x}_j - \mathbf{x}_i}{\|\mathbf{x}_i - \mathbf{x}_j\|}, \quad (4)$$

where k is the spring stiffness, $C(i)$ is the set of points connected to \mathbf{x}_i by springs, and l_j is the rest length of the spring connecting \mathbf{x}_i and \mathbf{x}_j . An example of such a helix shown in Fig. 1.



Figure 1: Example of a discretized flagella.

2. Fluid Coupling

Since bacteria exist in a low Reynolds number regime (typically $10^{-4} - 10^{-2}$ [3]), it is reasonable to model the fluid using Stokes Equations:

$$\mu \nabla^2 \mathbf{u} - \nabla p = 0, \quad \nabla \cdot \mathbf{u} = 0. \quad (5)$$

We then consider the forces, \mathbf{F}_i arising from the springs to be regularized point sources, satisfying the regularized Stokes equations [1]

$$\mu \nabla^2 \mathbf{u} - \nabla p = - \sum \mathbf{F}_i \phi_\varepsilon, \quad \nabla \cdot \mathbf{u} = 0, \quad (6)$$

where the regularized delta function, ϕ_ε , is given by

$$\phi_\varepsilon = \frac{15\varepsilon^4}{8\pi(r^2 + \varepsilon^2)^{7/2}}, \quad (7)$$

which results in the fluid flow

$$\mathbf{u}(\mathbf{x}_i) = \frac{1}{8\pi\mu} \sum_j \left(\frac{r_j^2 + 2\varepsilon^2}{(r_j^2 + \varepsilon^2)^{3/2}} \mathbf{F}_j + \frac{(\mathbf{F}_j \cdot \mathbf{r}_j) \mathbf{r}_j}{(r_j^2 + \varepsilon^2)^{3/2}} \right), \quad (8)$$

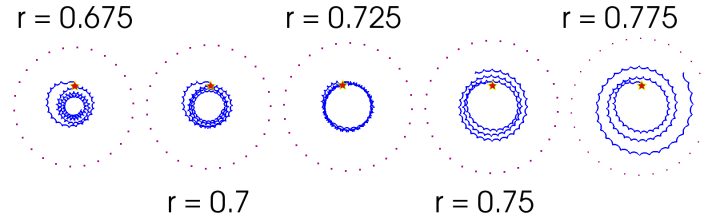


Figure 2: Trajectory of flagella swimming in various tube sizes. The star indicates the initial position, which is identical for all flagella.

where $\mathbf{r}_j = \mathbf{x}_i - \mathbf{x}_j$ and $r_j = \|\mathbf{r}_j\|$ and j ranges over the location of the spring nodes. We introduce motion to the system by applying a torque in the form of a regularized rotlet to the front of the flagella. In order to maintain a torque-free system, we place a second torque a small distance in front of the flagella, which we can think of as a crude approximation to a cell body. These torques impose an additional flow of the form

$$\mathbf{u}(\mathbf{x}_i) = \frac{1}{16\pi\mu} \sum_k \frac{2r_k^2 + 5\varepsilon^2}{(r_k^2 + \varepsilon^2)^{5/2}} (\mathbf{L}_k \times \mathbf{r}_k), \quad (9)$$

where k ranges over the locations of the torques and \mathbf{L}_k describes the strength and direction of the applied torque.

A solid tubular boundary can be approximated by placing a set of points on the surface of a tube and then computing the fluid flow at these points, $\mathbf{u} = [\mathbf{u}(\mathbf{x}_1), \mathbf{u}(\mathbf{x}_2), \dots, \mathbf{u}(\mathbf{x}_n)]$ as a result of the regularized Stokeslets (8) and rotlets (9). We can then enforce a no-slip boundary condition by solving for the forces $\mathbf{F} = [\mathbf{F}_1, \mathbf{F}_2, \dots, \mathbf{F}_n]$ at the points on the tube by rearranging the linear system (8) to have the form $\mathbf{u} = \mathbf{A}\mathbf{F}$.

3. Results

3.1. Free Space

For swimmers in free space, we can characterize much of the behavior by computing the non-dimensional number we refer to as the sperm number

$$Sp^4 = \frac{\xi^\perp \omega l^4}{\mathbf{E}\mathbf{I}}, \quad \xi^\perp = \frac{4\pi\mu}{\log\left(\frac{l}{r_F}\right)}, \quad \mathbf{E}\mathbf{I} = \frac{2E}{\kappa^2 l}. \quad (10)$$

Here, ω is the rotational frequency in hertz, and we approximate $\mathbf{E}\mathbf{I}$ by initializing the flagellum as if it were a straight rod and then bending it to a prescribed curvature κ and computing the resulting energy in the springs.

As demonstrated in Figures 3–4, the quantity Sp^2 collapses the distance each a flagella swims per revolution to a single (approximately cubic) curve, with the stiffer flagella swimming farther than the more flexible ones. This indicates the quantities encompassed by the sperm number, namely drag and flexibility, explain most of the observed behavior in the model. We note that in this case, the physical interpretation is that the stiffer flagella hold closer to their initial shape while the more flexible flagella stretch more which results in a smaller helical amplitude.

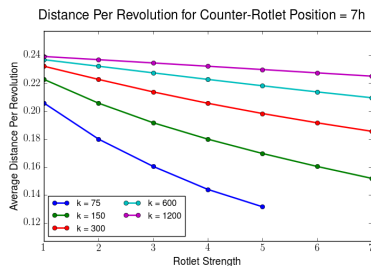


Figure 3: Distance per revolution as a function of applied torque. Note that the stiffer (large k) flagella swim farther per revolution than the more flexible flagella (small k).

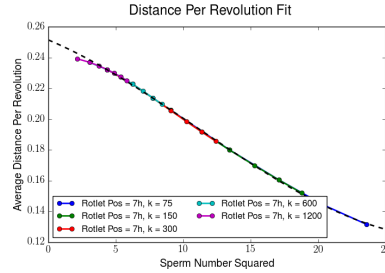


Figure 4: Distance per revolution plotted as a function of Sp^2 with a cubic fit.

3.2. Confined in Tubes

By simulating the flagella centered in tubes, we observe that the radii of the tube impacts the swimming dynamics. Figure 3 shows that the flagella swim a greater distance per revolution in tubes of smaller radii.

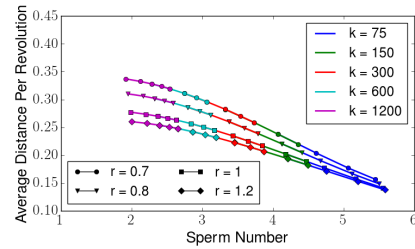


Figure 5: Distance per revolution plotted as a function of Sp for varying tube diameters.

A more interesting observation is that the flagella initialized at an angle with respect to the tube axis will center themselves in the tube for a sufficiently small radius, roll around the tube at an approximately fixed distance at a critical radius, and swim toward the tube wall at a sufficiently large radius. This effect is illustrated in Figure 2.

References

- [1] Ricardo Cortez, Lisa Fauci, and Alexei Medovikov. The method of regularized stokeslets in three dimensions: analysis, validation, and application to helical swimming. *Physics of Fluids*, 17(3):031504, 2005.
- [2] Heather Flores, Edgar Lobaton, Stefan Méndez-Diez, Svetlana Tlupova, and Ricardo Cortez. A study of bacterial flagellar bundling. *Bulletin of Mathematical Biology*, 67(1):137–168, 2005.
- [3] Eric Lauga. Bacterial hydrodynamics. *Annual Review of Fluid Mechanics*, 48:105–130, 2016.

Transport of swimming bacteria in porous media flows

Amin Dehkharghani¹, Nicolas Waisbord¹, Jörn Dunkel², and Jeffrey S. Guasto^{1*}

¹Department of Mechanical Engineering, Tufts University
200 College Avenue, Medford, MA 02155
Jeffrey.Guasto@tufts.edu

²Department of Mathematics, Massachusetts Institute of Technology
77 Massachusetts Avenue, Cambridge, MA, 02139

Abstract

Swimming bacteria live in porous environments characterized by dynamic fluid flows, where they play a crucial role in processes ranging from the bioremediation to the spread of infections. We study bacterial transport in a model microfluidic porous medium, which is complemented by Langevin simulations. Measured cell trajectories and the local cell number density reveal the formation of complex filamentous cell concentration patterns within the pores, which arise from the rotational alignment of the elongated bacteria with the Lagrangian stretching experienced within the porous media flows. Moreover, the effective diffusion coefficient of the motile bacteria is severely hindered in the transverse direction to the flow due to decorrelation of the cells' persistent random walk by hydrodynamic rotation. The hindered lateral diffusion has the surprising consequence of strongly enhancing the longitudinal bacterial transport through a dispersion effect. These results demonstrate the significant role of the flow and geometry in bacterial transport through porous media with potential implications for understanding ecosystem dynamics and bioengineering of industrial systems.

Keywords: swimming cells, porous media, transport, active matter, microfluidics

1. Introduction

Swimming bacteria thrive in confined porous environments, often in the presence of complex fluid flows. They are integral to numerous environmental, human health, and engineering processes including biodegradation, spread of infections, and oil recovery. Elucidating the mechanisms underlying the transport properties of motile bacteria in porous media flows is paramount to understanding and controlling these processes. In addition to intricate pore structure and flow paths within porous media, self-propulsion, cell morphology, and the biological behaviours of the swimming bacteria further complicate the dynamics of cell transport. Studies that consider these essential elements in describing motile cell transport in porous media are lacking [2]. To remedy this, we use microfluidic experiments complemented by Langevin simulations to show how geometry, motility, and flow conspire to locally enhance cell concentration, while severely affecting their macro-scale transport properties.

2. Microfluidics experiments and Langevin simulations

A transparent microfluidic channel was designed to elucidate the cell-scale mechanisms mediating the transport of swimming bacteria in porous media flows. The quasi-two-dimensional model porous medium consists of a square lattice of circular pillars in a rectangular cross-section microchannel with five different angles between mean flow direction and the lattice direction (Fig. 1). Different angles of the porous media lattice generate different flow field topologies with minimal change in the device design and fabrication. Dilute suspensions of wild-type *Bacillus subtilis* are flowed through the device at different flow rates using a syringe pump and imaged on an inverted microscope.

A Lagrangian model of bacterial motility was also implemented to capture cell trajectories over a broader range of parameters than is possible experimentally. The equations of

motion are developed by considering the self-propulsion of a bacterium, their translation due to fluid advection, and their rotation due to fluid vorticity, the coupling between the elongated cell shape and fluid extension, and the tumbling events arising from the unbundling of the bacterial flagella[3,4]. These equations are integrated for 1000 simulated bacteria to steady state to obtain their trajectories.

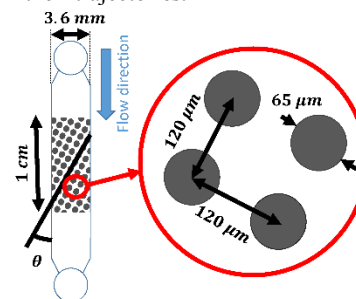


Figure 1. **Microfluidic porous medium.** Schematic representation of the model porous medium channel where $\theta = 0^\circ, 7.5^\circ, 15^\circ, 30^\circ, 45^\circ$, and the depth is $125 \mu\text{m}$.

3. Heterogeneous bacterial densification

In the absence of external forces, surfaces, or stimuli, bacteria are known to perform an unbiased random walk, which homogenizes their spatial distribution. In our porous microfluidic devices, the distribution of cells becomes highly heterogeneous when fluid flow is introduced. The topology of this heterogeneity is dependent upon the topology of the flow fields (Fig. 2 A - E). The resulting filamentous densification patterns of bacteria are well-captured by the Langevin model (not shown here). Cells, while being carried with fluid flow, cross the streamlines within the porous media flow due to their self-propulsion. This behaviour was shown to enable densification, even in simple Poiseuille flows [4].

*Supported by NSF grants CBET-1511340 and CAREER-1554095.

In porous media flows, the residency time of these elongated cells at each streamline depends on their average rotational alignment with that streamline. The rotational alignment of elongated particles arises from the Lagrangian stretching experienced within the porous media flow [3]. Cells located on streamlines with larger stretching tend to have a larger residency time, resulting in their larger concentration on those streamlines. This observation is supported by the strong correlation between the bacterial density and the stretching field within the porous media (Fig. 2 E-F, $\theta = 45^\circ$).

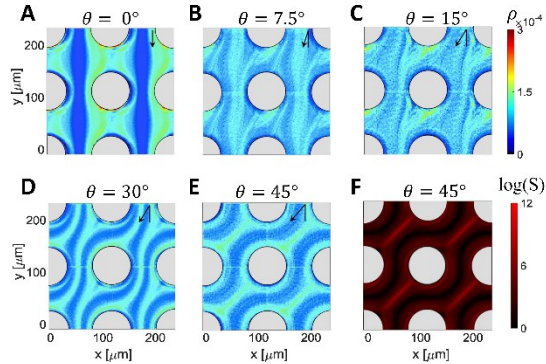


Figure 2. **Heterogeneous bacterial densification in porous media.** A-E, Bacterial density maps obtained from experimental trajectories. F, Stretching map for flow through $\theta = 45^\circ$ lattice obtained by calculating the logarithm of the eigenvalue of the left Cauchy-Green tensor.

4. Hindered effective diffusion amplifying longitudinal dispersion of bacteria

The canonical random walk motility of bacteria has long-motivated the extension of advection-diffusion models to bacterial transport in porous media flows. However, we observe that this analogy breaks down as increasing the flow hinders the transport of bacteria in the transverse flow direction. In general, we can relate the effective diffusion coefficient of the swimming bacteria to the persistence of their random walk motion. In a quiescent fluid, the velocities of the bacteria decorrelate exponentially due to the tumbling events, modelled as a rotational diffusion process with a coefficient of D_r . However, the hydrodynamic vorticity in the flow rotates the bacteria and reduces the persistence of the swimming. The competition between rotational diffusion and hydrodynamic vorticity is expressed as the non-dimensional rotational Peclet number: $Pe_r = \bar{\omega}/D_r$, where $\bar{\omega}$ is the average vorticity [4].

Effective bacterial diffusion coefficients are computed in the transverse direction to flow (D_\perp) based on the well-known Green-Kubo expression (Fig. 3). At high rotational Peclet numbers, the effective diffusion coefficients reduce rapidly with rotational Peclet number for $\theta = 0^\circ, 45^\circ$. This result is reasonably well captured by the $D_\perp \sim Pe_r^{-2}$ scaling of the translational diffusion coefficient for a noisy circular swimmer [1], suggesting that hydrodynamic rotation is the main mechanism for hindering transverse transport. The simulations enable the exploration of higher rotational Peclet numbers, which corroborate the experiments.

Long trajectories from the simulations enable the computation of effective dispersion coefficients in the longitudinal flow direction (Fig. 3). The longitudinal dispersion coefficients increase at high rotational Peclet numbers being more pronounced in the $\theta = 0^\circ, 45^\circ$ lattices at which the flow paths look like parallel pipes. While one might expect a Taylor-

Aris-like dispersion in these parallel flow paths, we show that the enhancement in the longitudinal dispersion coefficients is even more rapid due to the decrease of D_\perp with Pe_r , which can be implemented in the Taylor-Aris dispersion model.

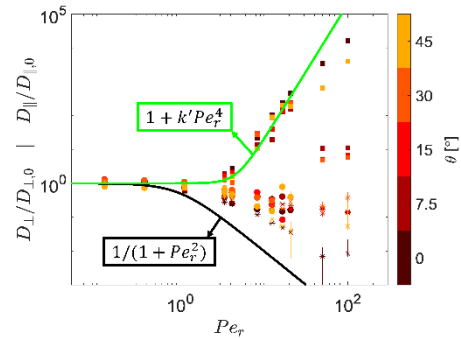


Figure 3. **Transport properties.** Effective dispersion coefficients in the transverse mean flow direction (D_\perp) from experiments (circles) and simulations (stars) and in the longitudinal direction (D_\parallel) from simulations (squares) normalized by their values in the absent of flow ($D_{\perp,0}$ and $D_{\parallel,0}$). Black curve is the normalized translational diffusion coefficient of a noisy circular swimmer in a simple shear flow, and the green curve is modified Taylor-Aris dispersion.

The transverse and longitudinal dispersion coefficients in other lattices fall between the dispersion coefficients of the $\theta=0^\circ, 45^\circ$ lattices. This is because in those lattices, the streamlines of the flow are aperiodic that leads to other hydrodynamic dispersion effects. The competition between these hydrodynamic dispersive effects and hindered effective diffusion coefficients results in slower reduction of transverse dispersion coefficients therefore smaller amplification of longitudinal dispersion coefficients.

5. Implications

The work presented here illustrates that fluid flows through porous media couple to cell shape and motility, which locally augment their concentration and impact transport. The resulting heterogeneous distribution of cells at the pore scale has the potential to impact microbial functions and biome dynamics ranging from biofilm formation to niche partitioning. The effect of flow on cell transport demonstrated here will undoubtedly lead to new discoveries in the physical ecology of biomes, the impact of the physical environment on the evolution, and a better understanding for bioengineering of industrial systems.

References

- [1] Friedrich B M and Jülicher F 2008 The stochastic dance of circling sperm cells: Sperm Chemotaxis in the plane *New J. Phys.* **10**
- [2] Long T and Ford R M 2009 Enhanced transverse migration of bacteria by chemotaxis in a porous T-sensor *Environ. Sci. Technol.* **43** 1546–52
- [3] Parsa S, Guasto J S, Kishore M, Ouellette N T, Gollub J P and Voth G A 2011 Rotation and alignment of rods in two-dimensional chaotic flow *Phys. Fluids* **23** 43302
- [4] Rusconi R, Guasto J S and Stocker R 2014 Bacterial transport suppressed by fluid shear *Nat. Phys.* **10** 212–7

Relationship between bacterial motility and biofilm-preventive properties on coatings with from soft to stiff mechanical properties

Mathieu Veuillet^{1,2}, Charline Soraru^{1,2}, Aissam Airoudj^{1,2}, Yannick Goubeyre³, Emmanuelle Gaudichet-Maurin³, Vincent Roucoules^{1,2} and Lydie Ploux^{1,2,*}

¹ Université de Haute-Alsace, CNRS, IS2M UMR 7361, F-68100 Mulhouse, France

² Université de Strasbourg, F-67000 Strasbourg, France

³ Veolia Research and Innovation, F-78520 Limay, France

*lydie.ploux@uha.fr

Abstract

We developed new hydrogel thin film coatings for (i) preventing biofilm formation on a large range of materials and (ii) providing tunable model platforms for studying bacterial motility and adhesion on surfaces with from soft to stiff mechanical properties. First *in situ* study of *Escherichia coli* behaviour on such surfaces were conducted under various hydrodynamic conditions, providing (i) confirmation of biofilm-preventive properties of coatings with low Young's modulus and high hydration rate; (ii) the Young's modulus range offering such properties; (iii) for the first time the evidence of a strong link between Young's modulus, motility (population percentage, bacteria's velocity) and biofilm-protective performances of polymer thin films, even enhanced under hydrodynamic flow.

Keywords: bacterial surface colonization, bacteria motility, biofilm-preventive coatings, mechanical surface properties

1. Introduction

Biofilms are a major issue in many health or economic domains, especially due to their ability to resist diffusion of molecules such as antibiotics and other antibacterial products, and to promote genetic selection of resistant microbial cells [1]. Many strategies seeking to provide biofilm-resisting surfaces without any use of biocide agent have focused on the modification of the surface chemistry including surface free energy and surface topography [2-4]. Despite of some efficacy in curbing the population of pioneer adherent bacteria, the reported solutions are mainly restricted to special situations (bacterial species, specific conditions of use) and are prone to be rapidly degraded by conditioning films.

Recently, we explored a new route to overcome these limitations by playing with mechanical properties of surfaces. Aside from weak probability of significant changes even in presence of conditioning film, mechanical properties were shown to significantly affect bacterial adhesion [5,6] and proliferation [5]. We especially reported that bacteria fail to adhere to and to colonize surfaces with elastic modulus less than 1 MPa [5].

In this work, we investigated this antibacterial effect under variable hydrodynamic conditions, especially aiming at understanding whether it may be related to specific behaviours in terms of motility. Therefore we developed a tuneable and well controlled coating offering a large range of elastic modulus, here used as a surface model of from soft to stiff coatings. Adhesion, motility and proliferation of the microbial cells were thoroughly analyzed by fluorescence confocal microscopy equipped with a specific, home-made flow cell. This allowed live imaging and *in situ* analysis under variable hydrodynamic culture conditions.

2. Materials & Methods

2.1. Preparation and properties of the coatings

Coatings are based on hydrogel thin films synthesized by plasma polymerization [7]. Plasma polymerization was performed in an electrodeless cylindrical glass reactor, in which the precursor molecule (2-hydroxyethyl methacrylate –HEMA-) was introduced by evaporation under evacuation at 0.1 mbar. By playing with external plasma parameters (pressure, input energy, duty cycle), the balance between crosslinking and hydrogen bonding was controlled, leading to different softness conditions. Young's modulus (E_s) values of the coatings ranged from 600 kPa to 4.5 MPa when immersed in aqueous liquid. Thickness (400 nm) and roughness ($R_a \approx 0.5$ nm) remained similar, while surface chemistry varied according to the input energy, however with only slight variations of amount functional groups in the range of surface stiffness from 0.6 to 1.8 MPa. Five different coatings

2.2. Microbiological culture and analysis

Bacterial behaviour on the coatings was investigated with GFP-fluorescent *Escherichia coli* (*E. coli*). Cultures without hydrodynamic constraints were performed on coatings with elastic modulus from 600 kPa to 4.5 MPa placed in Petri dishes. Cultures under hydrodynamic culture conditions were performed in a home-made flow cell in which 1 reference material (silicon wafer), 1 "soft" coating (600 kPa) and 1 "stiff" coating (1.8 MPa) were placed. Rising steps were strictly controlled to avoid any creation of air-surface interface. All bacteria remaining on the surface were considered as mobile or immobile but attached cells. *In situ* imaging up to 20h after inoculation was conducted under confocal microscope. Micrographs were treated and analysed with ImageJ® and plugins, or Comstat 2.1 (TUD, Denmark). Colonization was described in terms of total population of attached cells (hereinafter referred to "total population"), mobile and

*Footnotes may appear on the first page only to indicate research grant, sponsoring agency, etc. These should not be numbered but referred to by symbols, e.g. *,+. The footnote text may be produced in a small font.

immobile subpopulations (referred to “mobile population” and “immobile population”, respectively), and displacement and velocity of the mobile bacteria. All experiments were repeated at least 3 times, corresponding to at least 6 samples per material type.

3. Results & Discussion

Under static culture condition, the level of colonization after 2 h strongly varied with E_s value (Figure 1A). Two families of hydrogel are distinguished: (i) Surfaces with E_s values lower than 1.8 MPa are associated to a lower “total population” than the reference surface. Colonization was even reduced by 90% on the surface with E_s of 600 kPa in accordance with previous results we obtained on other coatings [5]. (ii) Surfaces with E_s values equal or higher than 1.8 MPa are associated to total populations equal or higher than on the reference surface, respectively. Interestingly, “total population” on all coatings was composed of two, immobile and mobile, subpopulations, whose percentage relative to total population varied strongly with E_s value: Mobile population accounted for up to 70% on soft surfaces while it was less than 5% on reference and stiff surfaces. Similarity of chemical composition and topographical features of all coatings with E_s value up to 1.8 MPa allows us to attribute these strong differences in bacterial motility and colonization to the surface mechanical properties.

Velocity of bacteria, *in situ* measured under confocal microscope, also showed significant differences in bacterial motility (Figure 1B). On reference and “stiff” coatings, the main population was composed of bacteria previously identified as immobile. They revealed a $0.25 \mu\text{m}\cdot\text{s}^{-1}$ average velocity, which was associated to slight vibrations around the bacteria’s gravity centre. In contrast, immobile bacteria were rare on “soft” coatings and had typical average velocity of ca. $0.5 \mu\text{m}\cdot\text{s}^{-1}$. The main population was mobile and displayed long displacements. Corresponding average velocity was ca. $1.3 \mu\text{m}\cdot\text{s}^{-1}$ while some bacteria moved up to $4 \mu\text{m}\cdot\text{s}^{-1}$. This range of velocity agrees the values reported for twitching ($0.06\text{--}1.00 \mu\text{m}\cdot\text{s}^{-1}$), which conforms with ability of *E.coli* K12 to express type IV pili.

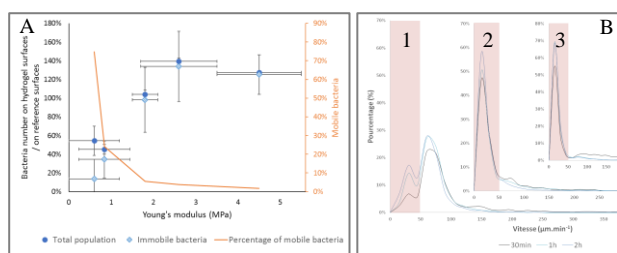


Figure 1: A) Total, immobile (*left y-axis*) and motile (*right y-axis*) (sub)populations of adhered bacteria referred to on the reference surface. B) Distribution of bacteria’s velocity on $E_s = 600 \text{ kPa}$ (1), $E_s = 1.8 \text{ MPa}$ (2) and reference (3) surfaces.

Under hydrodynamic conditions (Figure 2A), cell displacement and cell orientation with the stream were enhanced on the surface with E_s of 600 kPa compared to E_s of 1.8 MPa. This resulted in more frequent detachment of cells on the “soft” surface. One daughter bacterium was also frequently unsuccessful to adhere to the “soft” surface adhesion during cell division. As a result, after 20h of culture under flow, the “soft” surface carried only $20 \pm 18 \text{ cells/field}$ ($0.004 \mu\text{m}^3 \cdot \mu\text{m}^{-2}$) (Figure 2B), while biofilm quantity was ca. $45 \mu\text{m}^3 \cdot \mu\text{m}^{-2}$ on “stiff” and

reference surfaces. Thus, “soft” surfaces are shown to slow down proliferation, leading to biofilm-preventive properties beside the prevention of bacterial adhesion.

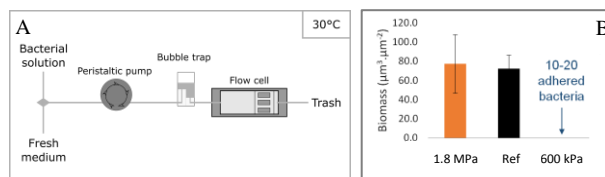


Figure 2: A) Experimental set-up for *in situ* analysis under hydrodynamic culture conditions. B) Biofilm quantity measured on $E_s = 600 \text{ kPa}$, reference and $E_s = 1.8 \text{ MPa}$ surfaces.

4. Conclusions

Aside from a promising way as biofilm-preventive coatings with efficiency against a large range of species, hydrogel thin films as here developed are precious model platforms to study bacterial motility, and potential further anchoring, on surfaces with from soft to stiff mechanical properties. In this work, they provide confirmation of the biofilm-preventive properties of coatings with low Young’s modulus E_s and high hydration rate and allow us to specify the E_s range of coatings revealing such properties. We also demonstrated for the first time a strong link between E_s , motility (bacterial population ratio and bacteria’s velocity) and final biofilm-protective effects on polymer thin films, even enhanced under some hydrodynamic features.

References

- [1] Mathieu, L., Francius, G., El Zein, R., Angel, E., and Block, J.-C., Bacterial repopulation of drinking water pipe walls after chlorination, *Biofouling*, 32, pp. 925–934, 2016.
- [2] Rzhepishevskaya, O., Hakobyan, S., Ruhul, R., Gautrot, J., Barbero, D., and Ramstedt, M., The surface charge of antibacterial coatings alters motility and biofilm architecture, *Biomater. Sci.*, 1, pp. 589–602, 2013.
- [3] Boks, N. P., Kaper, H. J., Norde, W., van der Mei, H. C., and Busscher, H. J., Mobile and immobile adhesion of staphylococcal strains to hydrophilic and hydrophobic surfaces, *J. Colloid Interface Sci.*, 331, pp. 60–64, 2009.
- [4] Helbig, R., Günther, D., Friedrichs, J., Röbber, F., Lasagni, A., and Werner, C., The impact of structure dimensions on initial bacterial adhesion, *Biomater. Sci.*, 4, pp. 1074–1078, 2016.
- [5] Cottenye, N., Anselme, K., Ploux, L., and Vebert-Nardin, C., Vesicular structures self-assembled from oligonucleotide polymer hybrids: Mechanical prevention of bacterial colonization upon their surface tethering through hybridization, *Adv. Funct. Mater.*, 22, pp. 4891–4898, 2012.
- [6] Wang, Y., Guan, A., Isayeva, I., Vorvolakos, K., Das, S., Li, Z., Phillips, K.S., Interactions of *Staphylococcus aureus* with ultrasoft hydrogel biomaterials, *Biomaterials*, 95, pp. 74–85, 2016.
- [7] Veillet, M., Ploux, L., Airoudj, A., Gourbeyre, Y., Gaudichet-Maurin, E., and Roucoules, V., Macroscopic control of DMAEMA and HEMA plasma polymerization to tune the surface mechanical properties of hydrogel coatings, *Plasma Process. Polym.*, 14, e1600215, 2016.

Transport and diffusion of micro-particles in microswimmer suspensions

Blaise Delmotte¹ and Eric Keaveny² and Franck Plouraboué³ and Eric Climent³

¹*Courant Institute of Mathematical Sciences, New York University
251 Mercer Street, New York, NY, 10012, USA
delmotte@cims.nyu.edu*

²*Department of Mathematics, Imperial College
michelle.driscoll@northwestern.edu
741 Huxley Building, South Kensington Campus London SW7 2AZ
e.keaveny@imperial.ac.uk*

³*Institut de Mécanique des Fluides de Toulouse
1, Allée du Professeur Camille Soula 31400 Toulouse
fplourab@imft.fr, eric.climent@imft.fr*

Abstract

In addition to enabling movement towards environments with favourable living conditions, swimming by microorganisms has also been linked to enhanced mixing and improved nutrient uptake by their populations. Experimental studies have shown that Brownian tracer particles exhibit enhanced diffusion due to the swimmers, while theoretical models have linked this increase in diffusion to the flows generated by the swimming microorganisms, as well as collisions with the swimmers. In this study, we perform detailed simulations based on the force-coupling method and its recent extensions to the swimming and Brownian particles to examine tracer displacements and effective tracer diffusivity in squirmer suspensions. By isolating effects such as hydrodynamic or steric interactions, we provide physical insight into experimental measurements of the tracer displacement distribution. In addition, we extend results to the semi-dilute regime where the swimmer-swimmer interactions affect tracer transport and the effective tracer diffusivity no longer scales linearly with the swimmer volume fraction.

Keywords: tracer dispersion, squirmers, active suspensions, simulations

1. Introduction

Mixing and transport of microscopic, inert particles by motile microorganisms have been a topic of recent interest as such suspensions are a prime example of out-of-equilibrium systems. The particles experience Brownian motion due to their small size and are further affected by hydrodynamic interactions and collisions with the micro-swimmers. Enhanced particle transport in active suspensions has been observed in the presence of collective motion [8], but also in the absence of it [4, 5]. Understanding the mechanism of enhanced tracer transport can provide insight into biological processes such as predator-prey interactions and the plankton food chain, and can help in the design of novel biomimetic micro-fluidic devices that use similar strategies for enhanced mixing and stirring at small scales. We present results from simulations exploring tracer transport in dilute and semi-dilute suspensions of squirmers [3]. In our simulations, we employ recently developed numerical tools based on the force-coupling method (FCM) [1, 2] that allow for multibody hydrodynamic interactions between active and passive particles, polydispersity in particle size, particle Brownian motion that satisfies the fluctuation-dissipation theorem, and steric interactions.

2. Numerical tools

In our simulations, we consider N_p squirmers dispersed in fluid containing N_t tracers giving a total number of particles $N = N_p + N_t$. All particles are spherical, however the squirmers have radius a_{sw} , while the smaller tracers have radius a . The position of particle n is denoted by \mathbf{Y}_n , while its orientation is \mathbf{p}_n . The dynamics of the squirmers and tracers are governed

by the overdamped Langevin equations. To compute the velocities and angular velocities of all particles, we rely on the force-coupling method (FCM) and the combination of two recent extensions of FCM to active particles [2] based on the steady squirmer model [6] and to Brownian suspensions [1] using concepts from fluctuating hydrodynamics.

3. Simulations parameters and set-up

In our simulations, we set our parameters to match the *C. rheindardtii* experiments of Leptos *et al.* [5]. We set the swimmer to tracer radius ratio to $a_{sw}/a = 5$ and set the swimming speed to match $U = 100\mu\text{m s}^{-1} = 20a_{sw}s^{-1}$. The simulations are carried out in a triply periodic domain with edge length $L = 23a_{sw}$. The Stokes equations are solved using a Fourier spectral method with $N_g = 192$ grid points in each direction. The number of tracers is set to $N_t = 1255$, resulting in a tracer volume fraction of less than 0.34%. The number of swimmers is varied from $N_p = 12$ to 451 to examine very dilute swimmer suspensions of $\phi_v = 0.4\%$, as well as semi-dilute cases where $\phi_v = 15\%$. Finally, the thermal energy $k_B T$ is set to obtain the same distribution of tracers displacements as [5] in the absence of swimmers. A snapshot taken from a representative simulation is shown in Fig. 1a.

4. Results

4.1. Dilute regime

In their experiments, Leptos *et al.* [5] measured the time-dependent probability distribution function, $P(\Delta x, \Delta t)$, for

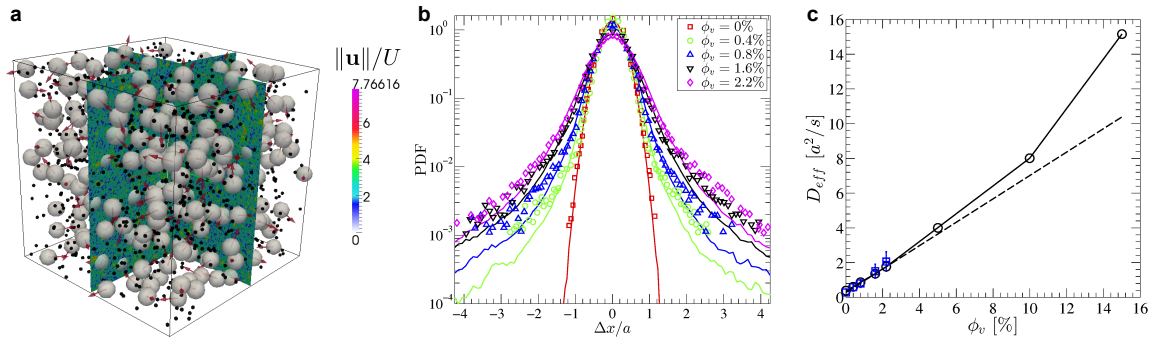


Figure 1: **a**, Snapshot of the simulation domain containing $N_p = 301$ swimmers and 1255 tracers, with $a_{sw}/a = 5$. The volume fraction is $\phi_v = 10\%$. The large grey spheres are the squirmers and the small black dots correspond to the tracers. Vectors represent the swimmers' orientations \mathbf{p}_n , $n = 1, \dots, N_p$. The colour bar shows the norm of the fluid velocity field, $\|\mathbf{u}\|/U$, in the mid-planes. One can observe the fluid velocity fluctuations arising from the fluctuating stress. **b**, PDF for tracer displacements at time $\Delta t = 0.12s$ for swimmer volume fractions $\phi_v = 0 - 2.2\%$. Symbols represent the data from [5]. Solid lines correspond to the simulations. **c**, Effective diffusion coefficient of tracers D_{eff} . \circ : simulations. $---$: linear fit for the dilute regime $\phi_v = 0 - 2.2\%$. \square : data from [5].

tracer displacements for suspensions with swimmer volume fractions $\phi_v = 0 - 2.2\%$ over 0.3s. As the beat period for the flagella of *C. rheindartii* is $T = 0.02s$, this observation time corresponds to 15 beat cycles. They find that unlike previous experiments using bacterial baths [8], the tracer displacement distributions exhibit non-Gaussian tails. The non-Gaussian tails are attributed to rare entrainment events that occur when a tracer particle comes in close proximity to a swimmer's surface. We performed simulations corresponding to the same swimmer volume fractions and observation times as in the experiments of [5]. The resulting tracer displacement distributions from our simulations are shown in Fig. 1b. Our squirmer simulations adequately capture the Gaussian core of the distributions. We find, however, that the larger, but rarer, displacement events related to the tails are slightly underestimated by the model. We attribute this to the fact that in the near-field, the squirmer does not replicate the flow induced by swimming *C. rheindartii* and the tails of the PDF for short-time tracer displacements depend on the details of the flow near the swimming micro-organism. In addition to the tracer displacement distribution, [5] measured the mean-squared displacement of tracers as a function of time and observed that the motion of tracers is diffusive obeying $\langle \Delta x^2 \rangle = 2D_{eff}t$ for all times, where D_{eff} is the tracer effective diffusion coefficient. In Fig. 1c, we compare the effective diffusion coefficient from our simulations with those obtained by [5]. As predicted by theoretical studies, we observe a linear scaling between the diffusion coefficient and the swimmer volume fraction ϕ_v in the dilute regime ($\phi_v = 0 - 2.2\%$). We can see that the simulated values match the experimental ones within the statistical errors reported for the experiments.

4.2. Semi-dilute regime

We perform simulations on more concentrated suspensions ($\phi_v = 10 - 15\%$) with the same numerical parameters. For all volume fractions, we observe that the PDF $P(\Delta x, \Delta t)$ tends towards a Gaussian at long times and the excess kurtosis converges asymptotically to zero. However the convergence rate increases with volume fraction. Using an analysis based on singular flows fields, [9] state that the tracer displacement distribution should only be Gaussian for $\phi_v > 25\%$ if the flows generated by the swimmers decay like r^{-n} with $n \geq 2$. The appearance of a Gaussian, however, agrees with the theoretical predictions of [7], as well as the experimental observations of [4] that observed an increase in Gaussianity with concentration. This, perhaps, highlights the importance of resolving the finite-size of both

swimmers and tracers to the observation of a Gaussian distribution of displacements. As in the experiments of [4], our simulations show (Fig. 1c) the linear scaling, $D_{eff} \propto \phi_v$, breaks down for $\phi_v > 2.2\%$, though we do not observe a clear power-law as in [4].

References

- [1] B. Delmotte and E. Keaveny, "Simulating brownian suspensions with fluctuating hydrodynamics," *J. Chem. Phys.*, vol. 143, p. 244109, 2015.
- [2] B. Delmotte, E. Keaveny, F. Plouraboué, and E. Climent, "Large-scale simulation of steady and time-dependent active suspensions with the force-coupling method," *J. Comp. Phys.*, vol. 302, pp. 524–547, 2015.
- [3] —, "Simulations of brownian tracer transport in squirmer suspensions," *Submitted, arXiv:1711.01442*, 2017.
- [4] H. Kurtuldu, J. S. Guasto, K. A. Johnson, and J. P. Gollub, "Enhancement of biomixing by swimming algal cells in two-dimensional films," *Proceedings of the National Academy of Sciences*, vol. 108, no. 26, pp. 10 391–10 395, 2011.
- [5] K. C. Leptos, J. S. Guasto, J. P. Gollub, A. I. Pesci, and R. E. Goldstein, "Dynamics of enhanced tracer diffusion in suspensions of swimming eukaryotic microorganisms," *Physical Review Letters*, vol. 103, no. 19, p. 198103, 2009.
- [6] M. Lighthill, "On the squirming motion of nearly spherical deformable bodies through liquids at very small reynolds numbers," *Communications on Pure and Applied Mathematics*, vol. 5, no. 2, pp. 109–118, 1952.
- [7] J.-L. Thiffeault, "Short-time distribution of particle displacements due to swimming microorganisms," *arXiv preprint arXiv:1408.4781*, 2014.
- [8] X.-L. Wu and A. Libchaber, "Particle diffusion in a quasi-two-dimensional bacterial bath," *Physical Review Letters*, vol. 84, no. 13, p. 3017, 2000.
- [9] I. M. Zaid, J. Dunkel, and J. M. Yeomans, "Lévy fluctuations and mixing in dilute suspensions of algae and bacteria," *Journal of The Royal Society Interface*, vol. 8, no. 62, pp. 1314–1331, 2011.

A Spheroidal Squirmer in Shear Flow

Kai Qi¹, Elmar Westphal², Gerhard Gompper¹, and Roland G. Winkler¹

¹Theoretical Soft Matter and Biophysics, Institute for Advanced Simulation and Institute of Complex Systems, Forschungszentrum Jülich, D-52425 Jülich, Germany

k.qi@fz-juelich.de, g.gompper@fz-juelich.de, r.winkler@fz-juelich.de

²Peter Grünberg Institute and Jülich Centre for Neutron Science, Forschungszentrum Jülich, D-52425 Jülich, Germany
e.westphal@fz-juelich.de

Abstract

Squirmers are generic models for biological microswimmers like bacteria and algae. Here, the properties of a spheroidal squirmer in shear flow is investigated by hydrodynamic simulations via the multiparticle collision dynamics (MPC) method, a particle-based simulation approach for fluids. Due to the elongated shape of a spheroid, alignment along the shear direction is observed for both passive spheroidal colloids and squirmers for weak shear flows. When the shear rate exceeds a critical value, alignment changes from the shear to the vorticity direction. Both, shear alignment and the transition reveal a clear dependence on the hydrodynamic dipole of the swimmer's flow field. Pullers with a large positive force-dipole coefficient exhibit gradual variations of the alignment direction, whereas pushers with a large negative coefficient show abrupt changes. Comparison between elongated and spherical squirmers reveals a significant shape dependence of their behaviors in shear flow.

Keywords: spheroidal squirmer, shear flow, alignment, tumbling

1. Introduction

From the largest animals to smallest organisms (single cells), motility is a fundamental characteristic of life. Cell swimming, in particular, underpins a wide range of fundamental biological phenomena, including microbial grazing—at the base of the food web—, parasitic infection—including severe diseases like malaria—, inter-microbial communication, and animal reproduction [1]. The understanding of biological microswimmer motility opens an avenue for control of their behavior and the design of artificial nanomachines, with a major impact on various fields ranging from life science and material science to environmental science. Propulsion and steering is intimately linked to various “taxes”, e.g., chemotaxis, phototaxis, or rheotaxis, where microswimmers react to external stimuli. In particular, *E. coli* bacteria have been shown to exhibit interesting rheotactic properties with a strongly concentration-dependent viscosity [2]. In the semidilute regime, such solutions exhibit a “superfluid-like” behavior with vanished viscous resistance is observed [2].

To investigate the properties of microswimmers under shear flow, we perform mesoscale hydrodynamic simulations using the multiparticle collision dynamics approach to describe the fluid [3], combined with molecular dynamics simulations for a microswimmer. Thereby, we apply a generic and coarse-grained description of the microswimmer by a so-called squirmer [1, 4]. We characterize the structural, dynamical, rheological properties of the squirmers for various shear rates and force-dipole moments.

2. Model and Method

A nonspherical squirmer as described as a prolate spheroidal rigid body with the prescribed surface velocity field [4]

$$\mathbf{u}_{sq} = -B_1(1 + \beta\zeta)(\mathbf{s} \cdot \mathbf{e}_z)\mathbf{s}, \quad (1)$$

with the spheroidal coordinates (ζ, τ, φ) , the tangent vector \mathbf{s} , and the unit vector \mathbf{e} in the swimming direction (cf. Fig. 1). The constant B_1 is related to the self-propulsion velocity U_0 via

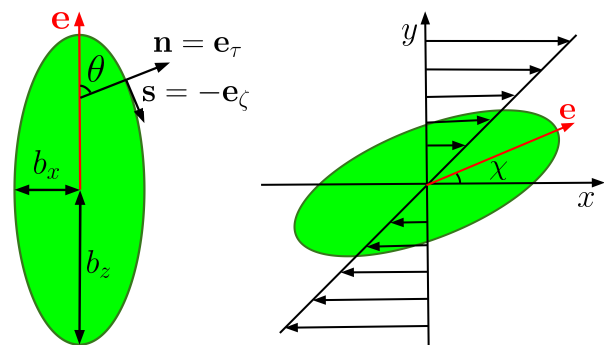


Figure 1: (Left) Model of a squirmer. Self-propulsion along the body-fixed orientation vector \mathbf{e} is achieved by an axisymmetric prescribed surface velocity in the direction of the tangent vector \mathbf{s} [4]. (Right) Illustration of a squirmer in shear flow.

$$U_0 = B_1\tau_0(\tau_0 - (\tau_0^2 - 1)\coth^{-1}\tau_0), \quad (2)$$

where $\tau_0 = b_z/\sqrt{b_z^2 - b_x^2}$, and β accounts for the active stress (force dipole, source quadrupole). Thereby, $\beta > 0$ corresponds to a puller, $\beta = 0$ to a neutral squirmer, and $\beta < 0$ to a pusher. The constants b_z and b_x are the semi-major and semi-minor axis, respectively. We consider $b_x = 3a$ and $b_z = 9a$.

A squirmer is embedded in fluid described by the multiparticle collision dynamics approach, which consists of two steps, i.e., streaming and collision. In the streaming step, fluid particles and squirmer move ballistically. Fluid particles colliding with the squirmer are reflected applying the bounce-back rule, thereby, fluid particles gain the local slip velocity. In this process, linear and angular momentum is conserved. The local stochastic interaction between particles and the squirmer is established by employing the stochastic rotation dynamics with angular momentum conservation (MPC-SRD+a) in the collision step [3]. Shear flow

with shear rate $\dot{\gamma}$ is induced by implementing Lees-Edwards periodic boundary conditions, with shear flow along the x -, gradient along the y -, and vorticity along the z -direction of the Cartesian reference system. The temperature of the system is maintained via a cell-level canonical thermostat [5].

In the following, lengths are measured in units of the collision cell size a . The simulations are performed with the mean number of particles per collision cell $\langle N_c \rangle = 10$, the rotation angle $\alpha = 130^\circ$, and the time step $h = 0.05\sqrt{ma^2/(k_B T)}$, which yields a fluid viscosity of $\eta = 8.1\sqrt{mk_B T/a^4}$, and a squirmer rotational diffusion coefficient around the minor axis of $D_R^\perp = k_B T/\xi^\perp = 2.6 \times 10^{-5}\sqrt{k_B T/ma^2}$, with the hydrodynamic rotational friction coefficient ξ^\perp of a spheroid. The Péclet number $Pe = U_0/2D_R^\perp b_z$ is $Pe = 95$.

3. Results

In response to shear flow, a squirmer exhibits a preferred orientation. The shear-rate dependence of the alignment, expressed by the Weissenberg number $Wi = \dot{\gamma}/D_R^\perp$, is presented in Fig. 2. Thereby, the angle χ between the propulsion direction and the flow direction is defined by

$$\tan(2\chi) = \frac{2e_x e_y}{e_x^2 - e_y^2}, \quad (3)$$

where e_x and e_y are the components of squirmer's orientation (propulsion direction). As shown in Fig. 2, the alignment angle decreases with increasing Weissenberg number. Thereby, passive colloids and squirmers at small $|\beta| \leq 1$ reveal a decrease of χ with the power-law $\tan(2\chi) \sim Wi^{-2/3}$, an exponent twice smaller than that found for passive polymers under shear flow. Here, activity seems to be irrelevant for the shear-induced orientation. However, the exponent becomes larger for stronger dipoles $\beta = \pm 5$. The dependence is close to that of passive polymers, i.e., a $Wi^{-1/3}$ dependence. The latter suggests a strong active flow-field effect on the orientation.

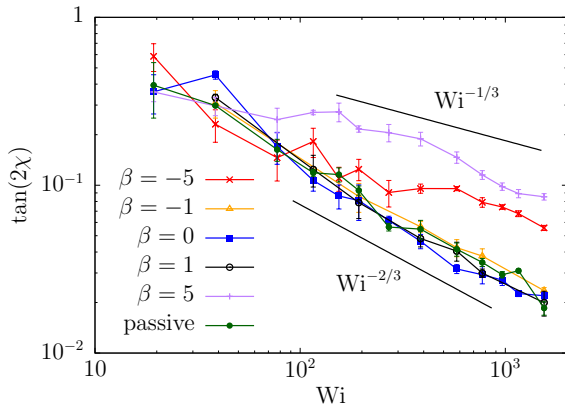


Figure 2: Flow alignment as a function of the Weissenberg number $Wi = \dot{\gamma}/D_R^\perp$ for various active dipole strengths β as indicated. The straight lines indicate the power-law dependencies.

Above a certain shear rate, we observe a transition from a preferred alignment with the shear flow to an alignment along the vorticity direction. This reorientation is quantified in Fig. 3 by the z component, e_z , of the squirmer orientation. At small

Weissenberg numbers, the average magnitude of e_z is somewhat smaller than the isotropic value $|e_z| = \sqrt{1/3}$, indicating a small preferred alignment in the xy -plane. With increasing Wi , $|e_z|$ decreases due to an enhanced alignment along the flow direction. However, above $Wi \approx 5 \times 10^3$, the spheroids reorient and point preferentially along the vorticity direction. Qualitatively, the transition is independent of the dipole strength β , especially, the passive spheroidal colloid exhibits the same transition, but quantitatively a stronger alignment effect is observed. Remarkably, pullers with $\beta = 5$ exhibit a qualitatively different behavior. First of all, they align already at lower shear rates with the flow, and, secondly, show a more gradual crossover to vorticity alignment. The reason for this behavior needs to be clarified.

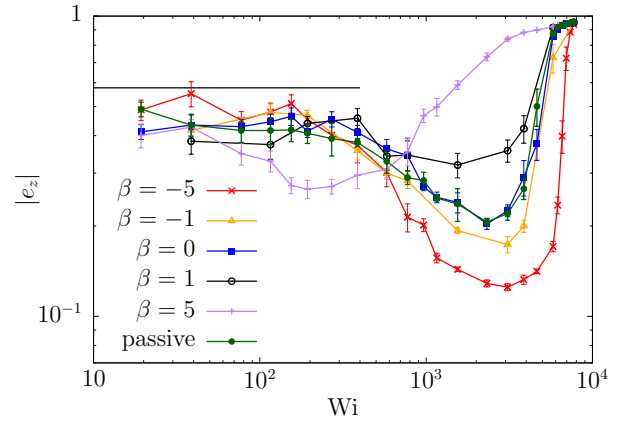


Figure 3: Absolute value of the z component of squirmer's orientation with respect to the reduced shear rate. The vertical line indicates the average value for an isotropic system.

Our simulations reveal that active microswimmers in flow fields exhibit a rich dynamical behavior. The presented structural properties are directly related to the microswimmers' dynamical and rheological behavior under flow. More results will be discussed and presented during the symposium.

References

- [1] Elgeti, J., Winkler, R.G. and Gompper, G., Physics of microswimmers-single particle motion and collective behavior: a review, *Rep. Prog. Phys.*, 78, 056601, 2015.
- [2] López, H.M., Gachelin, J., Douarche, C., Auradou, H., and Clément, E., Turning bacteria suspensions into superfluids, *Phys. Rev. Lett.*, 115, 028301, 2015.
- [3] Gompper, G., Ihle, T., Kröll, D.M., and Winkler, R.G., Multi-particle collision dynamics: a particle-based mesoscale simulation approach to the hydrodynamics of complex fluids, *Adv. Polym. Sci.*, 221, 1, 2009.
- [4] Theers, M., Westphal, E., Gompper, G., and Winkler, R.G., Modeling a spheroidal microswimmer and cooperative swimming in a narrow slit, *Soft Matter*, 12, 7372, 2016.
- [5] Huang, C.-C., Chatterji, A., Sutmann, G., Gompper, G., and Winkler, R. G., Cell-level canonical sampling by velocity scaling for multiparticle collision dynamics simulations *J. Comput. Phys.*, 168, 229, 2010.